

Catalytic selective ring opening of polyaromatics for cleaner transportation fuels

Author

Jampaiah, Deshetti, Murzin, Dmitry Y, Lee, Adam F, Schaller, David, Bhargava, Suresh K, Tabulo, Ben, Wilson, Karen

Published

2022

Journal Title

Energy & Environmental Science

Version

Accepted Manuscript (AM)

DOI

[10.1039/d1ee02363b](https://doi.org/10.1039/d1ee02363b)

Rights statement

© 2022 Royal Society of Chemistry. This is the author-manuscript version of this paper. Reproduced in accordance with the copyright policy of the publisher. Please refer to the journal website for access to the definitive, published version.

Downloaded from

<http://hdl.handle.net/10072/422351>

Griffith Research Online

<https://research-repository.griffith.edu.au>

Catalytic selective ring opening of polyaromatics for cleaner transportation fuels

Deshetti Jampaiah^a, Dmitry Y. Murzin^b, Adam F. Lee^{a*}, David Schaller^c, Suresh K. Bhargava^a, Ben Tabulo^c and Karen Wilson^{a*}

^a*Centre for Advanced Materials & Industrial Chemistry (CAMIC), School of Science,
RMIT University, Melbourne, VIC3000, Australia*

^b*Laboratory of Industrial Chemistry and Reaction Engineering, Abo Akademi University, Biskopsgatan 8,
20500, Turku/Abo, Finland*

^c*Southern Oil Ltd, 39 Guerassimoff Rd, Yarwun, QLD 4694, Australia*

*Corresponding Author: karen.wilson2@rmit.edu.au; adam.lee2@rmit.edu.au

Abstract:

The selective C-C bond cleavage of mono- and bicyclic naphthenic molecules via catalytic ring opening plays a vital role in refining low-quality fossil oils and pyrolysis oils derived from **municipal solid waste or waste biomass and tyres**. Diesel fuels derived from such oils exhibit high polyaromatic content and low cetane number (CN), resulting in significant particulate emissions upon (inefficient) combustion. Catalytic upgrading of these oils via ring opening to form paraffinic molecules enhances their CN, producing cleaner burning fuels, with reduced particulate and sulfur emissions. Supported **transition** metal catalysts are attractive candidates for obtaining high-quality fuels by selective C-C bond cleavage of naphthenic molecules with high conversion. Ring opening of model polyaromatics can proceed through several reaction pathways, dictated by the catalyst, feedstock and reaction conditions, producing hydrocarbons with the desired CN. Identification of the active sites in supported **transition** metal **nanoparticles** responsible for different ring opening pathways is essential for the development of next-generation catalysts exhibiting higher selectivity and stability. Here, we critically review recent advances in the **selective** ring opening (SRO) of naphthenic molecules to paraffinic hydrocarbons (with high CN and low aromaticity), and discuss the impact of catalyst design on performance and reaction mechanism. **Technical** challenges in designing **transition** metal catalysts for SRO are discussed, and **avenues explored** for improving diesel fuel quality from low-grade feedstocks, including **municipal solid waste**.

Keywords:

Oil refining, **Biomass**, Pyrolysis **oil**, Catalytic ring opening, **Cetane number**, Hydrogenolysis

1. Introduction

Consumption of liquid fuels in the transportation sector has risen continuously since the Industrial Revolution,¹ placing great demand on modern refinery streams to expand production and improve fuel quality. Such expansion must be tensioned against anthropogenic climate change, which imposes severe targets for reduced greenhouse gas emissions.^{2,3} Global crude oil consumption increased from 95 to >100 million barrels per day (Mb/day) from 2015-2019,³ although the COVID-19 pandemic derailed projections resulting in a sharp drop in production to 83 Mb/day in 2020. A slight increase post-pandemic is expected, but with more widespread availability of low emission energy sources, demand is predicted to fall further to 77 Mb/day by 2030.⁴ Although various scenarios indicate that crude oil use will peak by 2025⁵ due to the emergence of large scale, renewable energy technologies including biomass, solar, wind and hydrogen,⁶ ⁷ this timeline is a strong function of the model used. In 2020, the transportation sector constituted 32 % of global energy consumption and 60 % of global oil demand; while these values dropped dramatically due to COVID-19 (and will continue to fall road vehicle electrification), liquid fuel requirements for heavy duty freight is expected to continue rising by 1.4 % per year until 2030.^{8,9} Electrification plays an important role in reducing carbon emissions from cars and light duty vehicles, but is harder to implement for heavy and long distance transportation, with a reduced environmental impact for the latter only predicted towards 2050 through improved battery technology and renewable fuel availability (notably hydrogen or advanced biofuels).⁴ Demand for bioderived liquid transportation fuel is thus predicted to more than double by 2030, meeting 14 % of fuel needs, but with a continued reliance on petroleum-derived fuel for 70 % of needs.⁴

Transportation fuels are dominated by gasoline, diesel, and jet fuel. Diesel fuel, also called distillate fuel oil, offers performance, efficiency and safety features,¹⁰ and is generally defined as a hydrocarbon mixture comprising 12-20 carbon atoms of paraffins, aromatics and naphthenes (saturated hydrocarbons containing at least one carbon ring) with a boiling point spanning 170-360 °C.^{11, 12} The ignition and combustion properties of diesel are indicated by the Cetane Number, which is an inverse function of the fuel ignition delay as determined by variable compression engine test procedures (ASTM D613) employing reference mixtures of n-hexadecane (CN=100) and heptamethylnonane (CN=15).¹³ Most diesel engines operate well with fuels having a CN of 46-51,¹³ however lower CNs confer longer ignition delays and increased time for complete fuel combustion, resulting in rough engine operation, cold start issues and undesired particulate emissions.^{13, 14} The target for high-quality diesel fuel is a short ignition delay to increase combustion and reduce particulate emissions, coupled with a low concentration of polyaromatic hydrocarbons (PAH<11 wt%) and sulphur (<10-15 ppm).^{15, 16} Sweden and Finland have targeted the production of diesel fuel with more stringent specifications; in 1992, Sweden produced a diesel fuel with 2 to 5 ppm sulfur and a maximum of 5 wt% aromatics.¹⁷ Since 2003, diesel containing zero ppm sulfur and <1 wt% aromatics has been available on the Swedish market under the name of EcoPar.¹⁸ However, such ultra-low sulfur fuels need to be globally available if diesel fuel with a high CN and low particulate matter emissions are to find widespread use.^{14, 19}

Refined oil output has significantly increased in recent years due to expanded global refinery capacity. According to the European Automobile Manufacturers Association in 2021, 42.3 % of cars in Europe use diesel fuel.²⁰ Diesel-powered light commercial vehicles are dominant, with almost 90 % of EU van fleets and 97.8% of all EU truck fleets running on diesel. In Australia, 2.6 million diesel cars were registered in 2021, representing 16 % of the nation's 16.2 million-strong automobile fleet.²¹ Continued diesel use, coupled with the reduced availability of easily refined sweet crude oil, necessitates enhanced hydrocracking capability in refineries to improve diesel quality.^{22, 23} However, achieving this goal is problematic as oil refineries have different configurations and product profiles, including fuels, chemicals and asphalt.²⁴ The general operation of an oil refinery is shown in **Figure 1**, and illustrates how fuels including naphtha, gasoline, diesel, jet fuel and other fuel oils can be obtained from petroleum refining by processes such as hydrotreating, hydrocracking and catalytic reforming.²⁵

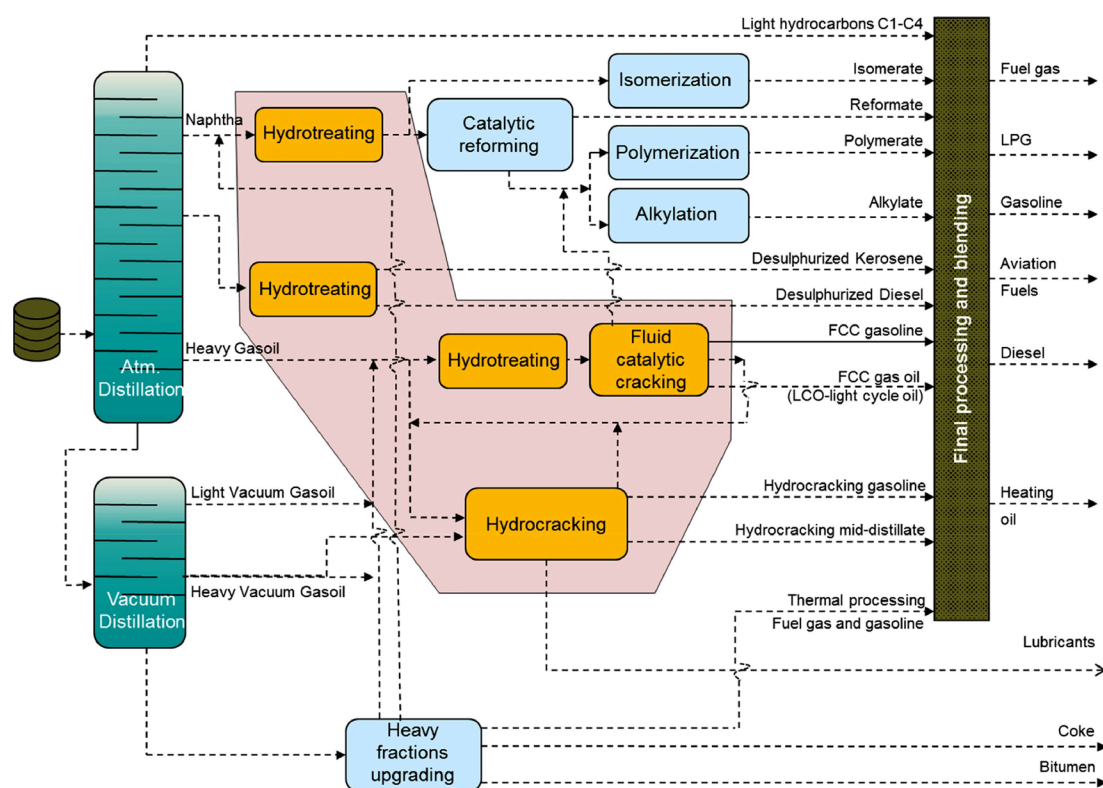


Figure 1. Schematic of refinery operation for fuels production from crude oil. Reproduced with permission from Ref²⁶.

For any oil refinery, the primary source is crude oil, which can be obtained from fossil fuels, biomass or synthetic sources like hydrotreated esters or plastic waste pyrolysis oils.²⁶ Petroleum refining industries have a well-developed infrastructure to produce diesel fuel,²⁷ and due to the existing processes, blending of leftover petroleum fraction (light cycle oil, LCO) obtained from fluid catalytic cracking with the diesel fraction is an attractive option. The LCO feedstock contains 84-87 wt% polyaromatics (20-30 % naphthenic and 40-60 % multiply-substituted aromatics with very short paraffinic side chains) and 2-4 wt% sulfur, with the balance heteroatoms including nitrogen (0.08 wt%).²⁸⁻³⁰ Despite a boiling point between 180-360 °C, the resulting blends have a CN of 27, far below the minimum standard of 51 used in developed countries

including the USA and Australia and hence LCO is unsuitable for use as a diesel feedstock without upgrading. Other attractive potential diesel feedstocks include pyrolysis oils derived from municipal solid waste (MSW), or biomass or tires waste. Utilisation of waste-derived pyrolysis oils for diesel production offers reduced landfill waste (and associated environmental pollution), an economic boost for the waste recovery sector and improved energy security.³¹ Global MSW generation is predicted to reach 2.3 Bt/yr by 2030, and typically comprises approximately 44-50 % biodegradable organic matter, 17% paper/cardboard and 12-15% plastics.³² Catalytic pyrolysis of MSW produces 15-30 wt% oil, containing ~50 % naphthenics (of which ~10% are naphthalene and its derivatives).³³ Simplified MSW models containing mixed biomass and plastics such as polyethylene terephthalate (PET), polypropylene (PP), high density polyethylene (HDPE), low density polyethylene (LDPE), and polystyrene (PS),³⁴ produce 6-12% aromatics. Fast pyrolysis of biomass typically produces 10-15 wt% aromatics (of which ~15 % are naphthalene). Polyaromatics can result from aldol condensation and cyclisation reactions,³⁵ or Diels Alder cycloaddition of biomass-derived furanic species with alkenes,³⁶ aromatics,³⁷ or hydrocarbon pool molecules^{38, 39, 40, 41} over zeolites to form toluene, xylenes, trimethylbenzenes, naphthalene, and their derivatives.⁴² The formation of branched decalins are also possible from the acid catalysed oligomerisation of biomass-derived cyclic alcohols.⁴³ Waste plastic is the third-largest contributor to MSW,^{44 45} and predicted increases⁴⁶ are likely to result in 12 Bt/yr of plastic waste will be landfilled by 2050.⁴⁷ Waste plastic pyrolysis at 450-500 °C^{44, 48} typically generates 45–50 wt% oils with a broad boiling point range.⁴⁹ Non-catalytic pyrolysis of polyolefins results in waste plastic oil (WPO) containing <3 wt% aromatics,⁵⁰ however catalytic pyrolysis of mixed plastics,^{51, 52} predominantly PE and PP with smaller quantities of PS, PET and poly(vinyl chloride) (PVC), over solid acids increases the oil fraction but also increases aromatic yields >95 %. In 2018, the French Plastic Odyssey project produced diesel fuel from mixed plastic (PP, and/or high density HDPE and low density LDPE) with a 70 % yield,⁵³ however this WPO contained significant aromatics and unsaturated hydrocarbons, expected to lower the CN and increase particulate emissions during combustion.⁵⁴ Approximately 1 billion waste tires are produced globally per annum;⁵⁵ pyrolysis oil derived from tire waste, in pre-commercial production by companies such as Southern Oil Refining, may contain >60 % polyaromatics.⁵⁶ Note that the production of diesel range hydrocarbons varies with pyrolysis conditions, with higher temperatures favouring polyaromatic hydrocarbons.⁴⁹

Diesel fuels derived directly from LCO or waste pyrolysis oils are either low yielding or poor quality due to their high aromatic content, and hence require improved upgrading technologies to remove naphthenics. Fluid catalytic cracking (FCC) and hydrocracking are commonly employed to upgrade heavy oil fractions into lighter components suitable for fuels (**Figure 1**). However, FCC of pyrolysis bio-oils leads to excessive char and coke formation, even at low reaction temperatures, and concomitant irreversible deactivation of FCC catalysts,²⁶ while further hydrocracking of LCO (itself obtained from a FCC unit) leads to a loss of diesel fraction and increase in light hydrocarbons.⁵⁷ Hydrocracking of pyrolysis bio-oils also produces lighter components with shortened hydrocarbon chains unsuitable for diesel, and the requirement

for high operating temperature and H₂ pressure would significantly increase processing costs.⁵⁸ Hydrocracking of deoxygenated pyrolysis oil and vacuum gas oil blends also yield diesel products with a reduced paraffinic and higher aromatic content than conventional diesel,⁵⁹ with an associated loss in CN. In general, hydrotreating of aromatics in pyrolysis oils generates 2+ ring cycloalkanes with a CN incompatible with diesel.⁶⁰ Although polyaromatics were reportedly removed over NiMo/Al₂O₃ hydrotreatment catalysts (at 350-375 °C and 80-100 bar H₂) to yield a fuel with CN 75,⁴⁶ no information was provided on whether polycyclic hydrocarbons remained or their impact on emissions.

Selective ring opening (SRO) is an alternative, emergent technology to reduce naphthenic levels in LCO and pyrolysis oils via ring hydrogenation and cleavage of endocyclic C-C bonds^{10, 54, 61} to produce paraffins with the same number of carbon atoms,⁶² and hence increase the CN of resulting diesel fuels. Hydrogenation of aromatics in combination with SRO of diesel feedstocks can further enhance the CN.^{12, 63} As an added benefit, SRO increases the volume of available product due to the gradual decrease in density resulting from loss of molecular weight during hydrogenation of complex polyaromatic compounds.⁶⁴ Major naphthenic molecules (those containing one or more saturated cyclic structures) remaining in distillate fractions after various levels of hydrogenation are naphthalene, tetralin, decalin and indan,^{65, 66} and are representative of the type of molecules present in real diesel feeds. As outlined earlier, diesel quality is in part determined by the presence of molecules with larger CN,⁶⁶ and catalytic SRO of bicyclic molecules such as the aforementioned can increase the CN. SRO studies are however hampered by analytical difficulties arising from the complexity of ring opening and competing reactions, e.g. isomerisation and cracking. Quantitative analysis of intermediates and products is necessary to obtain deeper insight into the SRO mechanism and thereby guide the design of improved catalysts. Although monocyclic naphthenes such as methylcyclopentane (MCP) and methylcyclohexane (MCH) are not components of real diesel feedstocks, studies of their SRO can shed valuable mechanistic insight. For example, ring contraction of a polycyclic six-membered molecule can produce five-membered ring isomers akin to methyl cyclopentane, whereas the hydrogenation of naphthalene generates tetralin, which comprises one aromatic and one-saturated ring (cyclohexane attached to benzene).⁶⁷ Knowledge of MCP and MCH ring opening as model molecules provides the basis for understanding the behaviour of more complex molecules such as naphthalene, tetralin, decalin and indan. The structure of exemplar mono- and bicyclic molecules, and their corresponding CN numbers, are shown in **Figure 2**.⁶⁶

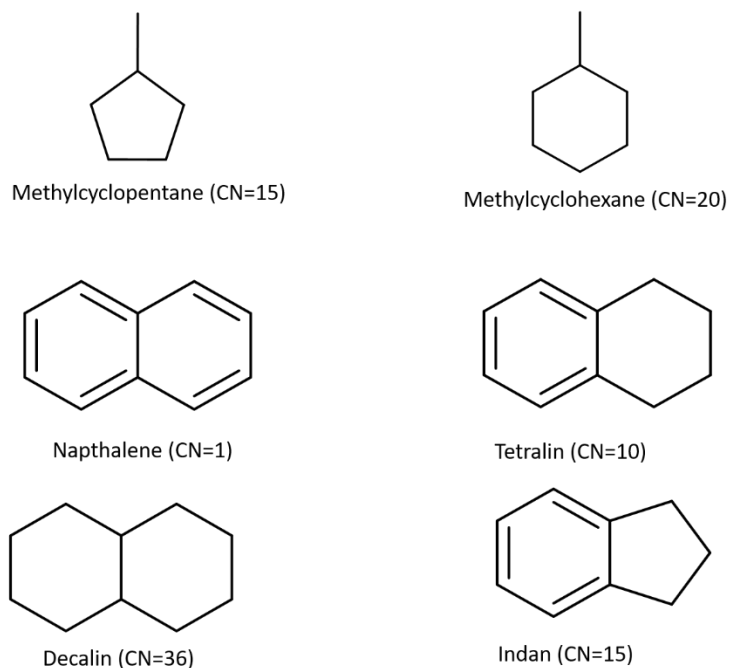


Figure 2. CN of prototypical monocyclic and bicyclic naphthenic molecules.

Despite the importance of SRO of naphthenic molecules for enhancing the CN of diesel fuel, and the potential for upgrading of waste-derived pyrolysis oils,^{43, 46,34} there are few reviews of ring opening catalysis.^{63, 65, 68, 69} Most such reviews exclusively focus on zeolite-supported noble metal catalysts and their performance benchmarking against model compounds. However, different reaction mechanisms and structure-reactivity relationships have not been systematically evaluated with respect to a broad range of relevant model compounds. It is widely acknowledged that catalyst properties, such as acidity, porosity and metal particle size strongly influence the SRO reaction. Thus, the present review discusses recent advances in SRO of monocyclic, saturated alkanes and polycyclic molecules, identifying links between physicochemical properties of catalysts and their corresponding conversion and selectivity towards specific products. Topics explored include the role of mono- and bimetallic active sites, the impact of support acidity, and their influence on different SRO pathways and resulting catalyst stability and lifetime. The SRO reaction over supported metal catalysts is discussed for both model compounds and real feedstocks, noting efforts to improve CN, resulting conversion and selectivity. Finally, we discuss current challenges facing the SRO approach, and offer perspectives on the future design of highly selective catalysts for the SRO of naphthenic molecules and suggest practical solutions for potential industrial implementation.

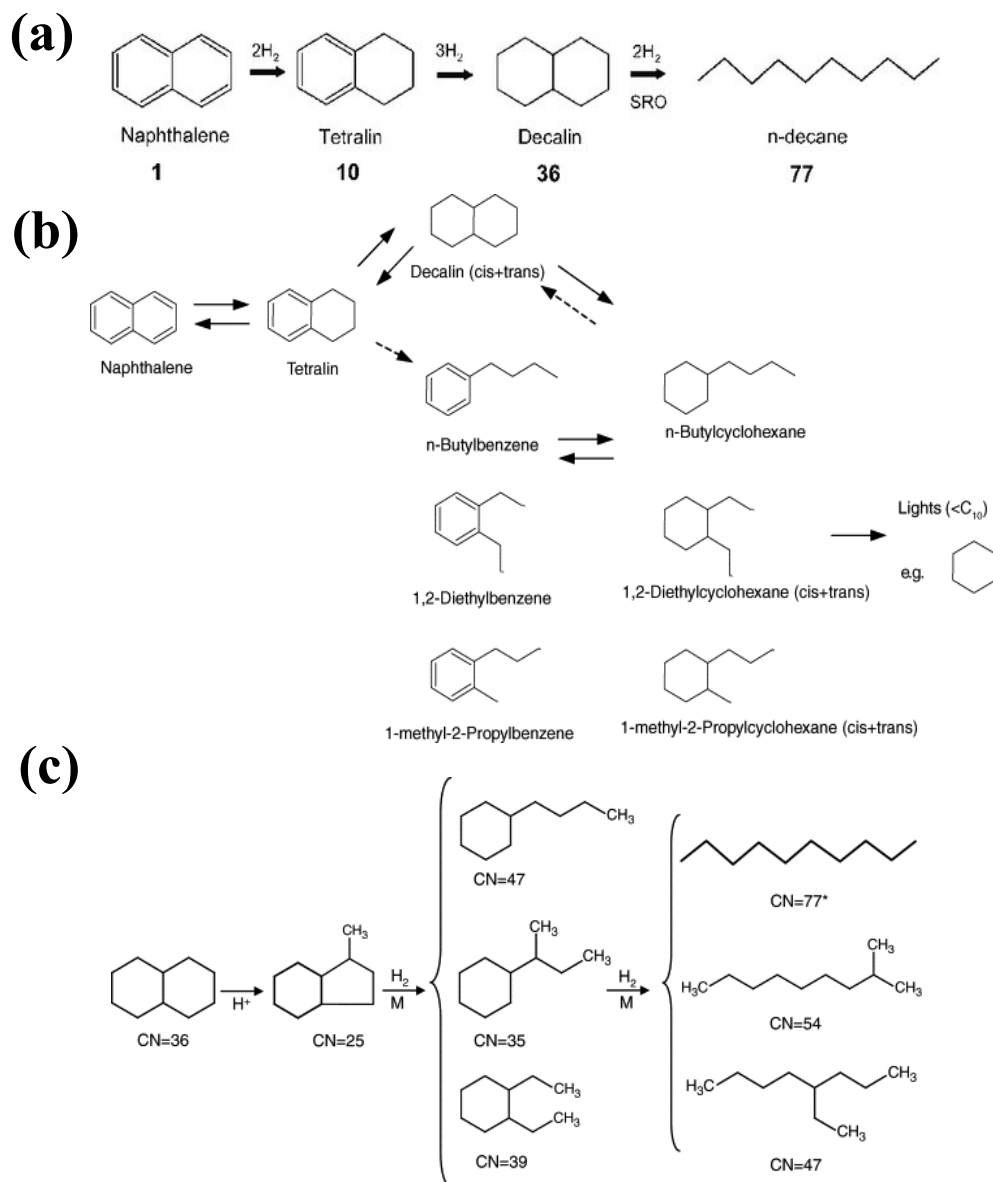
2. Selective Ring Opening Catalysts

The chemistry of SRO has been explored since the 1950s, predominantly using model compounds like MCP and MCH over noble metal catalysts. Since about 2000, the chemistry of catalytic SRO was extended

to various bicyclic model compounds, notably tetralin, decalin and indan, with the ability to control partial or complete hydrogenation of polyaromatics considered a significant advance.^{10, 70}

Generally, SRO requires transition metals active for hydrogenolysis and a support that may be either neutral or participate in the reaction via adduct formation (or possess acidity to actively direct secondary reactions). Using an external hydrogen source, partial hydrogenation of (poly)aromatic rings is followed by selective C-C bond cleavage to produce ring-opened products. Resasco and co-workers demonstrated that changes in CN of different compounds such as decalin, tetralin, and phenanthrenes were achieved when selective C-C bond breaking forms linear or mono-branched paraffins.^{13, 66} For example, a CN of 77 (n-decane) can be obtained from the SRO of decalin (CN=36) (Scheme 1a). However, the formation of SRO products with increased CNs is not achievable in a single step, and SRO is typically only performed after severe hydrotreating which can broaden the distribution of cyclic molecules thereby increasing the reaction network complexity, as shown in Scheme 1b. For polyaromatics, selective C-C cleavage to open the second ring is crucial to obtain a molecule with less branching and a high CN.⁶⁶ Uncontrolled hydrogenation and further C-C bond scission must be avoided, as such hydrocracking forms light hydrocarbons unsuitable for diesel fuel. Therefore, the selectivity, distribution and composition of the less-branched products heavily depends on operating conditions and characteristics of the catalytic system. It is therefore important to evaluate the possible reaction paths and understand the role of catalysts in selective C-C bond cleavage of naphthenic molecules, which could provide a pathway for upgrading diesel fuels. In general branched isoparaffins form when cleavage occurs at an unsubstituted C-C bond, decreasing the CN, whereas cleavage of a substituted C-C bond reduces branching and increases the CN: ring contraction followed by a ring opening (Scheme 1c) is proposed as a unique strategy to achieve a high level of control over the final product stereochemistry and hence CN.^{71, 66}

The existence of competing pathways in naphthene SRO necessitates an understanding of the thermodynamics of associated reactions to predict the relative product yields. Hydrocracking of paraffins and naphthenes can proceed via: (i) acyclic cracking where a paraffin molecule is cracked into two smaller species; (ii) exocyclic cracking where a side chain is removed from a naphthene; and/or (iii) endocyclic cracking where cleavage of ring C-C bond occurs.⁷² To simplify thermodynamic calculations, Govindhakannan et al considered SRO as a cracking reaction followed by a hydrogenation reaction.⁷² While the ΔH^\ominus for reaction is negative for all three of the preceding cracking reactions, the corresponding ΔS^\ominus is positive for acyclic and exocyclic cracking reactions but negative for endocyclic ring opening reactions. The negative ΔS^\ominus for endocyclic ring opening is a consequence of the entropy decrease for the hydrogenation step exceeding the entropy increase arising from C-C cleavage. Acyclic and exocyclic cracking are thermodynamically favoured relative to endocyclic cracking, with the latter becoming non-spontaneous at elevated temperature (>500 °C). Considering the ring opening of decalin, cracking (CR),



Scheme 1. (a) CN number enhancement from the conversion of naphthalene to n-decane; (b) reaction pathways for the hydrogenation of naphthalene to tetralin and hydrogenolysis of the model feed naphthalene and tetralin. (Reproduced with permission from Ref⁷³); and (c) role of initial ring contraction in altering CN. (Reproduced with permission from Ref⁶⁶).

ring contraction (RC), SRO and dehydrogenation (DH) products are all possible. For equimolar ratios of H₂ and decalin, cracking and dehydrogenation products dominate, and equilibrium calculations predict insignificant levels of total ring opening (TRO, sum of saturated and unsaturated) products.⁷² Excess H₂ can suppress competing pathways and increase TRO, with an optimum H₂:decalin molar ratio of 4:1 predicted (Figure 3). TRO is also temperature sensitive, with decalin ring opening mildly exothermic and ring contraction products more endothermic. Consequently, equilibrium yields for TRO products decrease dramatically between 500-600 K, and hence to be viable, any SRO process should operate <600 K. Kubička et al⁷⁴ proposed a simplified scheme for the hydrocracking of decalin, wherein the cis- and trans- bicyclic isomers are in equilibrium with each other and with ring contraction products (precursors to ring opening and cracking products) as shown in Figure 4. Applying the thermodynamic data for selected products at

500 K,⁷² reveals that the preferred route from decalin to ring opened products is through ring contraction. Although higher temperatures promote ring contraction, they also disproportionately favour cracking, and hence more active and selective catalysts are required for low temperature SRO which suppressing competing cracking pathways.

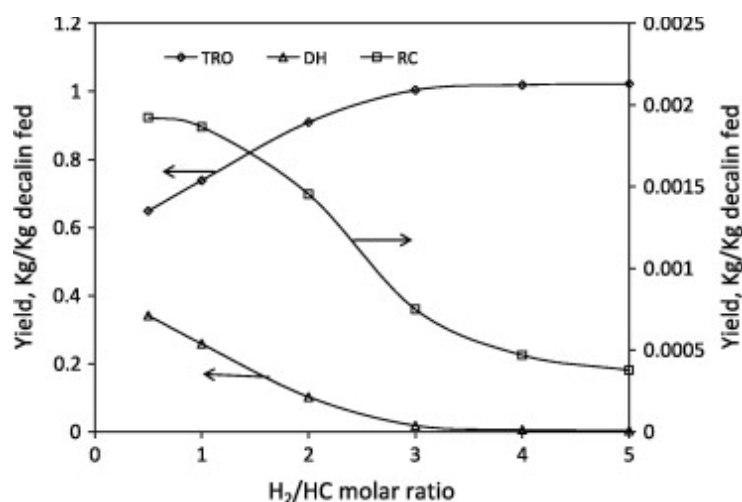


Figure 3. Yields of total ring opening (TRO), dehydrogenation (DH) and ring contraction (RC) products as a function of hydrogen:decalin molar feed ratio at 500 K determined from thermodynamic equilibrium calculations. Reproduced with permission from ⁷².

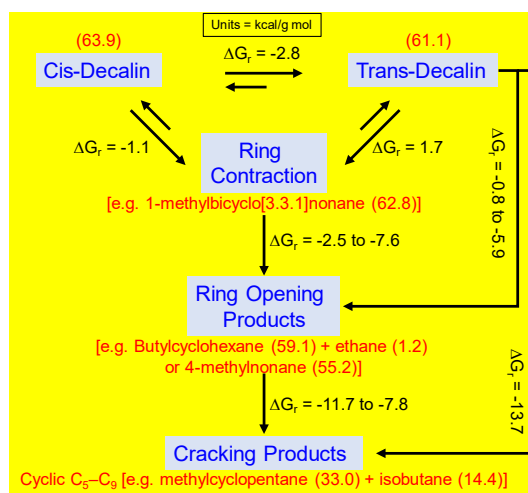


Figure 4. Gibbs free energy changes for the ring opening of decalin based on thermodynamic data from Ref ⁷² and proposed reaction cycle from Ref ⁷⁴. Values in brackets are the standard Gibbs free energy of formation of selected stable molecules identified as potential products of RC, SRO and CP pathways.

Three classes of solid catalysts show promise for C-C bond cleavage of naphthenic molecules without significant changes in the molecular weight of products, and hence are candidates for SRO: (i) solid acids; (ii) supported transition metals; and (iii) bifunctional catalysts containing Brønsted acid and transition metal sites. **Figure 5** summarises the advantages and disadvantages of each catalyst class.

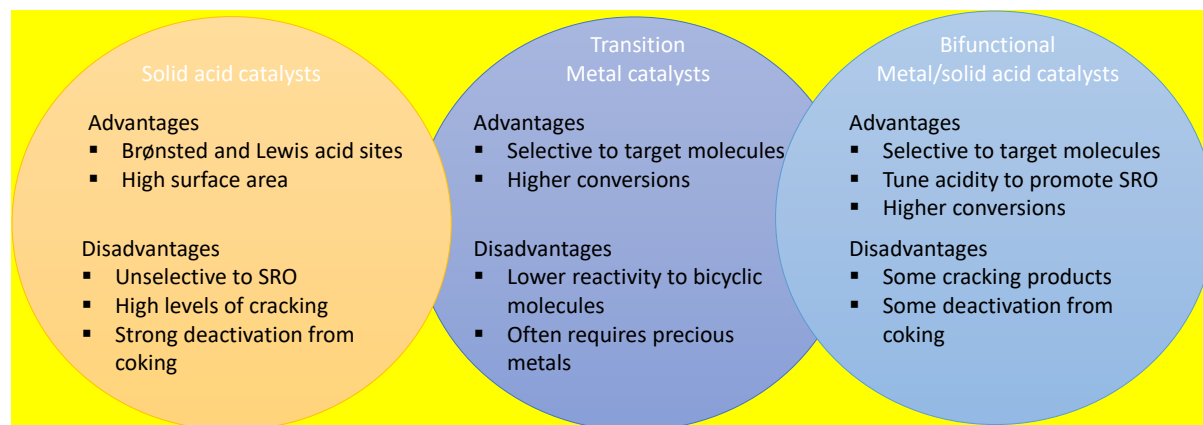


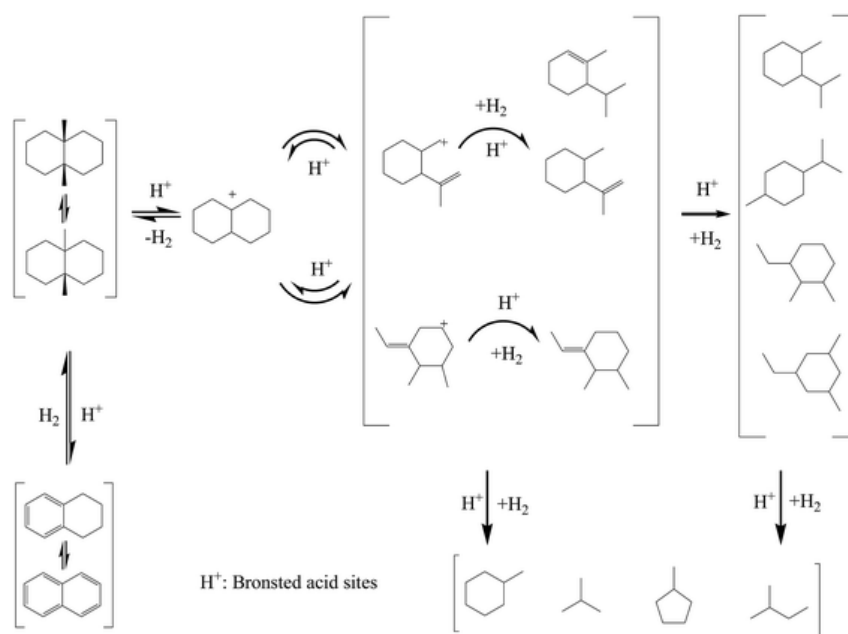
Figure 5. Summary of main catalysts employed for selective ring opening (SRO).

The following sections provide an overview of solid acid, transition metal and bifunctional metal/solid acid catalysts employed in SRO, and compare their activity/selectivity for key steps involved in the SRO mechanism (hydrogenation, hydrogenolysis of C-C bonds, isomerisation and cracking) to offer insight into the optimal formulation of active and selective catalysts for targeted SRO reactions.

2.1. Solid acid catalysts

Solid acid-catalysed ring opening of naphthenes has mainly been studied on zeolites,⁷⁵⁻⁷⁷ wherein Brønsted acidic sites protonate the cyclic molecule, leading to isomerisation and subsequent C-C bond cleavage. The most well-known solid acid catalysts are proton-modified zeolites, including H-Beta, H-Y, H-Mordenite, and H-ZSM5.⁷⁷⁻⁸⁴ H-ZSM-5 (Si/Al=20), which have been explored for the ring opening of monocyclic molecules such as MCP and MCH at 250 °C and 6 MPa H₂ pressure.⁷⁹ Complete conversion of both reactants was observed, but with 99 % selectivity towards cracking products, which is undesirable for diesel application. Corma et al. investigated medium-pore (10-membered ring, MCM-22, ZSM-5, and ITQ-2), large-pore (12-membered ring, Beta, USY), and ultra-large pore (UTD-1) zeolites for the ring opening of tetralin and decalin at 450 °C and demonstrated that 12-membered ring zeolites could open the molecular rings, with Beta-type zeolites most selective. However, the major focus of this study was tetralin and decalin cracking, and hence little information was provided on ring opening products. In a similar study, SRO was reported for decalin using USY, ZSM-5 and mordenite zeolites,^{85, 86} however, no isomeric or ring opening products were observed. Kubička et al. compared solid acids such as H-Beta-25, H-Beta-75, H-Y-12, H-Mordenite-20, and H-MCM-41 (where the number after the zeolite represents the SiO₂:Al₂O₃ ratio) for decalin ring opening at 300 °C and 2 MPa H₂ to assess the impact of acidity on ring opening. The Brønsted acidity of the zeolite catalysts was determined by pyridine adsorption at 250 °C and followed the order H-Mordenite-20 (331 μmol/g) > H-Beta-25 (269 μmol/g) > H-Y-12 (255 μmol/g) > H-Beta-75 (147 μmol/g) > H-MCM-41 (26 μmol/g). Mildly acidic zeolites exhibited modest ring opening yields (5-8 wt%) along with isomers (50 wt%), cracking products (23 wt%), and other heavy products (10 wt%); conversion and ring opening yields correlated with the Brønsted acid site densities of the catalysts.

The mechanism of C-C bond cleavage in decalin over Brønsted acid catalysts is illustrated in Scheme 2, wherein protolytic dehydrogenation forms a carbocation at acid sites. The next step involves β -scission and hydride transfer, resulting in the formation of isomers such as methylbicyclononane, dimethylbicyclononane, dimethylbicyclooctane and trimethylbicycloheptane, which are finally hydrogenated to yield corresponding saturated ring opening products.



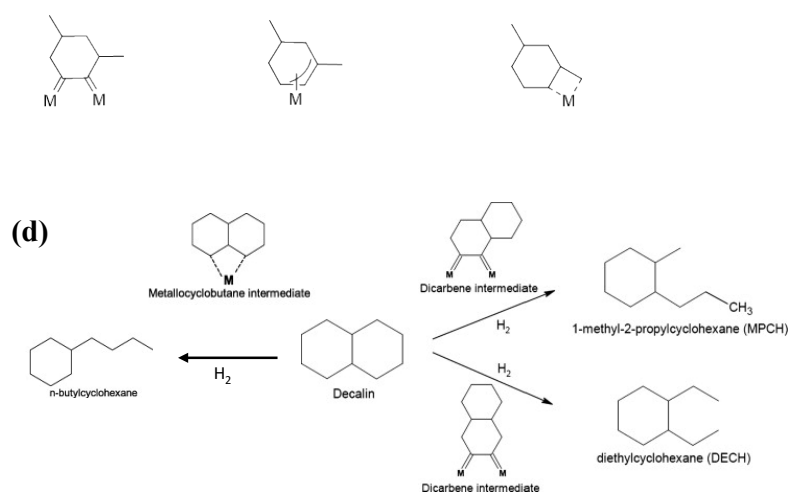
Scheme 2: Proposed mechanism for isomerisation and ring opening of decalin over Brønsted acid catalysts. Reproduced with permission from ⁷⁷.

The most common ring opening products from decalin (CN=36) are 1-ethyl-3,5-dimethylcyclohexane (CN=30), 1,2,3,5-tetramethylcyclohexane (CN=18), methyl-isopropylcyclohexane (CN=24) and isobutylcyclohexane (CN=36), which indicate solid acid catalysts alone cannot significantly increase the CN of naphthenics and hence are unsuitable for fuel upgrading.⁸⁷⁻⁸⁹ Zeolites also deactivate through coking, and form significant light hydrocarbons (CN between 15 and 29) at high conversions, being a function of acid strength and pore structure. Since the yields of ring opening products are low (5-10% at most),⁷⁴ and the products of acid-catalysed ring opening do not offer improved CN,^{76, 90} unpromoted solid acid catalysts are unsuitable for SRO.

2.2 Transition metal catalysts

Transition metal catalysts can open naphthenic ring compounds when the metal ensembles possess hydrogenolysis activity,⁹¹ for example Pt/ Al_2O_3 , Ir/ Al_2O_3 , Ir/ SiO_2 , Pt-Ir/ Al_2O_3 , Pt-Ir/ SiO_2 , Ru-Pd/ Al_2O_3 , Ru-Ir/ Al_2O_3 and Ni-Ir/ Al_2O_3 .^{12, 89, 92-94} Ring opening is proposed to occur via hydrogenolysis of endocyclic C-C bonds bound to metal sites in three different coordination modes (dicarbene, π -adsorbed olefin or

metallocyclobutane) as illustrated in **Scheme 3a-c**.⁶³ The selectivity and distribution of ring opening products will depend on which of these intermediates is formed.



Scheme 3. Three potential ring opening intermediates formed during activation of 1,3 dimethyl cyclohexane over transition metal catalysts: (a) dicarbene; (b) olefin; and (c) metallocyclobutane. Reproduced with permission from ⁶³. (d) Reaction pathways for decalin SRO via dicarbene and metallocyclobutane routes. Reproduced with permission from ^{66, 76}.

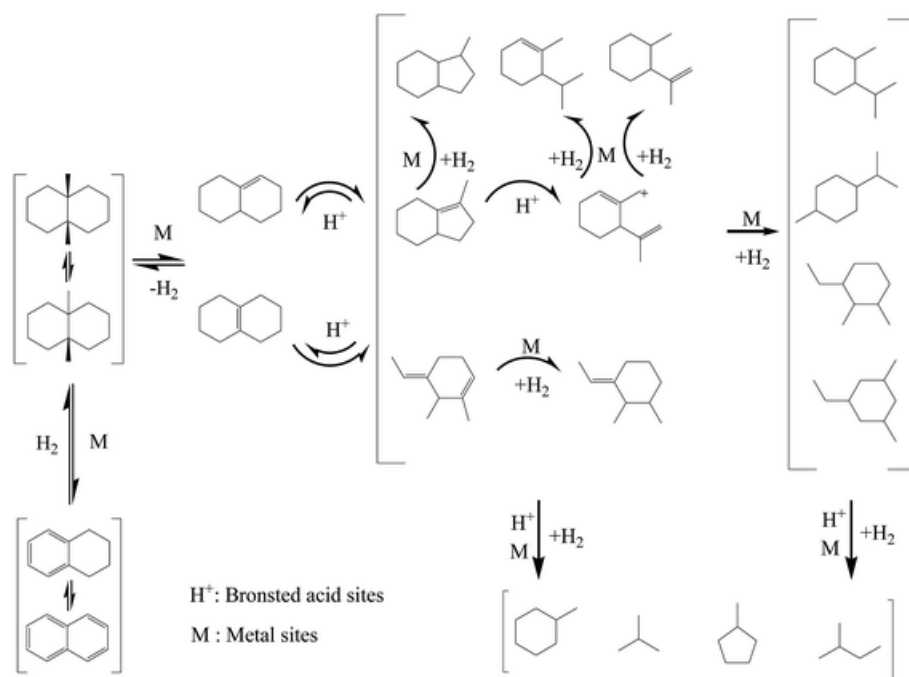
Scheme 3a shows the dicarbene intermediate, formed by the coordination of adjacent secondary carbon atoms to two metal sites, resulting in a perpendicular adsorption configuration which favours exclusive breaking of unsubstituted secondary-secondary C-C bonds. This is referred to as a ‘selective mechanism’ results in a predictable product distribution, and is often favoured over larger metal nanoparticles (NPs) where suitable metal ensembles dominate.^{95,89} In contrast, π -adsorbed olefin coordination (**Scheme 3b**) only requires bonding to a single metal atom, and results in a ‘non-selective mechanism’; this is favoured over highly dispersed metal sites. The flatter adsorption geometry leads to an equal probability for either secondary–secondary, secondary–tertiary or tertiary–tertiary C-C bond cleavage, and hence an unpredictable product distribution. The metallocyclobutane route (**Scheme 3c**) also involves coordination to a single metal atom, however, bonding to the ring and exocyclic side group in this geometry results in selective cleavage of substituted C-C bonds to produce only linear paraffins, and is highly desirable for diesel fuel production.⁹⁶ **Scheme 3d** illustrates potential product distributions arising from decalin ring opening over Ir catalysts via the di-carbene or metallocyclobutane intermediates. The former intermediate favours methyl-propylcyclohexane (MPCH) and diethylcyclohexane (DECH) from the two possible ring M=C-C=M coordination modes, whereas the latter selectively produces n-butylcyclohexane following secondary-tertiary C-C bond cleavage. Such mechanistic insight is often derived by comparing the observed product distributions against possible models; the metallocyclobutane mechanism is invoked when higher levels of paraffins are measured.⁹⁷ The reaction mechanism and associated product distribution and selectivity vary strongly with the hydrogenolysis metal (e.g. type and particle size), support and model compound investigated. In general, the selectivity for unsubstituted C-C cleavage in naphthenic molecules

follows the order Ir >> Rh \approx Ru \approx Ni > Pt, when proceeding via the di-carbene mechanism.¹² However, Pt shows superior activity for cleaving substituted C-C bonds, and also exhibits a strong particle size dependence, which are attributed to operation of an alternative metallocyclobutane pathway over smaller NPs.^{89, 12, 76} The activation barrier to the metallocyclobutane intermediate is higher than that of the di-carbene, and hence the former pathway most likely only operates when the di-carbene route is inhibited by e.g. site blocking from coke or steric hinderance of the reactant.⁸⁹ As discussed later, under certain conditions Ir favours the metallocyclobutane mechanism, but this is also strongly dependent on reaction conditions and support, with Ir/Al₂O₃ more selective towards paraffins than Ir/SiO₂, irrespective of metal dispersion.⁸⁹ Trends in the activity of transition metals also depend on the model compound studied. Although five membered MCP rings are easily opened by a noble metal at low temperature, ring opening of the six membered MCH is almost a hundred times slower.¹² Transition metals on non-acidic supports are generally not sufficiently active towards polycyclic molecules due to their low isomerisation activity.^{89,98} Combination with a tunable acidic support is therefore critical for the development of practical SRO transition metal catalysts.

2.3 Bifunctional solid acid supported transition metal catalysts

Bifunctional catalysts based on solid acid supported transition metals enable cooperativity between metal catalysed hydrogenolysis/hydrogenation and acid catalysed isomerisation to drive SRO. In general, such catalysts are fabricated by dispersing metal NPs on a solid acid support, with the acidic support generally promoting ring isomerisation, and subsequent ring opening to the SRO product proceeding on metal sites.⁹⁹ Bifunctional catalysts are mostly used for RO of molecules containing two or more six-membered rings, wherein the acidic support can isomerise six-membered rings to their 5-membered counterparts, and the transition metal able to more readily open the resulting contracted ring. For example, tandem acid-metal catalysed ring opening of decalin via a substituted C-C bond cleavage mechanism produces n-butylcyclohexane (CN=47), diethyl-cyclohexane (CN=39) and 1-methyl-2-propylcyclohexane (CN=39).⁶⁶ The increased CN indicates that bifunctional catalysts are better suited for fuel upgrading than solid acid catalysts alone.⁷⁶ Metals from Group VIII (Rh, Ru, Ir, Pt and Pd) are well known for their hydrogenolysis activity, and are reported as having excellent activity and selectivity towards ring opening when dispersed over solid acid supports such as zeolites and SiO₂-Al₂O₃. Zeolites with medium and large pores, such as USY, HY and H-Beta are considered the most suitable supports for dispersing the hydrogenolysis metal.^{82, 100} Examples of bifunctional catalysts investigated include Pt/HY, Pt/H-Beta, Pt/H-mordenite, Pt-Ir/H-Beta, Ir/H-Beta, Ir/WO₃/Al₂O₃, Ir/SiO₂-Al₂O₃, Rh-Pd/ SiO₂-Al₂O₃ and Ru-MCM-41.^{81, 101-105} Metal dispersion and support acidity both strongly influence the ring opening performance, with the selectivity to ring opening products tuned by varying support acidity, and composition of the metallic phase (mono- or bimetallic function, metal content and particle size).¹⁰⁶⁻¹⁰⁸ Strong interactions between the metal and support can also affect the metal hydrogenolysis activity, and conversely, metals can suppress support acidity.¹⁰⁹

The bifunctional mechanism is briefly illustrated in Scheme 4 for decalin SRO.¹¹⁰ In this mechanism, ring opening is considered to proceed indirectly, with dehydrogenation/hydrogenation occurring on the metal sites and skeletal isomerisation and β -scission facilitated by the acid sites; note that this is different to the simple metal catalysed hydrogenolysis mechanism (Scheme 2).



Scheme 4. SRO of decalin via a bifunctional mechanism. Reproduced with permission from ¹¹⁰.

Typical SRO reaction pathways for model polycyclic molecules, and the impact of their molecular structure on reactivity are introduced in the next section to identify trends in SRO activity and mechanism over different catalyst classes.

3. SRO of model polycyclic molecules

In principle, SRO is a promising route for upgrading low-value feeds to high-quality products, however in practice it continues to prove challenging due to the underlying complex chemistry.⁶⁵ Product characteristics depend not only on the composition of the feed, but also on the operating conditions and the selected catalyst. For example, even when starting from a single molecule (or two stereoisomers in the case of decalin), a complex mixture of ca. 200 hydrocarbons is formed due to the variety of possible reactions at metal and acid sites.¹¹¹ In this context, to gain fundamental insight into the mechanism of target reactions, the systems must be simplified, and hence model substances are commonly employed in SRO reactions. As discussed earlier, C–C bond scission without hydrogenation is endothermic, and it is the hydrogenation step that makes the overall SRO reaction mildly exothermic and thermodynamically feasible at low temperature.⁷² Product distributions can thus be controlled by varying the reaction temperature to shift

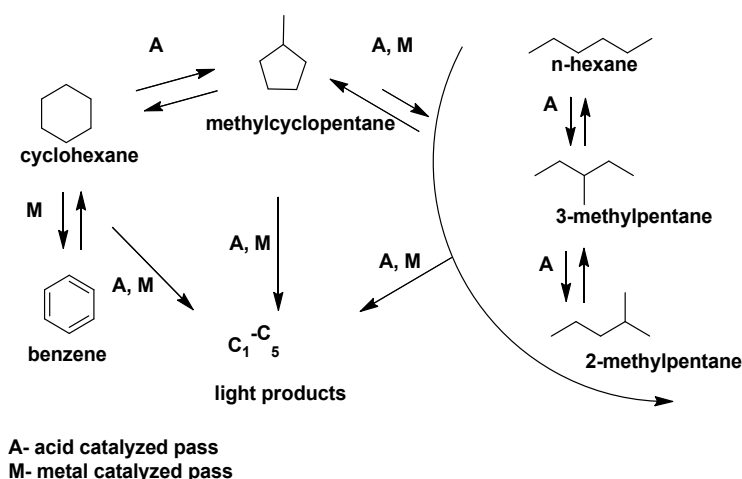
equilibria between different pathways.¹¹² The following sub-sections describe SRO mechanisms for mono- and bi-cyclic structures comprising five and six membered rings.

3.1 SRO of monocyclic compounds

Various noble and transition metals catalysts on supports including MCM-41, WO₃, USY, HZSM-5, Al₂O₃, SiO₂, SiO₂-Al₂O₃ and TiO₂ are reported to catalyse the conversion of monocyclic molecules such as MCP and MCH into C₆ and C₇ alkanes, respectively, although selectivity towards paraffins with a smaller number of branches (high CN) is generally poor.

3.1.1. SRO of MCP

The conversion of MCP over metal-supported catalysts generally produces three types of products, including ring enlargement (cyclohexane and benzene), ring cracking (C₁-C₅ light products), and ring opening (2-methylpentane (2-MP), 3-methylpentane (3-MP), and n-hexane (n-H)).¹¹³ MCP conversion and product selectivity depends on the hydrogenolysis metal employed, the support acidity and reaction temperature. The general scheme for MCP conversion over a metal-supported catalyst is shown in **Scheme 5**.¹¹⁴ Endo C-C bond cleavage of MCP forms the major RO products (n-H, 2-MP, and 3-MP), and from a CN point of view, n-hexane is preferred due to its higher CN (45) when compared to 2-MP (CN=33) and 3-MP (CN=30).



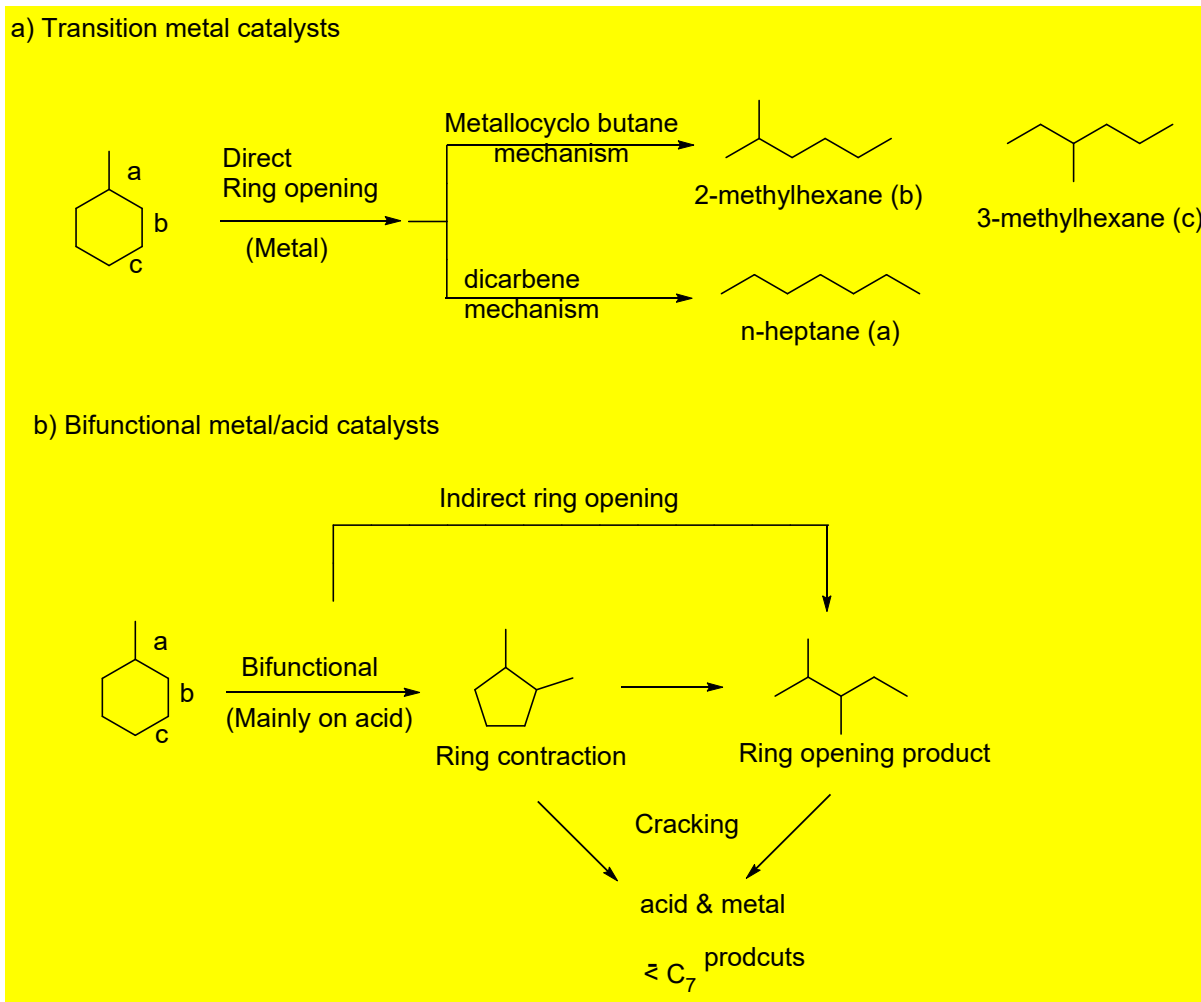
Scheme 5: Ring opening of MCP by hydrogenation, isomerisation and hydrogenolysis over solid acid supported transition metal catalyst. Reproduced with permission from Ref¹¹⁴.

Bifunctional catalysts employed in SRO of MCP include Pt/mordenite,¹⁰² Pt/KLT¹¹⁵, Ir/USY,¹¹⁶ Ir/MoO₂,¹¹⁷ Pt-Ir/MoO₂¹¹⁷ and Rh/HY.⁸⁷ In addition to the hydrogenolysis character of metal, the acidic properties of the support significantly affect the catalyst selectivity and mechanism of MCP ring opening.¹¹⁸ Generally, transition metals favour 2-MP and 3-MP. The most common statistical distributions are 2:2:1

(2-MP:n-H:3-MP) or 2:1 (2-MP:3-MP) respectively for the non-selective or selective hydrogenolysis mechanism. For bifunctional metal/solid acid catalysts, ring opening may occur on both metal and acid sites, producing a similar statistical distribution of ring-opened alkanes, but can also isomerise MCP which (at low H₂ pressure and high temperature) may dehydrogenate to benzene. The latter ring enlargement (RE) can also occur when noble metals are located inside the channels of zeolite supports, with adduct sites at the interface between the metal and support proposed to catalyse isomerisation. Ring enlargement occurs at adduct sites without surface migration of the activated reactant and intermediates. For example, Jacobs et al.¹¹⁹ reported that Pt-zeolite adduct sites could drive benzene formation via acid catalysed isomerisation and metal catalysed aromatisation (shown in **Scheme 5**). However, excess surface acidity favoured light alkane products due to preferential cracking. Thus, the ratio of 2-MP:3-MP and n-H:2-MP formed during MCP conversion is influenced by the support acidity and morphology,¹¹⁸ the presence of adduct sites at the perimeter of metal NPs,¹²⁰ and metal-support interactions.

3.1.2 SRO of MCH

MCH conversion is more complex than that of MCP, due to additional reaction pathways leading to ring opening (RO), ring enlargement (RE), ring contraction (RC), and cracking product (CP) formation.¹²¹ Akin to MCP, SRO of MCH can be direct or indirect, with the corresponding product distribution varying with catalyst.⁹³ According to **Scheme 6**, C-C bond cleavage in MCH can occur at three positions: a, b and c, and can be classified as direct ring opening (as for transition metal catalysts) or indirect ring opening (as for bifunctional metal/acid catalysts). In transition metal catalysis (**Scheme 6a**), MCH ring opening follows two reaction pathways, described as the dicarbene and metallocyclobutane mechanisms as discussed in **Section 2.2**.



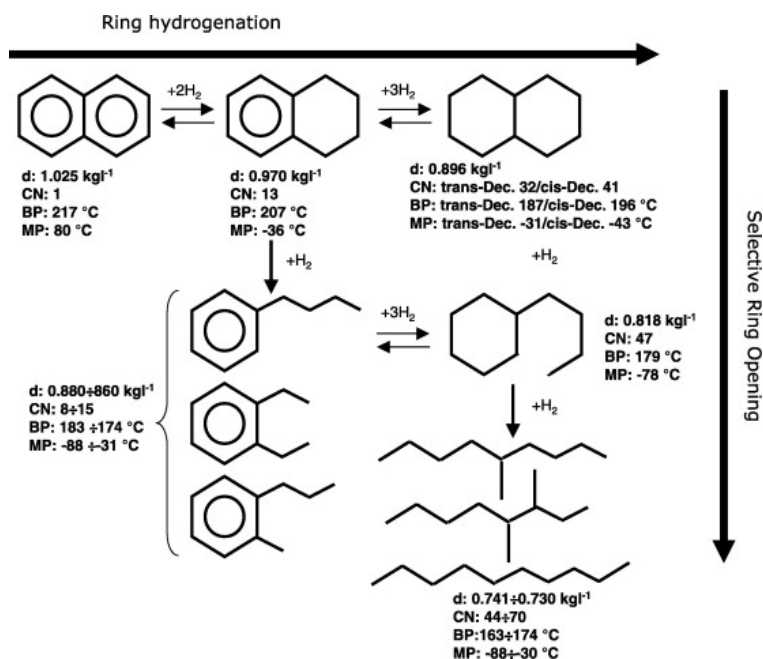
Scheme 6. Reaction pathways for the SRO of MCH via (a) direct ring opening on metal sites and (b) a bifunctional mechanism involving metal and acid sites. Reproduced with permission from Ref⁹³.

The dicarbene pathway results in cleavage of unsubstituted C-C bonds to produce 2-methylhexane (2-MH, CN=35) and 3-methylhexane (3-MH, CN=17), whereas the metalocyclobutane mechanism results in n-heptane (n-HP, CN=53) formation via cleavage of a substituted C-C bond.¹²² In contrast, the bifunctional mechanism (Scheme 6b) produces 2,3-dimethylpentane (CN=22) as a major ring opening product owing to ring contraction being favoured over acid sites.⁶⁶ However, keeping the selectivity of ring opening products high while simultaneously reducing the formation of undesired products, such as those from cracking and dehydrogenation, is challenging. As for MCP, supported noble metals are also active for MCH conversion, with the most investigated being Pt, Pd, Ru, Rh and Ir supported on Al₂O₃, SiO₂ and TiO₂.^{12, 75, 100, 121} Over bifunctional metal/acid catalysts, acid catalysed ring contraction of MCH is proposed to occur first, with the metal subsequently participating in hydrogenolysis to form ring opening products. Many studies focus on Ir due to its specificity for cleavage of endo C-C bonds in cycloalkanes, and it is widely reported that Ir catalysts favour opening of C5 versus C6 rings.^{12, 121} Comparison of RO of MCH over a bifunctional Ir/USY zeolite and Ir/SiO₂ at 275 °C and 2.8 MPa H₂ revealed higher MCH conversion and RO selectivity for the former. Although similar conversions were observed for MCH, RO selectivity was lower with RC products favoured. Bifunctional catalysts are thus the best candidates for ring opening

of C6 hydrocarbons.¹²³ Detailed discussions of different catalyst classes and their structure-activity relationships towards MCP and MCH ring opening are presented in **Section 4**.

3.2. SRO of bicyclic compounds

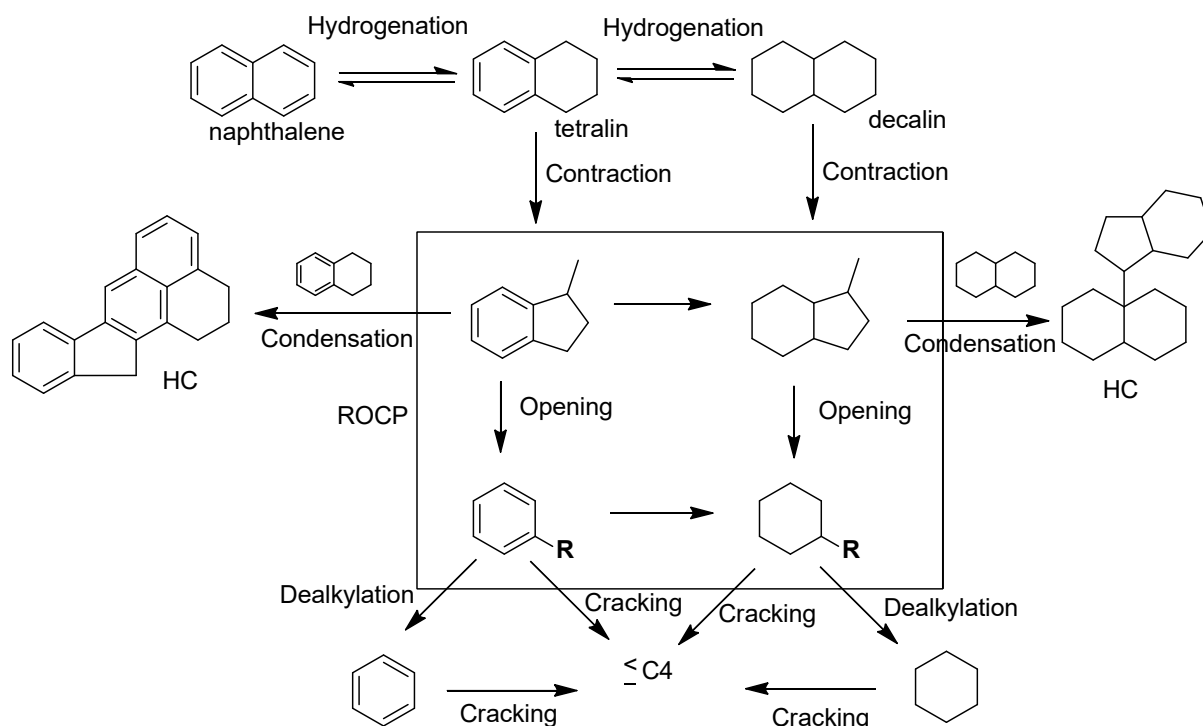
Substituted naphthalenes, tetralin and decalin are the major polycyclic constituents of the diesel fraction boiling-point range from oil refining and petrochemical plants,¹²⁴ and a significant component of waste plastic and tyre pyrolysis oils.¹²⁵ Typical polyaromatic concentrations are between 66-88 wt% for fossil derived oils (prior to hydrotreating) depending on the feedstock source,¹²⁶ and 10-30 wt% for plastic derived pyrolysis oil.¹²⁵ LCO from fluid catalytic cracking refineries has the highest polyaromatic content (88 wt%),⁵⁷ which cannot be easily blended into diesel, hence conversion of naphthalene into high-value products with a high CN is desirable.¹²⁷ Naphthalene is a representative component of real LCO feedstocks,¹²⁸ and its derivatives, such as tetralin and decalin, are important model compounds for studies of ring opening and resulting CN enhancement over supported metal catalysts.¹²⁹ The mechanism proposed for naphthalene (CN=1) conversion to n-decanes (CN=72-76) is shown in **Scheme 7**, wherein the first two reaction steps involve selective hydrogenation to tetralin and eventually decalin, and subsequent SRO to the n-butyl cyclohexane via endo C-C bond cleavage,⁶⁸ and potentially n-alkanes with a concomitant CN improvement (up to 72-76) at each stage. Ring hydrogenation and SRO also decrease fuel density from 1.025 to 0.730 g/cm³, which can increase engine performance and lower particulate matter (PM) emissions.¹⁰⁰ However, high H₂ inputs are required to obtaining n-alkanes with such high CNs; a 5:1 molar ratio of hydrogen:naphthalene is required to saturate the molecule (**Scheme 7**) increasing the CN to 36. Since a CN of 46-51 is acceptable for most diesel engines,¹³ complete hydrogenation of polycyclic aromatics is not essential, and hence their partial hydrogenation followed by SRO is an attractive strategy to improve CN while avoiding excessive H₂ costs. To this end, deeper insight is required into the various factors affecting the ring opening positions, e.g. C-C bond substitution (high CNs), catalyst selection (acid or metal or bifunctional), active metal particle size, feedstock and reaction conditions.^{12, 130} Tuning the product selectivity to achieve partial ring hydrogenation and SRO remains challenging, and the following section discusses mechanisms of ring opening of polycyclic aromatic and saturated hydrocarbons.



Scheme 7. Summary of naphthalene hydrogenation and SEO pathways to improve fuel density and CN. Reproduced with permission from Ref ¹⁰⁸.

3.2.1 SRO of naphthalene, tetralin, and decalin

Scheme 8 presents a plausible mechanism for the ring opening of naphthalene, tetralin, and decalin model compounds over zeolite supported transition metal catalysts.¹³¹ Reaction likely proceeds by hydrogenation of naphthalene to tetralin and decalin, followed by isomerisation and ring opening.^{73, 131} In this mechanism, acid catalysed contraction of a six-membered ring to a five-membered ring is a critical step, as opening five-membered rings is more facile.¹³² As shown in **Scheme 8**, the major products can be classified into four groups: isomerisation (or RC), RO, dehydrogenation (DH) and CP.¹³¹ Other reactions such as dealkylation and condensation are also observed, which can respectively result in an undesired carbon loss or the formation of polycyclic molecules, with the latter likely to yield hydrocarbons closer to lubricants than diesel (following hydrogenation and SRO). Note that linear paraffins are not observed for naphthalene SRO,¹²⁷ only alkyl-benzene and alkyl-cyclohexane, with subsequent zeolite promoted dealkylation at high temperature ($340 \text{ }^\circ\text{C}$) favouring cracking versus SRO as discussed earlier.



Scheme 8. Possible reaction network for SRO of naphthalene, tetralin and decalin over zeolite supported transition metal catalysts. Modified from Refs ^{127,131}

In contrast to MCP and MCH, the distribution of RO products from a two-membered ring is complex. However, some of the important ring opening products and open chain decanes (OCDs, also referred to as secondary ring opening products) form from decalin over transition metal and bifunctional metal/acid catalysts via dicarbene and metallocyclobutane reaction pathways as previously discussed. Products of decalin SRO over metal and metal/acid catalysts are shown in Table 1, which indicate that both catalyst classes can produce ring opening and OCD products with higher CN. Secondary ring-opened products obtained via the metallocyclobutane pathway have slightly better CNs than those obtained via the dicarbene pathway. Figure 6 plots the relationship between CN and specific volume for some of the major ring opening products, highlighting that the complete hydrogenation of naphthalene produces saturated cycloalkanes (CN=40) and a hydrocarbon mixture with a specific volume of ~1.1 mL/g, similar to the parent polyaromatic.^{13, 66} Although SRO can also produce ring opening molecules with higher CN (>50) and specific volumes (1.3-1.4 mL/g) of saturated hydrocarbons, reaction selectivity is critical since a significant loss in CN will occur if branched alkanes are produced during ring opening. Selective ring opening at substituted C–C bonds is therefore desirable to increase the specific volume without lowering CN, which in turn necessitates tuning of mono- and bifunctional catalysts to direct the desired reaction pathway.

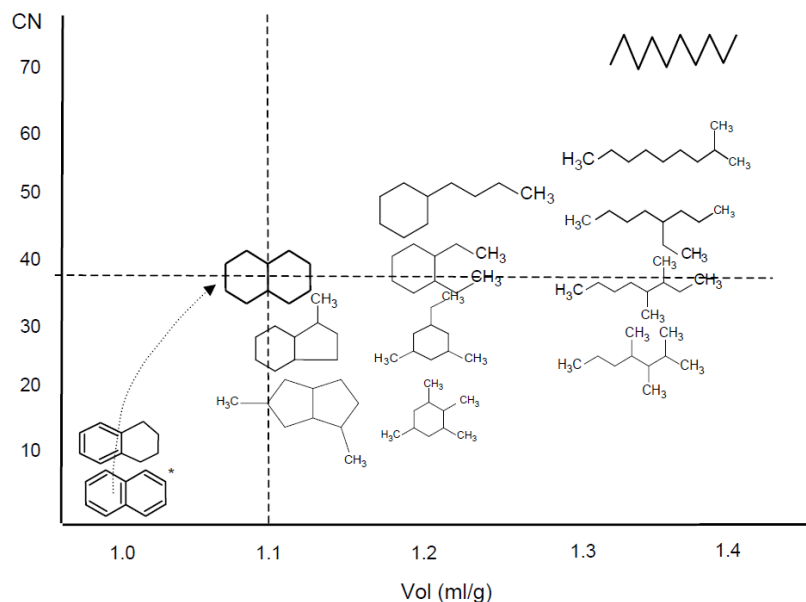
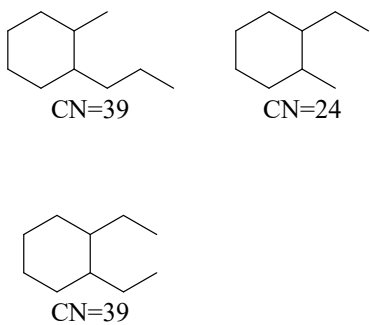
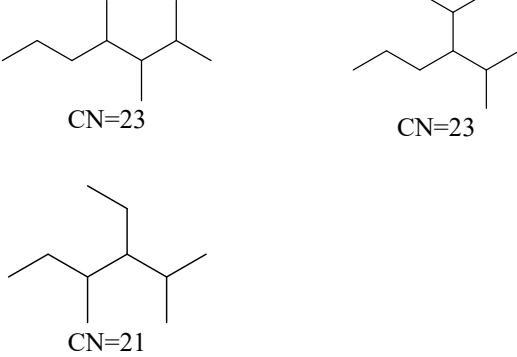
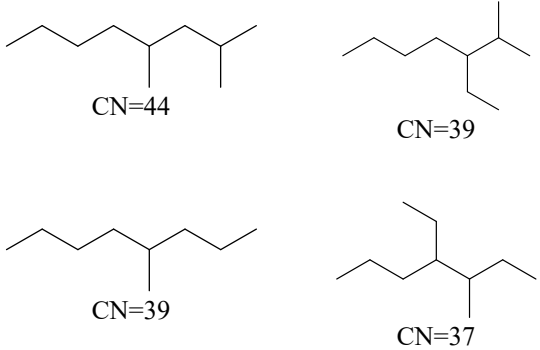
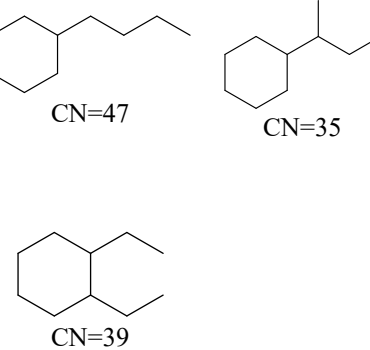
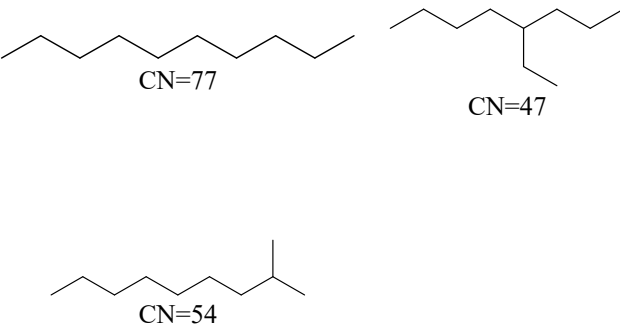
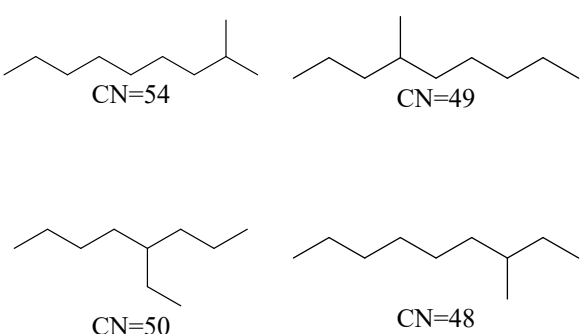


Figure 6. CN and specific volume of typical products formed from SRO of naphthalene. *Naphthalene specific volume is at 100 °C all others at 20 °C. Reproduced with permission from Ref⁶⁶

In summary, although monocyclics such as MCP and MCH readily form ring opening products over transition metal catalysts,¹³³ this is not the case for bicyclic six-membered rings (naphthalene and tetralin). High reaction temperatures and H₂ pressures can increase the conversion of polycyclic compounds over transition metal catalysts, this results in cracking at the expense of ring opening. For example, Pt-Rh/Al₂O₃ and Rh/Fe₂O₃-TiO₂ can achieve 80-90 % conversion during the ring opening of naphthalene (at >350 °C and >6 M Pa),^{131, 132, 134-137} but only deliver low ring opening yields (<2 %) due to extensive cracking and cross-coupling reactions between RO products. Decalin is more easily opened by transition metal catalysts due to the absence of aromaticity, however bifunctional metal/acid catalysts are preferred for SRO of naphthalene, tetralin, and decalin.¹³⁸ Acidic supports facilitate cracking, dealkylation and isomerisation, whereas transition metals promote hydrogenolysis and (de)hydrogenation. Optimal catalysts should balance both active sites to achieve high RO yields in two-membered rings at low reaction temperatures (<250 °C).

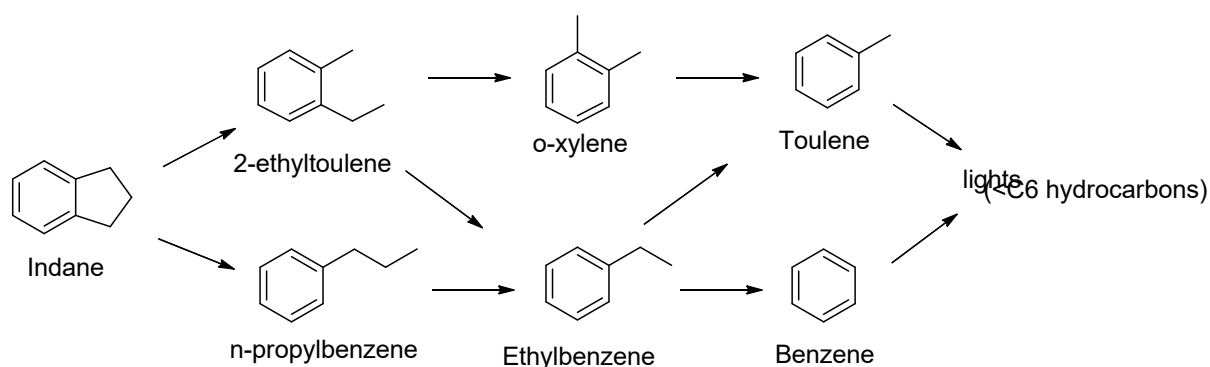
Ring opening of tetralin is easier than naphthalene due to the former's saturated ring. As shown in Scheme 8, there are two possible reaction pathways over bifunctional catalysts: partial hydrogenation of tetralin to octalin followed by further hydrogenation to decalin on the metal site, and subsequent ring contraction and isomerisation to saturated ring opening products; or formation of aromatic ring opening products by the direct protonation of tetralin, with ring contraction of the corresponding carbocation leading to methylindan (through deprotonation) and subsequent competitive β -scission resulting in n-alkylbenzene formation.

Table 1: CN of ring opening products and OCDs from metal- and /metal/acid catalysed ring opening of decalin. Reproduced with permission from Ref⁶⁶

Reaction type	Ring opening products	Open chain decanes	
	Metal or Metal/acid Catalysed	Metal catalysed	Metal/acid catalysed
Dicarbene mechanism (unsubstituted C-C bond cleavage)	 CN=39 CN=24 CN=39	 CN=23 CN=23 CN=21	 CN=44 CN=39 CN=39 CN=37
	 CN=47 CN=35 CN=39	 CN=77 CN=47 CN=54	 CN=54 CN=49 CN=50 CN=48

3.2.2. SRO of Indan

Indan is another model compound that is used to represent possible reaction intermediates during the hydrotreatment of bicyclic aromatic molecules over RO catalysts (via the isomerisation or ring contraction of tetralin to form methyl-substituted indan).¹⁰⁰ Indan comprises a C5 naphthenic ring adjacent to a benzene ring, with the C5 ring strain rendering it more susceptible to opening than C6 counterparts.¹⁰⁰ Consequently, indan model compounds are suitable for low pressure (1 bar) ring opening, in contrast to model compounds such as decalin or tetralin that require high H₂ pressures (20-40 bar).¹³⁹ Indan vapours may react with hydrogen over a metal ring opening catalyst in several ways (Scheme 9)⁶² to form 2-ethyltoluene (CN=12), n-propylbenzene (CN=16), o-xylene (CN=10), ethylbenzene (CN=7), toluene (CN=4), benzene (CN=0) and light hydrocarbons (e.g. methane).⁷¹ 2-ethyltoluene and n-propyl benzene are desired products, formed by cleavage of the five-membered rings to leave the molecular weight unchanged. However, dealkylation also results in formation of o-xylene, ethylbenzene, toluene, benzene and light hydrocarbons.



Scheme 9. Reaction network for low pressure indan SRO over transition metal catalysts. Reproduced with permission from Ref

62

In summary, the low reactivity of bicyclic molecules presents a challenge to supported metal catalysts. Bifunctional catalysts offer increased activity through metal-acid co-operativity, however low operating temperatures (<250 °C) are necessary to minimise cracking. Structure-activity relationships are critically discussed in the next section.

4. SRO catalysts

4.1 Transition metal catalysts

Noble metals such as Pt, Ir, Ru, Rh and Pd are widely investigated for the SRO of monocyclic and bicyclic molecules due to their high hydrogenolysis activity. These metals are particularly effective for opening monocyclics, but less effective for opening bicyclic naphthene. Ring opening of such molecules has been studied for transition metals over supports including Al₂O₃, TiO₂ and SiO₂,^{12, 62, 140} with metal particle size and synergy between metals commonly explored as means to tune SRO selectivity. **Table 2** summarises the performance of mono- and bimetallic transition metal catalysts towards SRO of model mono- and polycyclic molecules.

4.1.1 Monometallic catalysts

Altering the size of metal nanoparticles is a common strategy to modify the performance of heterogeneous catalysts, and one which has been exploited in SRO of mono- and bicyclic molecules. Pt nanoparticles are of significant interest in the SRO of naphthenic molecules, being selective for breaking the endo C-C bond as shown in **Scheme 10**, however Pt can also catalyse hydrogenation during ring opening, and produce cracking products, and hence its properties require careful tuning to optimise ring opening.

In the 1980s, Kramer and co-workers published several papers on MCP ring opening over Pt/Al₂O₃, and Pt/SiO₂ catalysts,^{91, 120, 141} demonstrating that SRO of MCP is structure sensitive (**Table 2, entry 1**),^{91, 142} as summarised in **Scheme 10**, with both “selective” and “non-selective” pathways available. In the selective mechanism, C-C cleavage can occur between unsubstituted carbons ‘b’ and ‘c’, whereas the non-selective mechanism occurs through C-C bond breakage between substituted ‘a’ and unsubstituted ‘b’ or ‘c’ carbons. Pt particles <2 nm cleaved the C-C bond at substituted and unsubstituted C-C bonds via a non-selective mechanism. Low-coordinate surface atoms which dominate smaller NPs were proposed to bind C5 rings via a single metal atom via a π -coordinated intermediate, resulting in n-hexane, 2-MP and 3-MP products in a statistical distribution of 2:2:1.^{91, 120, 142, 143} The selective mechanism is dominant for larger (>2 nm) Pt particles, with reactants coordinating between unsubstituted carbons (b and c) to form a di-carbene intermediate bound to two metal atoms, favouring endocyclic C-C bond cleavage.⁹¹ Such a coordination geometry results in a predictable (and selective in the authors’ terminology) product distribution, dominated by 2-MP and 3-MP in a 2:1 molar ratio. The different reaction pathways reflect the orientation of adsorbed MCP, being tilted away from the metal surface for larger Pt NPs (di-carbene mode) and parallel to the surface for highly dispersed NPs (π -coordinated).¹²⁰ Note that a metallocyclobutane intermediate likely accounts for n-hexane formation over larger NPs at temperatures >400 °C or in the presence of an acidic supports.¹¹³

Table 2. Ring opening of **mono- and bicyclic** naphthenics over **transition** metal catalysts.

Entry	Catalyst	Catalyst properties	Feedstock	Reaction conditions	Conversion (%)	ROP selectivity (%)	Product distribution (%)	Ref.	
Monometallics									
1	Pt/Al ₂ O ₃	<2 nm	MCP	20 mg, 237 °C, 0.1 MPa H ₂	9	100	39 (2-MP); 14.8 (3-MP); 46.2 (n-H)	142	
		2-3 nm			9	100	61.4 (2-MP); 20.5 (3-MP); 18.1 (n-H)		
		>3 nm			9	100	71.9 (2-MP); 19.5 (3-MP); 8.6 (n-H)		
2	0.5Pt/γ-Al ₂ O ₃	0.5 wt% Pt, ~ 1 nm, 127 m ² g ⁻¹	MCP	200 mg, 220 °C, 0.1 MPa H ₂ , H ₂ /feed=6, Pre-reduction at 400 °C for 12 h	5	100	2.3 (2-MP); 1 (3-MP); 1.7 (n-H)	144	
3	0.3Pt/Al ₂ O ₃	0.3 wt% Pt, <2 nm	MCP	350 °C, 2.8 MPa H ₂ , 15 h ⁻¹ WHSV, H ₂ /feed=5	10.4	97	42 (2-MP); 17 (3-MP); 41 (n-H)	12	
4	Pt/γ-Al ₂ O ₃	1.3 nm, 75% Pt dispersion, 215 m ² g ⁻¹	MCP	500 mg, 400 °C, 2.85 MPa H ₂ , H ₂ /feed=7.5, 6-12 h ⁻¹ WHSV	50	100	45 (2-MP); 23 (3-MP); 32 (n-H)	133	
5	0.6Pt(0.46Cl)/Al ₂ O ₃	0.6 wt% Pt, 1.5 nm, 215 m ² g ⁻¹ , Lewis acidity of 283 μmol.g ⁻¹	MCP	400 °C, 2.85 MPa H ₂ , WHSV = 12 h ⁻¹ , H ₂ /feed = 7.5	56	100	45 (2-MP); 22 (3-MP); 33 (n-H)	145	
	b	0.6Pt(1.36Cl)/Al ₂ O ₃			0.6 wt% Pt, 1.5 nm, 215 m ² g ⁻¹ , Lewis acidity of 342 μmol.pyridine.g _{cat.} ⁻¹	50	100		45 (2-MP); 23 (3-MP); 32 (n-H)
6	1Pt/Al ₂ O ₃	1.02 wt% Pt, 0.91±0.03 nm, 86.1% dispersion, 105 m ² g ⁻¹	MCP	20 mg, 300 °C, H ₂ /feed = 3000, Pre-reduction at 450 °C for 1 h	1.6	100	36.3 (2-MP); 7.3 (3-MP); 56.4 (n-H)	146	
	b	9Pt/Al ₂ O ₃			9.25 wt% Pt, 2.37±0.07 nm, 47.7% dispersion, 105 m ² g ⁻¹	31.2	100		57 (2-MP); 20.3 (3-MP); 22.7 (n-H)
	c	21Pt/Al ₂ O ₃ -SiO ₂			21.3 wt% Pt, 2.41±0.06 nm, 46.8% dispersion; 105 m ² g ⁻¹	47.6	100		53.8 (2-MP); 20.7 (3-MP); 25.5 (n-H)
7	0.3Pt/SiO ₂	0.3wt% Pt, 1.4 nm, ~100 m ² g ⁻¹	MCP	150 mg, 280 °C, 2 MPa H ₂ , 30 h ⁻¹ WHSV, H ₂ /feed=20, Pre-reduction at 350 °C for 1 h	0.2	100	-	140	
8	0.94Pt/SiO ₂	0.94 wt% Pt, 3 nm, 285 m ² g ⁻¹	MCP	250 mg, 350 °C, 2 MPa H ₂ , 2 h ⁻¹ GHSV, H ₂ /feed=60, pre-reduction 450 °C for 3 h	1.5	92	-	114	
9	0.5Pt/TiO ₂	0.5wt% Pt, 1.2 nm, ~42 m ² g ⁻¹	MCP	200 mg, 260 °C, 0.1 MPa H ₂ , Pre-reduction at 500 °C for 12 h	9.9	-	4.5 (2-MP); 1.2 (3-MP); 4.2 (n-H)	147, 148	
10	0.5Pt/WO ₂	0.51 wt% Pt, <1nm, 2 m ² g ⁻¹	MCP	200 mg, 470 °C, 0.1 MPa H ₂ , Pre-reduction at 500 °C for 4 h	29	-	1.1 (2-MP); 0.1 (3-MP); 1.1 (n-H)	149	
11	1.4Pt/Al ₂ O ₃	1.4 wt% Pt, 1.2 nm, ~200 m ² g ⁻¹	MCH	300 °C, Prereduction 350 °C for 4 h	2	0	-	121	
12	0.5Pt/Al ₂ O ₃	0.5 wt% Pt, < 2nm	MCH	350 °C, 2.85 MPa H ₂ , 15 h ⁻¹ WHSV, H ₂ /feed=5	6.6	7	0.3 (2-MH); 0.1 (3-MH); 5.9 (n-H)	12	

13	Pt(0.46Cl)/Al ₂ O ₃	0.6 wt% Pt, 0.46 wt% Cl, ~215 m ² g ⁻¹ , 283 μmol.pyridine.g _{cat} ⁻¹ of acidity	MCH	350 °C, 3.95 MPa H ₂ , 2.1 h ⁻¹ WHSV, H ₂ /feed=8	7.1	50	-	145
14	0.9Ir/Al ₂ O ₃	0.9 wt% Ir, < 2nm	MCP	275 °C, 2.8 MPa H ₂ , 30 h ⁻¹ WHSV, H ₂ /feed=5	52	99	70 (2MP); 29 (3-MP); 1 (n-H)	12
15	Ir/γ-Al ₂ O ₃	0.6 wt% Pt, 1.1 nm, 215 m ² g ⁻¹ , 85% Ir dispersion	MCP	500 mg, 290 °C, 2.85 MPa H ₂ , H ₂ /feed=7.5, 6-12 h ⁻¹ WHSV	94	100	69 (2MP); 29 (3-MP); 3 (n-H)	133
16	0.5Ir/TiO ₂	0.5 wt% Ir, 1.3 nm, ~42 m ² g ⁻¹	MCP	200 mg, 260 °C, 0.1 MPa H ₂ , Pre-reduction at 500 °C for 12 h	100	3.5	1.7 (2MP); 1 (3-MP); 0.9 (n-H)	147, 148
17	0.3Ir/SiO ₂	0.3 wt% Ir, 2-5 nm	MCP	150 mg, 280 °C, 2 MPa H ₂ , 1 h ⁻¹ WHSV, H ₂ /feed=40, Pre-reduction at 350 °C for 1 h	10.5	98.6	70.3 (2MP); 28.1 (3-MP); 0.2 (n-H)	150
18	0.5Ir/γ-Al ₂ O ₃	0.5 wt% Ir, ~ 1nm, 128 m ² g ⁻¹	MCP	200 mg, 220 °C, 0.1 MPa H ₂ , Pre-reduction at 400 °C for 12 h	65.7	88.3	40.8 (2MP); 13.7 (3-MP); 13.6 (n-H)	144
19	0.5Ir/WO ₂	0.47 wt% Ir, <1nm, 2 m ² g ⁻¹	MCP	200 mg, 340 °C, 0.1 MPa H ₂ , Pre-reduction at 500 °C for 4 h	2.4	73	1.4 (2MP); 0.1 (3-MP); 1.1 (n-H)	149
20	0.3Ir//Al ₂ O ₃	0.3 wt% Ir, 1.3 nm, ~200 m ² g ⁻¹	MCH	220 °C, Prereduction 350 °C for 4 h	10	-	-	121
21	0.9Ir/Al ₂ O ₃	0.9 wt% Ir, < 2nm	MCH	275 °C, 2.85 MPa H ₂ , 30 h ⁻¹ WHSV, H ₂ /feed=5	14.5	87	37 (2-MH); 58 (3-MH); 5 (n-HP)	12
22	1Ir/SiO ₂	1 wt% Ir, 7.4 nm, 0.55 μmol.ammonia.g _{cat} ⁻¹ of acidity	MCH	320 °C, 3.5 MPa H ₂ , 0.2 h ⁻¹ WHSV, H ₂ /feed=30	36	62	-	92
	1Ir-2K/SiO ₂	1 wt% Ir, 2.1 atoms Knm ⁻² of SiO ₂ , 2 nm, 1.8 μmol.ammonia.g _{cat} ⁻¹ of acidity	MCH	Pre-reduction at 450 °C for 2 h	24	82	-	
23	Ir/Al ₂ O ₃	1.8 wt% Ir, < 2 nm, 155 m ² g ⁻¹	MCH	350 °C, 5 MPa H ₂ , 0.2 h ⁻¹ WHSV, H ₂ /feed=24, Pre-reduction at 350 °C for 1 h	79	55	-	75, 76
24	0.9Ir/γ-Al ₂ O ₃	0.9 wt% Ir, < 2 nm, 250 m ² g ⁻¹	1,2 DMCH	320 °C, 3.54 MPa H ₂ , 0.15 h ⁻¹ WHSV, H ₂ /feed=30	80	45	-	89
			1,3 DMCH		90	44	-	
25	0.9Ir/Al ₂ O ₃	0.9 wt% Ir, < 2 nm	Decalin	275 °C, 3.54 MPa H ₂ , 1.6 h ⁻¹ WHSV, H ₂ /feed=5	4.4	4	-	12
26	Ir/Al ₂ O ₃	1.8 wt% Ir, 1.4 nm, 155 m ² g ⁻¹	Decalin	500 mg, 350 °C, 5 MPa H ₂ , 1 h ⁻¹ WHSV, H ₂ /feed=50, Pre-reduction at 350 °C for 1 h	11	89	-	76
27	Ir/Nb ₂ O ₅	0.3 wt% Ir, 74 m ² g ⁻¹ , 4.4±2.0 nm, 21% metal dispersion, 80 m ² g ⁻¹ . Total acidity of 260 μmol.ammonia.g _{cat} ⁻¹	Decalin	1000 mg, 350 °C, 3 MPa H ₂ , 4.5 h ⁻¹ WHSV, H ₂ /feed=50, Pre-reduction at 500 °C for 4 h	40	42	42 (RO); 31 (RC); 19 (DH); 15 (CP)	151
28	2wt%Ir/boehmite	2 wt% Ir, < 2 nm, 370 m ² g ⁻¹	Indan	300 mg, 325 °C, 0.1 MPa H ₂ , 1.4 h ⁻¹ WHSV, H ₂ /feed=63, Pre-reduction at 450 °C for 1 h	79	68	61 (2-ET); 7 (n-PB); 32 (OP)	152

29	2wt%Ir/CeO ₂	2 wt% Ir, 1.1 nm, 137 m ² g ⁻¹	Indan	325 °C, 0.1 MPa H ₂ , 2.7 h ⁻¹ WHSV, H ₂ /feed=63, Pre-reduction at 400 °C for 1 h	58	77	67 (2-ET);10 (n-PB); 33 (OP)	100
30	Ir/γ-Al ₂ O ₃	1.6±0.2 nm, Pd/Ir (0/0.178) wt%, 155 m ² g ⁻¹	Indan	336 °C, 0.1 MPa H ₂ , 2.7 h ⁻¹ WHSV, H ₂ /feed=4800, Pre-reduction at 359 °C for 1 h	99	12	11 (2-ET);1 (n-PB); 88 (OP)	153
31	Rh/γ-Al ₂ O ₃	0.6 wt% Rh, 215 m ² g ⁻¹ , 56% Rh dispersion, 1.5 nm	MCP	500 mg, 300 °C, 2.85 MPa H ₂ , H ₂ /feed=7.5, 6-12 h ⁻¹ WHSV	94	100	61 (2MP); 32 (3-MP); 7 (n-H)	133
32	Rh/SiO ₂	5 wt% Rh, Si/Al=2.6, ~ 4 nm	MCP	200 mg, 300 °C, H ₂ /feed=18, pre-reduction at 400 °C for 2 h	79.1	94.2	59.4 (2MP); 26 (3-MP); 2.6 (n-H)	87
33	Ru/γ-Al ₂ O ₃	0.6 wt% Ru, 215 m ² g ⁻¹ , 41% Ru dispersion, 2 nm	MCP	500 mg, 300 °C, 2.85 MPa H ₂ , H ₂ /feed=7.5, 6-12 h ⁻¹ WHSV	75	100	65 (2MP); 33 (3-MP); 2 (n-H)	133
34	Re/γ-Al ₂ O ₃	0.6 wt% Re, 215 m ² g ⁻¹ , 30% Re dispersion, 3.1 nm	MCP	500 mg, 300 °C, 2.85 MPa H ₂ , H ₂ /feed=7.5, 6-12 h ⁻¹ WHSV	36	100	51 (2MP); 35 (3-MP); 14 (n-H)	133
35	0.97Ru/Al ₂ O ₃	0.97 wt% Ru, 1.2 nm, ~200 m ² g ⁻¹	MCH	227 °C, Prereduction at 350 °C for 4 h	46	45	-	121
36	1.5Ru/SiO ₂	1.5 wt% Ru, 1-2 nm	MCH	275 °C, 2.85 MPa H ₂ , 30 h ⁻¹ WHSV, H ₂ /feed=5	52.9	65	-	12
37	Pd/γ-Al ₂ O ₃	2.3±0.4 nm, Pd/Ir (0.16/0) wt%, 155 m ² g ⁻¹	Indan	336 °C, 0.1 MPa H ₂ , 2.7 h ⁻¹ WHSV, H ₂ /feed=4800, Pre-reduction at 359 °C for 1 h	1	0	-	153
38	Ru/γ-Al ₂ O ₃	0.16 wt% Ru, 2.3±0.4 nm, 155 m ² g ⁻¹	Indan	336 °C, 0.1 MPa H ₂ , 2.7 h ⁻¹ WHSV, H ₂ /feed=4800, Pre-reduction at 359 °C for 1 h	51	9	8 (2-ET);1 (n-PB); 91 (OP)	154
39	30Ni/Al ₂ O ₃	30 wt% Ni, 227 m ² g ⁻¹	MCP	300 °C, 1 MPa H ₂ , 1.2 h ⁻¹ , H ₂ /feed=33; Pre-reduction at 450 °C for 12 h	34	100	23 (2MP);20 (3-MP); 57 (n-H)	155
40	60Ni/SiO ₂	60 wt% Ni, 286 m ² g ⁻¹	MCP	300 °C, 3 MPa H ₂ , 1.8 h ⁻¹ WHSV, H ₂ /feed=40, Pre-reduction at 350 °C for 2 h	82.6	84.3	48 (2MP); 16 (3-MP); 6 (n-H)	156
41	15Ni/Al ₂ O ₃	15 wt% Ni, 155 m ² g ⁻¹	MCH	275 °C, 2.85 MPa H ₂ , 30 h ⁻¹ WHSV, H ₂ /feed=5	2.3	100	-	12
42	60Ni/SiO ₂	60 wt% Ni, 176 m ² g ⁻¹ , 92 μmol.ammonia.g ⁻¹ of acidity	MCH	500 mg, 300 °C, 3 MPa H ₂ , 1.8 h ⁻¹ WHSV, H ₂ /feed=40, Pre-reduction at 260 °C for 1 h	82.6	100	-	156
43	Ni/γ-Al ₂ O ₃	Up to 50 nm, 155 m ² g ⁻¹	Indan	336 °C, 0.1 MPa H ₂ , 2.7 h ⁻¹ WHSV, H ₂ /feed=1500, Pre-reduction at 359 °C for 1 h	<1	-	-	94
Bimetallic or trimetallics								
44	0.25Pt-0.25Ir/γ-Al ₂ O ₃	0.25 wt% Pt, 0.25 wt% Ir, 124 m ² g ⁻¹ , ~ 1 nm	MCP	200 mg, 220 °C, 0.1 MPa H ₂ , Pre-reduction at 400 °C for 12 h	29	100	24 (2MP); 2 (3-MP); 4 (n-H)	144
45	0.25Pt-0.25Ir/TiO ₂	0.25 wt% Pt, 0.25 wt% Ir, ~42 m ² g ⁻¹	MCP	200 mg, 260 °C, 0.1 MPa H ₂ , Pre-reduction at 500 °C for 12 h	88.9	80.6	46 (2MP); 17 (3-MP); 10 (n-H)	147, 148
46	0.25Pt-0.25Ir/WO ₂	0.25 wt% Pt and 0.23 wt. % Ir, <1nm, 2 m ² g ⁻¹	MCP	200 mg, 470 °C, 0.1 MPa H ₂ , Pre-reduction at 500 °C for 4 h	32.7	11.9	3 (2MP); 0.4 (3-MP); 1.2 (n-H)	149

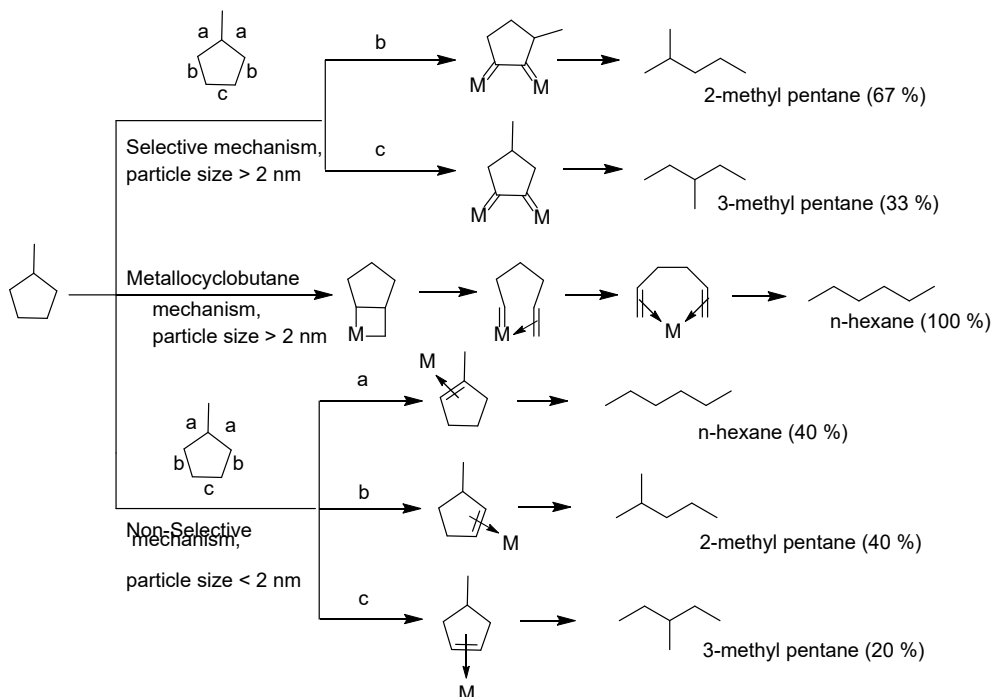
47	0.3Ir-10Co/SiO ₂	0.27 wt% Ir, 9.9 wt% Co, 3.4±0.5 nm, 55 H ₂ desorption/μmol.g _{cat} ⁻¹ , ~100 m ² g ⁻¹	MCP	150 mg, 280 °C, 2 MPa H ₂ , 1 h ⁻¹ WHSV, H ₂ /feed=40, Pre-reduction at 350 °C for 1 h	21.9	76.9	48 (2MP); 28 (3-MP); 3 (n-H)	150
48	Ir-10Co/SiO ₂	0.98 wt% Ir, 9.9 wt% Co, 3.2±0.5 nm, ~100 m ² g ⁻¹	MCP		12.7	79.8	48 (2MP); 29 (3-MP); 3 (n-H)	
49	0.2Pt-0.3Ir-10Co/SiO ₂	0.19 wt% Pt, 0.3 wt% Ir, 9.8 wt% Co, 3.6±0.7 nm, 68.4 H ₂ desorption/μmol.g _{cat} ⁻¹ , ~100 m ² g ⁻¹	MCP	150 mg, 280 °C, 2 MPa H ₂ , 30 h ⁻¹ WHSV, H ₂ /feed=20, Pre-reduction at 350 °C for 1 h	35	75.8	48 (2MP); 27 (3-MP); 3 (n-H)	140
	0.2Pt-10Co/SiO ₂	0.21 wt% Pt, 10.5 wt% Co, 3.2±0.6 nm, 58.2 H ₂ desorption/μmol.g _{cat} ⁻¹ , ~100 m ² g ⁻¹	MCP		2	76.9	43.4 (2MP); 29.8(3-MP); 4(n-H)	
	0.3Ir-10Co/SiO ₂	0.27 wt% Ir, 9.9 wt% Co, 3.4±0.5 nm, 55 H ₂ desorption/μmol.g _{cat} ⁻¹ , ~100 m ² g ⁻¹	MCP		4.5	76.5	42.8 (2MP); 31 (3-MP); 4 (n-H)	
50	Ir-Ni/Al ₂ O ₃	0.3wt% Ni and 0.9wt% Ir	MCH	330 °C, 3.54 MPa H ₂ , H ₂ /feed=30	28	70	-	93
51	Pt-Mg-Ir/Al ₂ O ₃	1 wt% Pt, 1 wt% Mg, 0.1 wt% Ir, 155 m ² g ⁻¹	Decalin	1000 mg, 350 °C, 3 MPa H ₂ , 4.5 h ⁻¹ WHSV, H ₂ /feed=30, Pre-reduction at 500 °C for 1 h	1.5	18	18 (RO)	157
52	Pt-Na-Ir/Al ₂ O ₃	1 wt% Pt, 2 wt% Ir, 0.5 wt% Na, 155 m ² g ⁻¹	Decalin	1000 mg, 325 °C, 3 MPa H ₂ , 4.5 h ⁻¹ WHSV, H ₂ /feed=30, Pre-reduction at 500 °C for 4 h	30.4	45	45 (RO)	158
53	Pt@Ru/SiO ₂	3.3 wt% Pt, 1.7 wt% Ru, 22.1±4.4 nm Pt, 12.9±2.6 nm Ru, 176 m ² g ⁻¹	Decalin	1000 mg, 300 °C, 8.1 MPa H ₂ , 1.8 h ⁻¹ WHSV, H ₂ /feed=49, Pre-reduction at 450 °C for 1 h	61	26	26 (RO)	159
54	2wt%Pt ₂₅ Ir ₇₅ /boehmite	0.2 wt% Pt, 1.8 wt% Ir, 370 m ² g ⁻¹	Indan	300 mg, 325 °C, 0.1 MPa H ₂ , 1.4 h ⁻¹ WHSV, H ₂ /feed=63, Pre-reduction at 450 °C for 1 h	40	80	72 (2-ET); 8 (n-PB); 20 (OP)	152
55	2wt%Pt ₅ Ir ₉₅ /CeO ₂	0.1 wt% Pt, 1.9wt% Ir, 1.5 nm, 137 m ² g ⁻¹	Indan	325 °C, 0.1 MPa H ₂ , 2.7 h ⁻¹ WHSV, H ₂ /feed=63, Pre-reduction at 400 °C for 1 h	56	79	68 (2-ET); 11 (n-PB); 21 (OP)	100
56	Pd@Ir/γ-Al ₂ O ₃	2.7±0.5 nm, Pd/Ir (0.269/0.385) wt%, 155 m ² g ⁻¹	Indan	336 °C, 0.1 MPa H ₂ , 2.7 h ⁻¹ WHSV, H ₂ /feed=4800, Pre-reduction at 359 °C for 1 h	91	47	41 (2-ET); 6 (n-PB); 52 (OP)	153
	Industrial Pt-Ir/γ-Al ₂ O ₃	0.2 wt% Pt, 1.8 wt% Ir, < 2nm, 155 m ² g ⁻¹	Indan		62	30	26 (2-ET);4 (n-PB); 70 (OP)	
57	Ru ₁ Ir ₄ /γ-Al ₂ O ₃	0.02 wt% Ru, 0.16 wt% Ir, 1.9±0.3 nm, 155 m ² g ⁻¹	Indan	336 °C; 0.1 MPa H ₂ , 2.7 h ⁻¹ WHSV, H ₂ /feed=4800, Pre-reduction at 359 °C for 1 h	55	62	57 (2-ET); 5 (n-PB); 38 (OP)	154
58	Pd ₁ Ru ₄ /γ-Al ₂ O ₃	0.02 wt% Pd, 0.07 wt% Ru, 2.9±0.6 nm, 155 m ² g ⁻¹	Indan	350 °C, 0.1 MPa H ₂ , 2.7 h ⁻¹ WHSV, H ₂ /feed=1500, Pre-reduction at 359 °C for 1 h	27	64	59 (2-ET); 5 (n-PB); 34 (OP)	62
59	Ni@Ir/γ-Al ₂ O ₃	3.2±0.6 nm, 155 m ² g ⁻¹	Indan	336 °C; 0.1 MPa H ₂ , 2.7 h ⁻¹ WHSV, H ₂ /feed=1500, Pre-reduction at 359 °C for 1 h	64	60	51 (2-ET); 9 (n-PB); 40 (OP)	94
	Ni ₁ Ir ₁ /γ-Al ₂ O ₃	2.3±0.5 nm, 155 m ² g ⁻¹	Indan		-	81	64 (2-ET);17 (n-PB); 19 (OP)	

2-MP=2-methylpentane, 3-MP=3-methylpentane, n-H=n-hexane, 2-MH=2-methylhexane, 3-MH=3-methylhexane, n-HP=n-heptane, RO=Sum of all ring-opening products, RC=Ring contraction, DH=Dehydrogenation, CP=Cracking products, 2-ET=2-ethyl toluene, n-PB=n-propyl benzene

For MCP, ROP selectivity is the sum of 2-MP+3-MP+n-H; For MCH, ROP selectivity is the sum of 2-MH+3-MH+n-HP

For Indan, ROP selectivity is the sum of 2-ethyltoluene and n-propyl benzene

OP=Other products such as dealkylation products including o-xylene+ethylbenzene+toluene



Scheme 10. Proposed mechanisms for MCP hydrogenolysis over Pt/Al₂O₃ (values in parentheses represent the statistical product distribution).¹²⁰

Reported RO product distributions (**Table 2**) can be largely accounted for by the different pathways in **Scheme 10**. **Table 2 (Entry 1)** shows that 2-MP and 3-MP are the dominant ring opening products for Pt NPs >2 nm, and the n-hexane yield is enhanced for particles <2 nm.¹⁴² Selectivity towards n-hexane can be further enhanced by inducing metal-support interactions between <2 nm Pt particles and alumina. The resulting partial encapsulation of Pt NPs promotes adduct formation between reactive intermediates at the metal-support interface.¹²⁰ While similar effects can also be induced for Pt/SiO₂, the partially encapsulated domains are less stable than for Pt/Al₂O₃.⁹¹ Higher reaction temperatures enhance MCP conversion (**Table 2, Entry 1-4**) without significantly influencing the product distribution. A few studies have examined Cl doping of Pt/Al₂O₃ catalysts, however this had negligible impact on product distribution (**Table 2, Entry 2**), indicating that selectivity is predominantly governed by Pt particle size for neutral/weakly acidic supports.

Particle size effects on 2MP, 3MP and n-hexane (n-H) production during MCP ring opening were explored by Zhao et al. using first-principles calculations over flat Pt(111) and stepped Pt(211) surfaces as models for large and small NPs respectively.¹⁶⁰ Activation energies for C-C bond scission to form 2-MP and 3-MP over Pt(111) are lower than for C-C bond scission to form n-H (75 versus 116 kJ/mol). In contrast, the barrier for C-C cleavage to n-H drops to 94 kJ/mol over Pt(211) whereas that to 2-MP and 3-MP formation increases to 100 kJ/mol. Accordingly, smaller Pt NPs favour linear products with a higher

CN because the activation barrier to selective cleavage of 'b' and 'c' carbon bonds in **Figure 10** is disfavoured.

Support effects in Pt catalysed MCP ring opening have also been explored. SiO₂ and TiO₂ supported Pt NPs exhibit negligible conversions at 260-300 °C (**Table 2, Entry 7-9**),^{60, 147, 148} and only 1 % conversion was observed for 1 wt% Pt/Al₂O₃ (**Entry 6a**).¹⁴⁶ These findings suggest that support effects are negligible when particle sizes are < 2nm. However, for >2 nm Pt particles on alumina (**Entry 6b**) a 20-fold increase in MCP conversion is observed relative on silica (**Entry 8**), evidencing some influence of the support. To further understand particle size and support effects, Le Valant et al. used Al₂O₃ and Al₂O₃-SiO₂ (Al₂O₃:SiO₂=4.6) supported Pt NPs with loadings of 1-21 wt% for SRO of MCP (**Table 2, Entry 6**).¹⁴⁶ MCP conversions followed the order: 21wt% Pt(2.4 nm)/Al₂O₃-SiO₂ (47.6%) > 9wt% Pt(2.4 nm)/Al₂O₃ (31.2%) > 10wt% Pt(1.9 nm)/Al₂O₃-SiO₂ (28%) > 5wt% Pt(1 nm)/Al₂O₃-SiO₂ (12.9) > 1wt% Pt(1.2 nm)/Al₂O₃ (2.8%) > 11wt% Pt(1 nm)/Al₂O₃ (1.9%) > 1wt% Pt(0.9 nm)/Al₂O₃ (1.6%). These results demonstrate a strong Pt structure sensitivity for MCP conversion, which is favoured over larger NPs. Significant support effects were only observed for small (<1.9 nm) NPs, with Pt on Al₂O₃-SiO₂ more active than when dispersed on silica; this can be rationalised by the larger metal-support interface for smaller NPs. The corresponding RO product distribution was also structure sensitive (**Figure 7a-b**), with smaller Pt particle favouring the non-selective mechanism and concomitant n-H production, consistent with the preceding first-principles calculations for different Pt facets. The percentage of Pt atoms present in different surface coordination environments for various fcc truncated octahedral NPs^{161, 162} (from the Van Hardeveld and Hartog model) was correlated with the experimentally observed ROP distribution from MCP (**Figure 7c**). The Pt NP size (d) was estimated from the mid-sphere diameters (**Figure 7d**), and the resulting atomic distribution shown as a function of particle size in **Figure 7e** for particles up to 10 nm. The greatest proportion of corner atoms are obtained for Pt particles <2 nm, and show an inverse relationship to the proportion of atoms in (111) faces. The proportion of surface atoms in edge sites increase to a maximum value of 33.2 % for d = 1.85 nm, before decreasing for larger particles. These trends in NP geometry mirror experimental results for MCP ring opening (**Figures 7e-f**), wherein low coordination corner atoms favour n-H formation and face and edge atoms favour 2-MP and 3-MP. As predicted by Zhao et al (**Figure 7g-h**),¹⁶⁰ n-hexane formation preferentially occurs at corner and (some) edge sites, whereas 2-MP and 3-MP are predominately formed on close-packed faces.

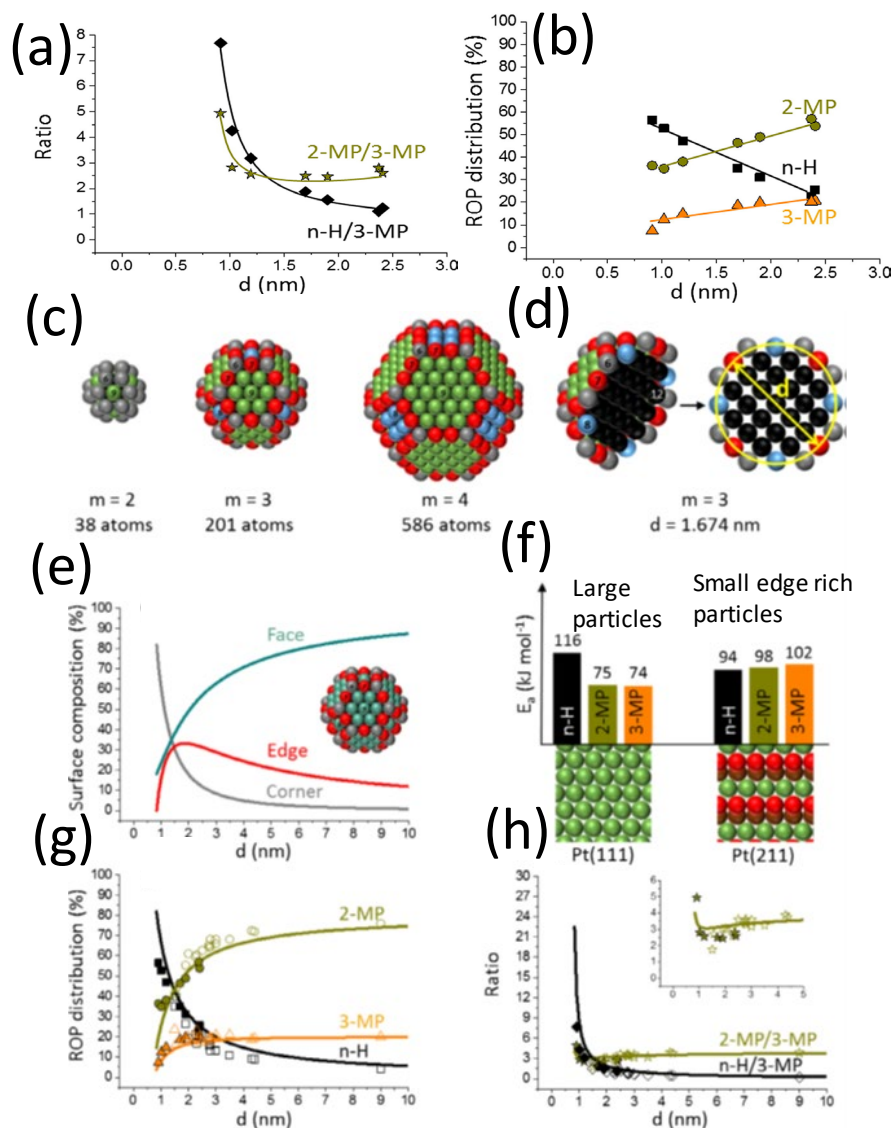


Figure 7. (a) ROP distribution, (b) and product ratio versus Pt particle size for the hydrogenolysis of MCP at 573 K, (c) ideal representations of perfect fcc truncated octahedra, and (d) corresponding particle size (denoted ‘d’ as shown for $m = 3$). Numbers shown on atoms, 6 (grey), 7 (red), 8 (blue), 9 (green), and 12 (black), represent respective coordination numbers for corner, edge, (100) and (111) facet, and bulk environments, respectively. (e) Evolution of calculated accessible surface composition versus Pt particle size. (f) Activation energies of the transition state for C–C scission in MCP ring opening reactions over Pt(111) and Pt(211) surfaces; green, brown and red atoms represent coordination numbers of 9, 10 and 7, respectively. (g) Calculated and observed ROP distribution, and (h) product ratios versus Pt particle size (full symbols represent experimental data and open symbols literature data, and solid lines represent statistical model calculations). Reproduced with permission from Refs ^{146, 160}.

Although Pt catalysts show promise for SRO of five-membered naphthenes, their reactivity towards 6-ring model compounds such as MCH, indan and decalin is promising. For example, while Pt/Al₂O₃ can ring-open MCP with 97-98 % selectivity to C₆ alkanes, it only exhibits 4–5 % selectivity (Table 2, entry 3 and 12) for ring opening of MCH to C₇ alkanes.¹² Similar observations (Table 2, entry 11 and 13) of low selectivity are attributed to dehydroaromatization, which is the dominant pathway during MCH ring opening at 300-350 °C.^{12, 121} When indan SRO was explored over 0.5 wt% Pt/Al₂O₃ in an atmospheric pulse reactor at 400 °C,¹⁶³ rapid catalyst deactivation and negligible indan conversion were observed.¹⁶³ Compared to five-membered cyclic molecules, ring opening of six membered bicyclics are scarcely

reported over Pt catalysts, due to their tendency to promote dehydrogenation and isomerisation pathways, and attendant poor activity and selectivity for RO products.

Iridium is also a promising candidate for SRO of mono- and bicyclic molecules. For example, Ir/Al₂O₃ exhibits 52 % MCP conversion and 52 % selectivity to ring opening products (**Table 2**), five times greater than for an analogous Pt (>2 nm)/Al₂O₃ catalyst and at a lower temperature (275 °C versus 350 °C for Pt). Ir (>2 nm)/Al₂O₃ catalysts follow the selective, dicarbene pathway (with cleavage at 'b' and 'c' bonds in **Scheme 10**), favouring the formation of 2-MP and 3-MP (**Table 2, Entry 14**), and again differing from Pt for which the non-selective mechanism is preferred (**Table 2, Entry 3**). These observations suggest that the Ir particle size may not affect the RO product distribution. Fogar and Anderson¹⁶⁴ and van Senden et al.¹⁶⁵ confirmed that SRO over Ir catalysts is structure insensitive, reporting 2-MP and 3-MP as the major products of MCP ring opening for Ir NPs between 1-20 nm. SRO of substituted cyclopentanes (**Figure 8**)^{12, 39} over Ir/Al₂O₃ also revealed a RO product distribution consistent with that predicted by the dicarbene intermediate mechanism.

Metal-support interactions can influence the reactivity of iridium, illustrated for MCP ring opening over Al₂O₃ and SiO₂ supported Ir NPs.¹⁴⁵ The activity of Ir/Al₂O₃ was nearly four times greater than Ir/SiO₂ at 225 °C, with the former also showing a greater yield of ring opening products (n-hexane), attributed to different SRO mechanisms over the different supports (**Table 2, Entry 14 and 17**).^{166,167} In the case of MCP SRO over Ir/MoO₂,¹¹⁷ low temperatures (220 °C) deliver a high 2-MP yield with a statistical distribution of 2-MP:3-MP:n-H (3.7:1:0.1) of ring opening products, which is higher than the expected statistical distribution of 2:1:2. However, Ir also promotes ring enlargement (RE) and thermodynamic cracking products at high temperatures (400 °C); the former due to the presence of electron deficient adduct sites at the Ir/MoO₂ interface which favour cyclohexane and benzene production, reducing the 2-MP yield (2-MP:3-MP=0.33:1). This differs from a classical bifunctional mechanism¹⁶⁸ wherein MCP isomerisation occurs at acidic sites on the support and reactive species then migrate to metal sites where ring opening occurs. In the proposed adduct mechanism, all reaction steps occur at a single site (where the metal NP perimeter contacts the support) thereby circumventing the requirement for surface diffusion of hydrocarbon species.

	Predicted "Dicarbene Mechanism"	Observed
	67	66
	33	34
	100	97
	100	98
	67	85
	33	15

Figure 8. Predicted and observed ring opening product distributions from isomeric C7 cyclopentanes over 0.9 wt% Ir/Al₂O₃. Reproduced with permission from Ref¹²

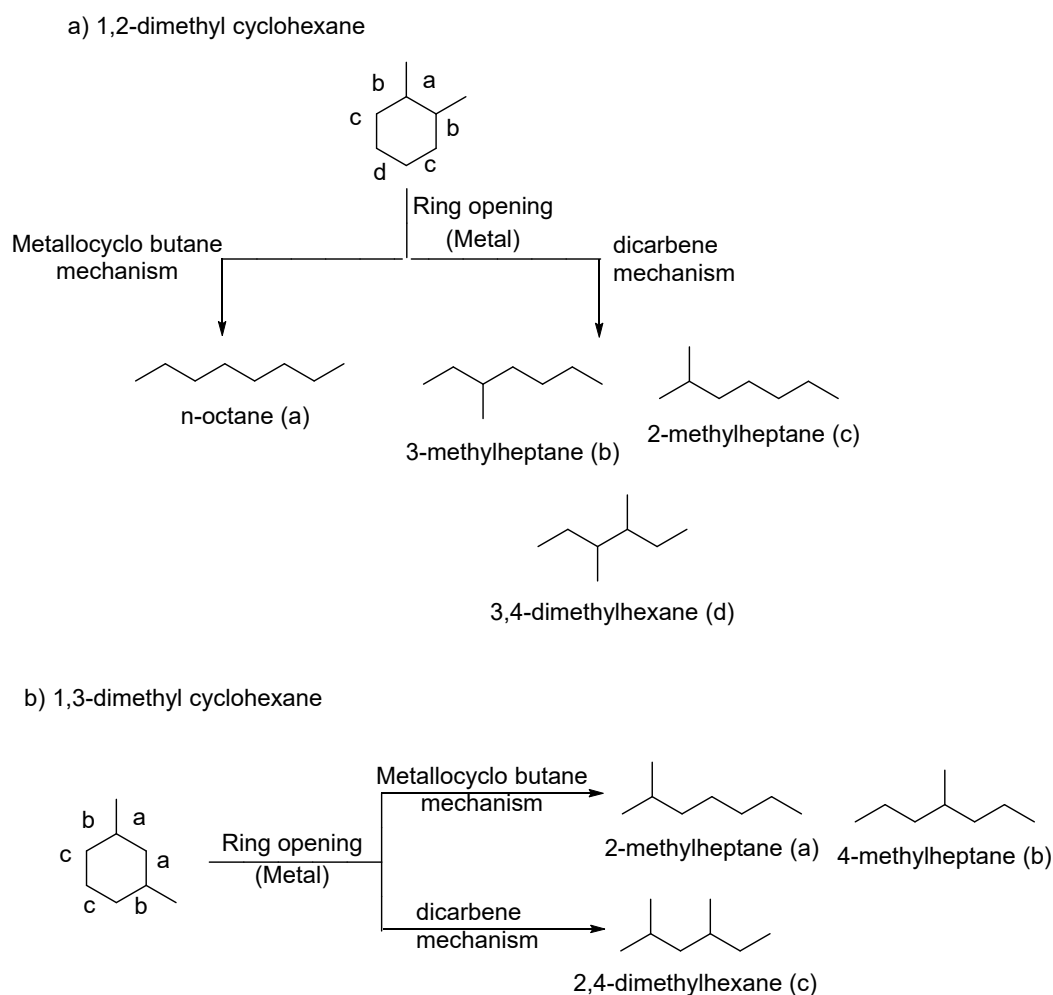
Ir is the only metal which displays a high RO selectivity for towards MCP (99 %) and MCH (87 %) (Table 2, Entries 14 and 21).¹² However, the RO product distribution is not statistical, with 2-MH and 3-MH formed in high proportions, e.g. for MCH over Ir/Al₂O₃ the 2-MH (37 %), 3-MH (58 %), and n-HP (5 %) products are completely different from the statistical distribution observed from MCP (Table 2, Entry 14). This is not entirely surprising, since planar adsorption of a cyclohexyl ring is not expected to be favourable.¹² Studies also indicate that SRO is sensitive to the substituents on cyclic reactants, with steric hindrance from alkyl substituents drastically lowering ring reactivity.¹⁶⁹ For substituted cyclohexanes over Ir/Al₂O₃, the RO selectivity follows the order benzyl (35 %) < methyl (87 %) < H (100 %).^{67, 169}

In common with the preceding trends for MCP, it is unsurprising that MCH conversion increases with reaction temperature over supported Ir catalysts. Piegsa et al. investigated MCH ring opening over Ir/Al₂O₃ in a fixed-bed reactor at temperatures between 220-350 °C.¹²² At low temperature (240 °C) MCH conversion was low (<10 %, Table 2, entry 20), but the selectivity towards 2-MH and 3-MH was 34 % and 54 %, respectively. Increasing the temperature to 300 °C increased MCH conversion (>95 %) at the expense of selectivity to both methylhexanes (which fell <5 %). Nevertheless, Ir is one of the most selective metals for MCH ring opening, even at low temperatures (<240 °C) which minimise competitive cracking.

Further studies highlight the impact of Ir loading on MCH conversion and ring opening. For Ir/Al₂O₃, conversion increased from 17 to 80 % as the metal loading increased from 0.5 to 2 wt%.⁷⁶ Initial rates of MCH SRO over Ir/Al₂O₃ catalysts were 0.03 mol.h⁻¹.kg⁻¹, 0.06 mol.h⁻¹.kg⁻¹ and 0.23 mol.h⁻¹.kg⁻¹ for respect catalysts possessing 0.6, 1.2 and 1.8 wt% Ir respectively. However, this higher activity simply reflects an

increase in the active metal surface area. Increasing Ir loading did not alter the RO product selectivity, which was attributed to the similar metal dispersions for all loadings, in accordance with the report of Walter et al.¹²¹

Although Ir can cleave unsubstituted C-C bonds in naphthenics via the dicarbene mechanism, this is not ideal for obtaining a high CN fuel (or blend) due to the associated formation of branched alkanes. Resasco and co-workers therefore investigated the effect of Al₂O₃, SiO₂ and TiO₂ supports on the cleavage of substituted C-C bonds in Ir catalysed 1,2 -DMCH and 1,3-DMCH⁸⁹ (at 320 °C, 3.54 MPa H₂ and a H₂:naphthenic ratio of 30, Table 2, Entry 24). Figure 9-b shows that alumina offered the increase in CN, with ΔCNs of 3.5 for 1,3-DMCH and 9.0 for 1,2-DMCH, presumably by enhancing the degree of substituted C-C bond cleavage via a metallocyclobutane intermediate.



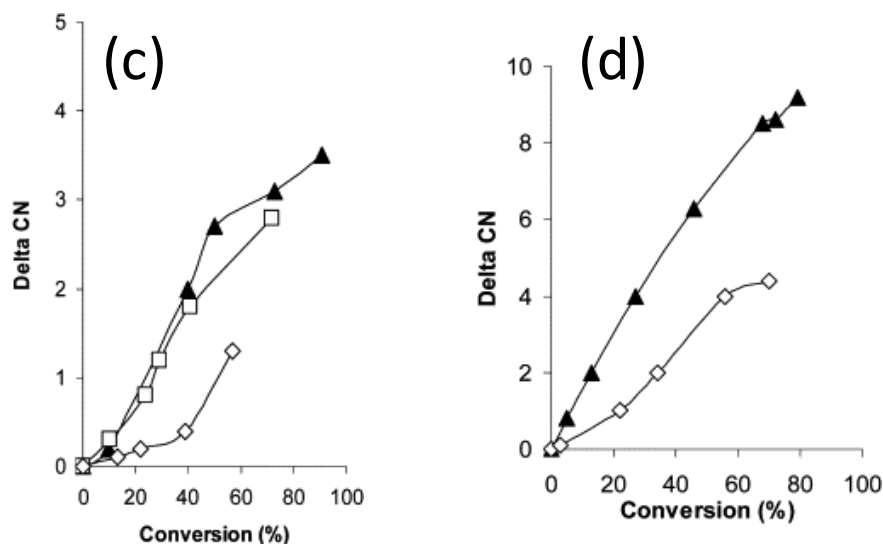


Figure 9. Possible reaction pathways for SRO of (a) 1,2-DMCH and (b) 1,3-DMCH, and experimentally observed increase in CN (Δ CN) for (c) 1,3-DMCH (d)1,2-DMCH over Ir catalysts (\blacktriangle Ir/Al₂O₃; \diamond Ir/SiO₂; \square Ir/TiO₂). Reproduced with permission from Ref⁸⁹.

Promotion of Ir/Al₂O₃ by K or Ni has also been investigated for SRO of 1,3-DMCH.⁹³ Potassium suppressed secondary hydrogenolysis without changing the ratio of substituted to unsubstituted ring opening products (Table 2, Entry 22a), whereas Ni suppressed substituted C-C bond cleavage and favoured branched products (akin to Ir/SiO₂) Formation of a metallocyclobutane intermediate, necessary for high n-alkane selectivity, is believed to occur on Ir sites at the Al₂O₃ boundary (via adduct formation). It is possible that adduct formation is hindered by surface Ni aluminate formed during catalyst calcination. In contrast, K doping of Ir/SiO₂⁹² appears to stabilise the metallocyclobutane intermediate thus favouring unbranched products (Table 2, Entry 22b).

Kinetic studies of SRO of MCH over Ir/Al₂O₃ have also probed the effect of Ir dispersion and H₂ pressure on hydrogenolysis of exo- versus endocyclic bonds.¹⁶⁹ Turnover frequencies (TOFs) for endo- and exocyclic C-C bond cleavage of MCH are shown in Figures 10a-b as a function of Ir dispersion (D). Exocyclic bond cleavage occurs through MCH demethylation, at a rate equal to the rate of cyclohexane (CH) production.⁶⁷ The TOF for endocyclic C-C bond cleavage is the difference between the overall TOF for MCH hydrogenolysis and that for exocyclic cleavage. As shown in Figure 10a, the TOF for endocyclic C-C bond cleavage initially decreases with falling Ir dispersion for average NP sizes spanning 1-2 nm (D >0.40), but increase dramatically for lower metal dispersion (D <0.30). In contrast, the TOF for exocyclic C-C bond cleavage (demethylation) increased continuously with falling Ir dispersion (D = 0.04–0.65), particularly for D <0.40 (Figure 10b). These observations of a pronounced structure sensitivity for MCH ring opening are distinct from MCP ring opening over Ir catalysts wherein demethylation was never observed.^{12, 65} Figure 10c-d highlight this structure sensitivity, with selectivity to ROPs (versus demethylation) increasing monotonically with Ir dispersion; endocyclic C-C bond cleavage to n-alkanes

with high CNs requires small Ir NPs. Isotope labelling studies (Figure 11)¹⁷⁰ revealed that either C–C bond cleavage or C–H(D) bond reformation may be rate-determining for ring opening, but that C–H(D) bond dissociation does not control the rate of C–C bond hydrogenolysis.

Ir catalysts exhibit superior activity for SRO of MCP and MCH compared to Pt, nevertheless Ir is still ineffective for opening 2+ring molecules like decalin under moderate conditions (e.g. 3.54 MPa H₂, LHSV = 1.6 and 275 °C). Only 4.4 % decalin conversion was observed over Ir/Al₂O₃ (Table 2, Entry 25) with trace OCDs formed,¹² despite the same catalyst exhibiting 68 % conversion of perhydroindan under similar conditions.¹² Contraction of six-membered to five-membered rings remains a key barrier to the activation of six member bicyclic feedstocks.

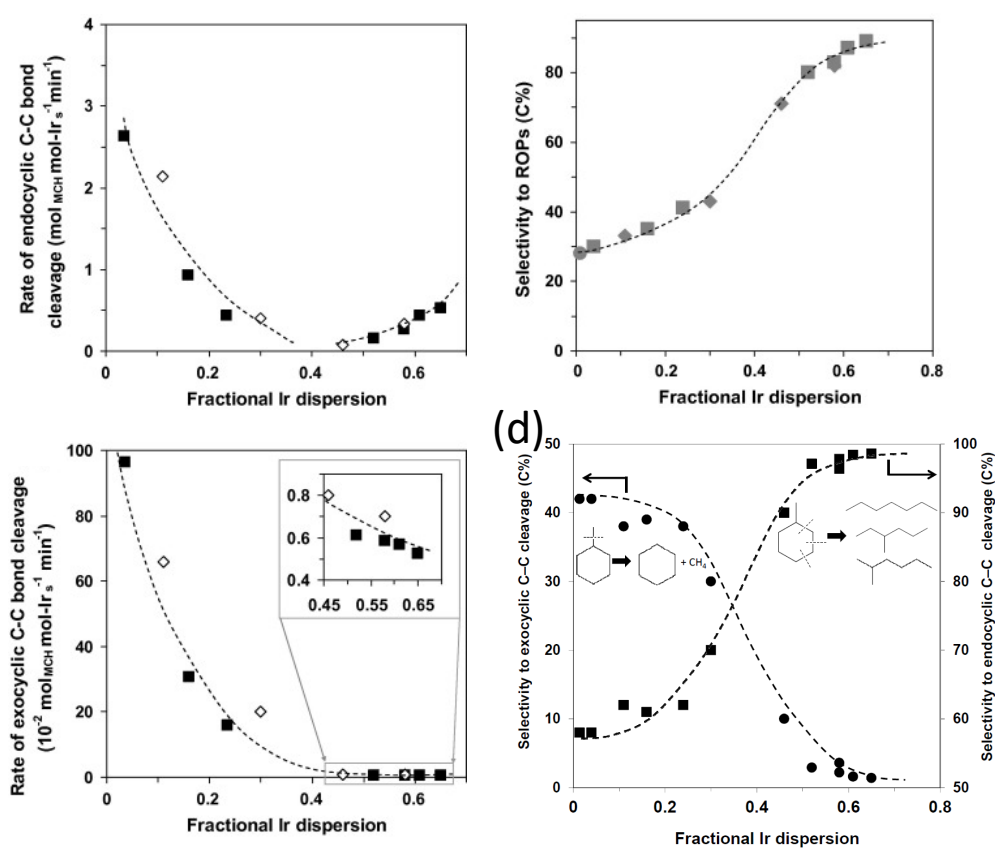


Figure 10. Turnover frequencies for (a) endocyclic and (b) exocyclic C–C bond cleavage of MCH over Ir/Al₂O₃ as a function of Ir dispersion (250 °C, 1.2 kPa MCH and 630 kPa H₂). Catalysts prepared from Cl-free precursor (■) or Cl-containing precursor (◇). Inset of (b) is enlarged section of highly dispersed catalysts (D = 0.46–0.65). (c) Total selectivity to ROPs as a function of Ir dispersion. (d) Dependence of endocyclic (■) and exocyclic (●) C–C bond cleavage on Ir dispersion over Ir black and Ir/Al₂O₃ catalysts. Reproduced with permission from Ref¹⁶⁹

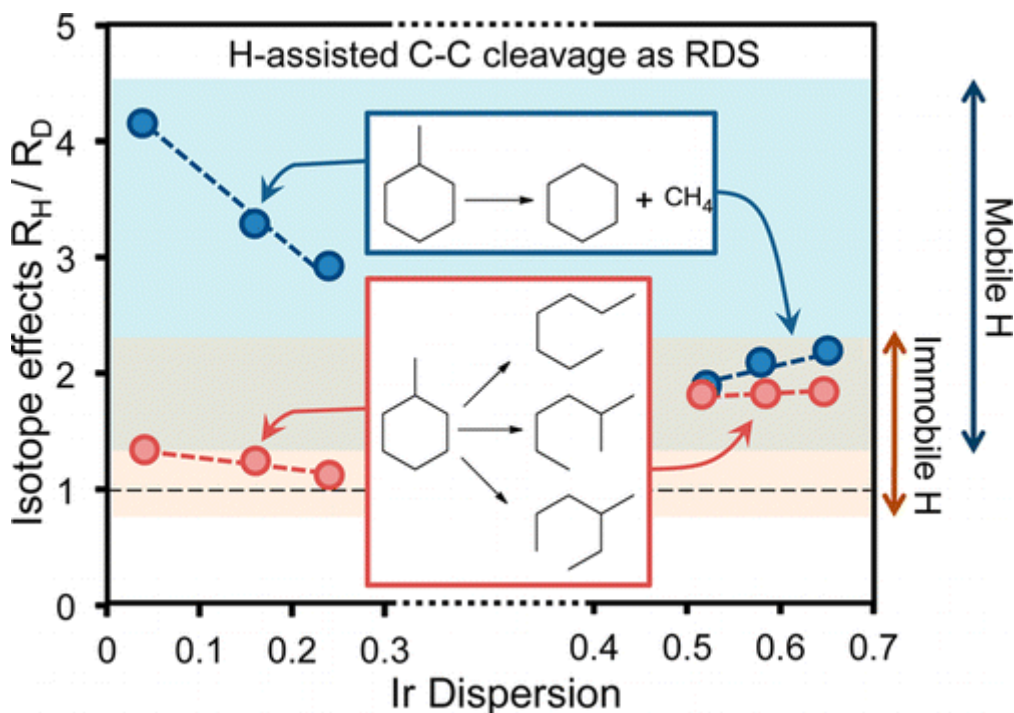


Figure 11. Effect of H/D isotopic substitution on MCH hydrogenolysis over Ir/Al₂O₃. Reproduced with permission from Ref¹⁷⁰

Alumina supported Rh, Ru and Re are also reported for SRO of MCP at temperatures spanning 200 to 475 °C and 2.85 MPa H₂ (Table 2, Entries 31, 33 and 34), benchmarked against Pt and Ir.¹³³ MCP conversions and TOFs at 300 °C decreased from Ir/Al₂O₃ ($127 \times 10^{-2} \text{ s}^{-1}$) > Rh/Al₂O₃ ($64 \times 10^{-2} \text{ s}^{-1}$) > Ru/Al₂O₃ ($50 \times 10^{-2} \text{ s}^{-1}$) > Re/Al₂O₃ ($44 \times 10^{-2} \text{ s}^{-1}$) >> Pt/Al₂O₃ ($1.3 \times 10^{-2} \text{ s}^{-1}$), although the trend in ROP selectivity followed the order Ir/Al₂O₃ > Pt/Al₂O₃ ~ Rh/Al₂O₃ > Ru/Al₂O₃ > Re/Al₂O₃. Ir produced <2 % of cracking products, even at 90 % MCP conversion. Although Ru exhibited high MCP conversion (>80 %) it favoured deep hydrogenolysis and hence cracking products. For Pt, significant MCP conversion (up to 50 %) and moderate RO selectivity (up to 45 %) were only achieved when the reaction temperature was increased to 400 °C. McVicker et al. observed similar trends comparing the hydrogenolysis activity of Ir, Pt and Ru for MCP conversion under similar reaction conditions,¹² with Ir affording 99 % ROP selectivity and <1 % cracking products (Table 2, entry 3). A related investigation of MCP conversion over Pt/SiO₂, Ru/SiO₂, Ni/Al₂O₃ and Ir/Al₂O₃ catalysts¹² found that MCP conversion followed the order Ru (52.9 %) > Ir (14.5 %) > Pt (6.6 %) > Ni (2.3 %), with ROP selectivity following Ir (87 %) > Ni (12 %) > Pt (5 %) > Ru (4 %) (Table 2, Entries 3, 12, 14, 21 and 41). Despite high MCP conversion, Ru was unselective to desirable n-H, 2-MH and 3-MH ring opening products, promoting cracking (50.2 %). Paál et al. demonstrated single site hydrogenolysis of MCH over Rh, Pd, Ir, and Pt, contrasting with deep hydrogenolysis (leading to shorter alkanes) over Co, Ni, Cu, Ru, Ag and Re metals.¹⁷¹ Iridium thus emerges as the most active and selective metal for the ring opening of C5 and C6 model compounds.

Non-noble Ni transition metal catalysts are also reported for SRO of mono- and bi-cyclic molecules. In 1975, Miki et al. investigated a 30 wt%Ni/Al₂O₃ (Table 2, Entry 39) for SRO of MCP at 260 °C and 1 MPa H₂, but observed extensive secondary cracking of primary C₆ alkane hydrogenolysis products to C₁–C₅ paraffins.¹⁵⁵ A corresponding study of 14 wt% Ni/Al₂O₃ for SRO of MCH also noted low conversion (2.3 %) and selectivity to ring opening products (12 %).¹² Interestingly, switching to a silica support to disperse high Ni loadings (60 wt%) improved performance resulting in 83 % conversion and 84 % ROP selectivity (Table 2, Entry 42).¹⁵⁶

In summary, transition metals are effective catalysts for the SRO of monocyclic molecules like MCP and MCH, but show poor ring opening activity towards bicyclics due to the higher activation barrier for the latter. Pt exhibits the highest selectivity for cleaving substituted C–C bonds in cyclic molecules (to afford desirable high CN linear alkanes) but is generally less active than Ir, Rh and Ru, and is unsuitable for SRO of six-membered rings due to competing dehydrogenation and isomerisation reactions. Cleavage of C–C bonds at substituted positions is critical to enhancing the CN of naphthenic feedstocks and requires molecular coordination via a metallocyclobutane intermediate (often as a metal-support adduct). Ring opening is structure sensitive over Pt, being influenced affected by NP size and support selection; substituted C–C bonds are preferentially cleaved for <2 nm particles. Ir offers enhanced conversion and ROP selectivity compared to Pt, but exhibits a similar structure sensitivity, with linear and branched alkanes from endocyclic bond cleavage favoured over small (<1 nm) particles. Support modification by the introduction of chlorine has little influence on the performance of Ir. Small metal NPs (<2 nm), moderate reaction temperatures (~300 °C) and use of an Al₂O₃ support emerge as important elements for high conversion and ring opening selectivity of naphthenes. Ir/Al₂O₃ is the best monofunctional catalyst for SRO of monocyclic model compounds, but is less effective towards bicyclics.

4.1.2 Bimetallic or trimetallic catalysts

The behaviour of metal active sites can be modulated by interactions with other (typically less active) metals. Such interactions may manifest as electronic and/or geometric effects, in which the electron density or atomic arrangement of the primary metal is altered respectively to e.g. enhance reactant activation, stabilise specific intermediates, or destabilise products. Alternatively, additional metals may directly participate in reactions, acting as co-catalysts.¹⁷² Bi- and trimetallic catalysts can offer unique catalytic performance relative to their monometallic counterparts, with improved activity, selectivity and/or stability. Bimetallic catalysts are widely used for SRO of naphthenes due to their improved (and tunable) activity resulting from synergy between the metal components. Various metal combinations, including Pt–Ir, Pt–Ru, Ir–Pd, Ru–Pd, Ni–Ir and trimetallic and Pt–Ir–Co catalysts have been studied for SRO of mono- and bicyclic molecules.

Pt–Ir catalysts have been explored for MCP conversion, with Pt–Ir/ γ -Al₂O₃ exhibiting higher conversion at 220 °C (29 %) than Pt/ γ -Al₂O₃ (5%), while retaining 100 % ROP selectivity (Table 2, Entry 2 and 44).¹⁴⁴ Although Ir/Al₂O₃ exhibits superior activity for MCP (66 % conversion), it is less selective, producing ~12 % cracking product; Pt doping therefore suppresses cracking reactions. Similar observations are reported for Pt–Ir/ TiO₂ wherein Pt addition to Ir/TiO₂ increases MCP conversion at 260 °C (from 72.3 % to 80.6 %, Table 2, Entry 45) and decreases cracking selectivity (from 27.7 % to 19.4%).¹⁴⁷ Synergy between Pt and Ir inhibits coke deposition and limits C–C deep hydrogenolysis.^{95, 164, 165}

Replacement of costly and Earth scarce Ir with noble metals such as Ru, Rh and Re has been attempted, however, the SRO activities of Pt–Ru,¹¹³ Pt–Rh¹⁷³ and Pt–Re¹⁷⁴ catalysts are intermediate between values for their respective monometallic catalysts (rather superior to either as desired). Other bimetallic catalysts including Rh–Sn/Al₂O₃,¹⁷⁵ Rh–Ge/Al₂O₃¹⁷⁶ and Rh–Ag/TiO₂¹⁷⁷ have also been explored, with little success. Cobalt has been added to Pt–Ir to form trimetallic systems, with the aim of further suppressing cracking during SRO of MCP. A series of Pt–Ir–Co catalysts prepared by a galvanic replacement were compared with bimetallic Pt–Co and Ir–Co catalysts for MCP ring opening.^{140, 150} In the galvanic replacement method, Ir atoms are preferentially deposited on the surface of Co NPs instead of the SiO₂ support (Figure 12a).

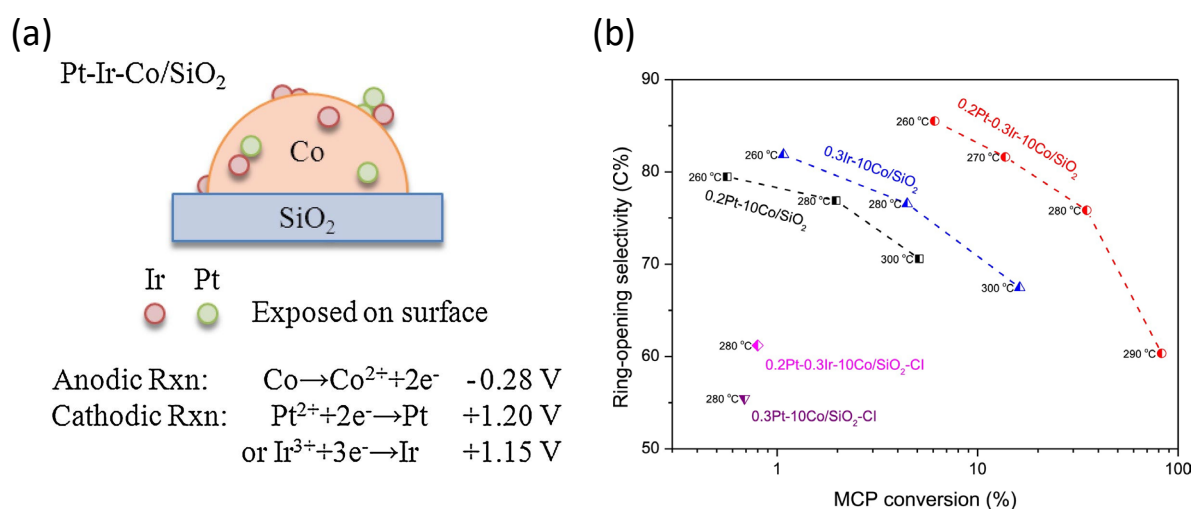


Figure 12. (a) Preparation of Pt–Ir–Co/SiO₂ via galvanic replacement. (b) Correlation between ring opening selectivity and MCP conversion over different catalysts. Reaction conditions: 0.15 g catalyst (diluted to 1 mL), $\text{WHSV}_{\text{MCP}} = 30 \text{ h}^{-1}$, $\text{H}_2:\text{MCP} = 20$ and 2 MPa H_2 . Catalysts pre-reduced at 350 °C for 1 h. Reproduced with permission from Ref¹⁵⁰.

Figure 12b shows that MCP conversion and RO selectivity of Pt–Ir–Co are superior to those of Pt–Co or Ir–Co, with the trimetallic system exhibiting a specific activity of $25 \text{ mol.gIr}_{\text{total}}^{-1}.\text{min}^{-1}$, significantly higher than for monometallic catalysts ($0.3\text{Pt}/\text{SiO}_2 = 0.08 \text{ mol.gPt}_{\text{total}}^{-1}.\text{min}^{-1}$ and $0.3\text{Ir}/\text{SiO}_2 = 0.2 \text{ mol.gIr}_{\text{total}}^{-1}.\text{min}^{-1}$). Catalytically active Ir atoms were highly dispersed over Co NPs, resulting in a significantly higher dispersion and greater Ir utilisation compared to pure Ir/SiO₂. As discussed in previous

sections, although monometallic catalysts are not active for SRO of bicyclic molecules, bimetallic catalysts show promise for the ring opening of decalin and indan. A comparative study of Pt-Ir supported on alumina or titania¹⁷⁸ delivered 9.5 % and 5.4 % decalin conversion respectively at 325 °C. Despite an improvement versus monometallic catalysts, the decalin conversion remains low and is attributed to: (i) the absence of acidic sites required to isomerise six-membered into five-membered rings; and (ii) strong metal-support interactions (SMSI) which can partial encapsulate metal NPs in Pt-Ir/TiO₂ thereby and lowering the active surface. Electropositive alkali metals can influence the hydrogenolysis activity of noble metals by increasing electron density on the latter. Improved decalin conversion (31 %) and ROP yields (45 %) were attained over 0.5wt% Na doped Pt-Ir/Al₂O₃ at 325 °C and 3 MPa H₂.¹⁵⁸ This was attributed to lowered dehydrogenation and cracking over the electronically perturbed noble metals, which helped to stabilise the desired ring opening products.

Ring opening of indan has been explored over bimetallic catalysts including Pt-Ir, Ru-Ir, Pd-Ir, Ru-Pd and Ni-Ir; corresponding conversions and product selectivities (Table 2, Entries 54-59). Indan SRO over 2 wt% Pt₅Ir₉₅ on supports including CeO₂, Al₂O₃, SiO₂-Al₂O₃, H-SA, ZrO₂, MgO and SiO₂¹⁰⁰ revealed the highest indan conversion (52 %) for ceria and the lowest (5 %) for silica (Figure 13a). The Pt₅Ir₉₅/CeO₂ catalyst also exhibited the highest selectivity to ROPs (68 % 2-ethyl toluene and 11 % n-propylbenzene) and lowest selectivity to light hydrocarbons (<C₅, 5 %). The high selectivity to ring opening can be attributed to the presence of acid and basic sites on ceria, this amphoteric character potentially limits secondary cracking reactions compared to purely acidic supports. In light of the superior performance of ceria supported metals, various Pt_xIr_y molar ratios were explored (x:y=100:0, 5:95, 15:85, 25:75, 50:50 and 0:100) (Figure 13b). Although Ir/CeO₂ showed the highest conversion, its initial ROP selectivity was only 5 % versus 67 % for Pt₅₀Ir₅₀/CeO₂ (note selectivities were unfortunately not calculated at iso-conversion). However, all catalysts exhibited similar deactivation profiles over the course of 5 h reaction, indicating gradual coking on the metallic phase and/or the support, as previously discussed.^{144, 165} Considering the relatively high reaction temperature in this study (325 °C), it would be interesting to explore whether cracking could be suppressed at lower temperatures while retaining significant SRO activity.

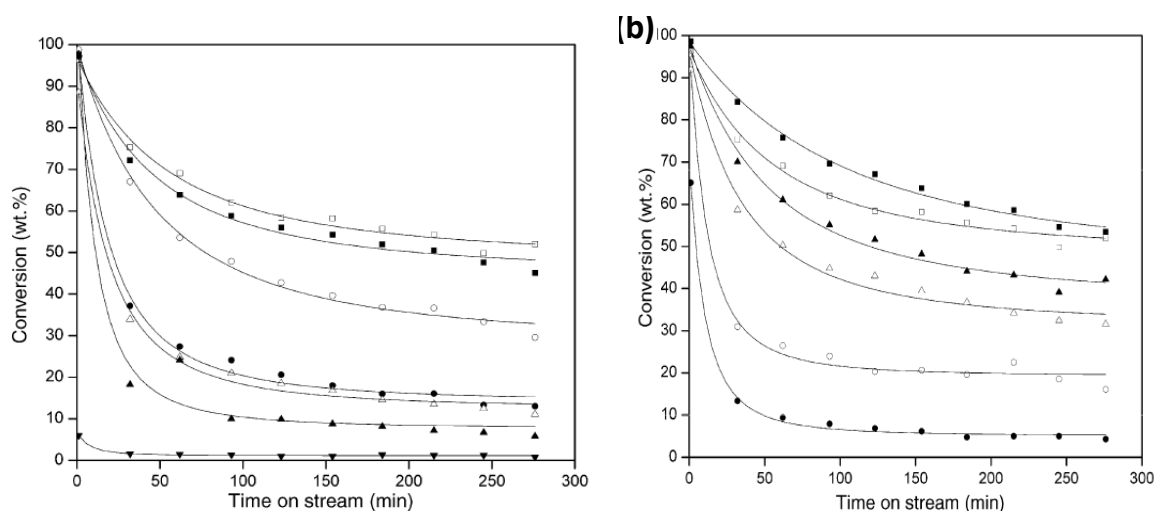


Figure 13. (a) Indan SRO at atmospheric pressure and 325 °C over supported 2 wt% Pt5Ir95 catalysts: CeO₂ (□); γ-Al₂O₃ (■), SiO₂-Al₂O₃ (○); H-SA (●); ZrO₂ (Δ); MgO (▲) and SiO₂ (▼). (b) Indan SRO at atmospheric pressure and 325 °C over CeO₂ supported 2 wt% Ir (■), Pt5Ir95 (□), Pt15Ir85 (▲), Pt25Ir75 (△), Pt50Ir50 (○) and Pt (●) catalysts. Reproduced with permission from Ref¹⁰⁰.

Bimetallic Ru-Ir/Al₂O₃ catalysts have also been studied for indan SRO at atmospheric H₂ pressure and 336 °C.¹⁵⁴ Ru₁Ir₄/Al₂O₃ exhibited 55 % conversion and 62 % selectivity to ROPs, superior selectivity to that of a monometallic Ru analogue (9 % selectivity), although the bimetallic performance was significant worse than monometallic Ir (99 % conversion and 74 % selectivity). However, the Ru-Ir bimetallic exhibited worse selectivity to ROPs than Ir/Al₂O₃. The lower activity of Ru-Ir versus Ir was attributed to the promotion of dealkylation reactions by Ru, in accordance with previous research.^{133, 179} For example, cyclohexane hydrogenolysis was unselective over a 1 wt% Ru/Al₂O₃ catalyst at 280 °C, with only light (C1–C3) hydrocarbons observed.¹⁷⁹

Monodispersed 1.6 nm Ir, 2.3 nm Pd and 2.7 nm Pd@Ir (core@shell NPs) prepared by a hydrogen-sacrificial reduction method, and 2.2 nm Pd₂Ir₁ alloy NPs, have been explored for the atmospheric pressure ring opening of indan at 336 °C.¹⁵³ HRTEM images (Figure 14a-d), revealed bimetallic Pd₂Ir₁ and Pd₁Ir₁ alloy NPs (2.2 ± 1 nm) were of similar size, but a wider distribution, than monometallic Pd (2.3 ± 0.4 nm) NPs. The Pd@Ir NPs were the largest (2.7 ± 0.5 nm) but with a narrow size, consistent with coating of preformed Pd cores by an Ir shell. The synthesis of Pd@Ir catalysts via hydrogen sacrificial reduction is shown in Figure 14e. Indan conversion followed the order Ir (99 %) > Pd@Ir (91 %) > Pd₂Ir₁ (9 %) > Pd (1 %); since Ir is currently twice as expensive as Pd, and one of the rarest elements on Earth, dispersion of Ir over a Pd core offers a promising means to reduce costs without compromising catalytic performance. High selectivity towards n-propylbenzene from C-C cleavage of the C5 indan ring is necessary to increase the CN, with Pd@Ir reaching 48 % (Table 2, Entry 56) in contrast to the monometallic Ir catalyst (10 %). In a related study, bimetallic Ni-Ir NPs were impregnated over an Al₂O₃ support by the hydrogen sacrificial method and tested for indan SRO.⁹⁴ Calculated TOFs (per surface Ir atom) for Ni@Ir/γ-Al₂O₃ of 0.83

$\text{mol}_{\text{indane}} \cdot \text{mol}^{-1}_{\text{Ir}} \cdot \text{min}^{-1}$ is significantly higher than that of Ir/ $\gamma\text{-Al}_2\text{O}_3$ ($0.43 \text{ mol}_{\text{indane}} \cdot \text{mol}^{-1}_{\text{Ir}} \cdot \text{min}^{-1}$) and Ni/ $\gamma\text{-Al}_2\text{O}_3$ ($<0.1 \text{ mol}_{\text{indane}} \cdot \text{mol}^{-1}_{\text{Ir}} \cdot \text{min}^{-1}$), evidencing more efficient utilisation of the more active Ir component in core-shell NPs. This study highlights that precious metal thriftiness can be achieved without loss of catalytic performance in SRO, and is a strategy that should be more widely explored for bimetallics.

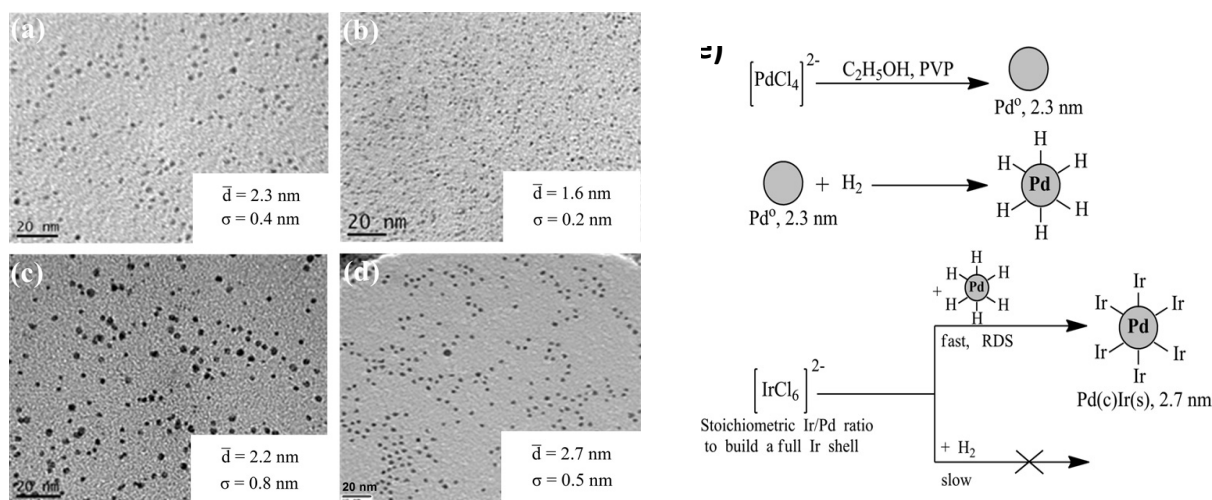


Figure 14. TEM images of Pd, Ir and bimetallic NPs: (a) Pd, (b) Ir, (c) Pd₂Ir₁, (d) Pd@Ir. (e) Schematic synthesis of Pd@Ir NPs formation by hydrogen-sacrificial reduction. Reproduced with permission from Ref¹⁵³

Indan SRO is also reported over bimetallic 2-3 nm Pd-Ru NPs with Pd:Ru molar ratios between 0 and 1.7,⁶² and Pd@Ru (core-shell) NPs prepared by stepwise growth synthesis (Figure 15a). The introduction of Pd doubled the selectivity of Ru towards n-propylbenzene, which reached levels comparable to Ir (Figure 15b). Moreover, comparison with monometallic Pd analogues suggests that the higher selectivity of bimetallic Pd@Ru towards n-propylbenzene reflects a different ring opening mechanism, proceeding via the olefin flat-lying intermediate, which also promotes hydrogenation increasing the light alkane yield.

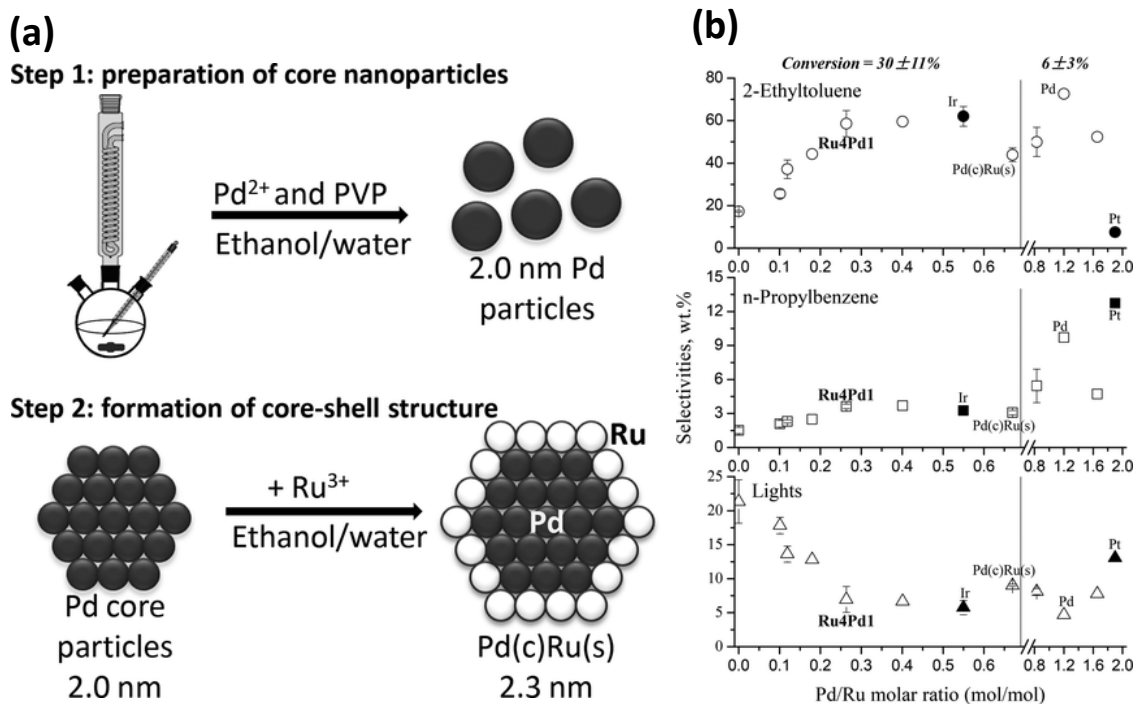


Figure 15. (a) Synthesis of Ru-Pd bimetallic NPs with Pd (Core)–Ru (shell) Structure (b) Selectivities vs. Pd-to-Ru molar ratio in the bimetallic and monometallic catalysts (monometallic Ir and Pt catalysts are included for comparison). The catalysts were grouped according to similar indan conversions for fair selectivity comparison. Reproduced with permission from Ref ⁶².

In summary, diverse combinations of noble and non-noble metals in bimetallic or trimetallic formulations offer a means to improve naphthene conversion and ROP selectivity. Pt and Ir combinations outperform monometallic Pt catalysts in both these performance measures, terms, and while Pt-Ir bimetallics are less active than monometallic Ir catalysts, they did offer enhanced ring opening selectivity by suppressing cracking pathways. Support effects are not widely explored for bimetallics, although the amphoteric character of CeO_2 is reportedly beneficial for indan ring opening over $\text{Pt}_5\text{Ir}_{95}$ alloy NPs. Limited attempts have been made to replace/reduced Ir use by incorporating Co or Ni in trimetallic formulations, which show promising ring opening activity compared to Ir. The most attractive metal systems are M@Ir core-shell catalysts which enable an extremely high dispersion of the more active Ir component over the a core of the les active component, and thereby enable thrifiting of the scarce and expensive former metal. Many studies are performed >300 °C, wherein cracking is thermodynamically favoured, and future studies should focus on creating more active active formulations able to operate at lower temperature where ring opening products are favoured.

4.2 Bifunctional metal/solid acid catalysts

Metal nanoparticles dispersed over solid acid supports generate bifunctional catalysts which possess the best balance of hydrogenolysis activity and selectivity for SRO of naphthenic molecules. In such bifunctional catalysts, metal sites promote (de)hydrogenation, while acid sites promote skeletal isomerisation. Most bifunctional catalysts investigated for the SRO of mono- and bicyclic molecules employ zeolites as the solid acid, whose pore structure, acidity (Si:Al ratio) and synergy with the metal determine the ROP overall yield and distribution. Examples include Y zeolite, HZSM-5, beta zeolite, mordenite, in addition to amorphous SiO₂-Al₂O₃ and WO₃ solid acid supports for active metals such as Pt, Ir, Pd, Ir, Rh, Ni, Mo and W (as mono- or bimetallic NPs). This section highlights recent advances in developing bifunctional SRO catalysts, whose performances are summarised in **Table 3** for of mono- and bicyclic reactants.

4.2.1 Transition metal/solid acid catalysts

Pt is widely used in bifunctional SRO catalysts, often in conjunction with zeolites. A study on Pt/H-ZSM-5 for MCP ring opening¹⁸⁰ identified a new reaction pathway compared to Pt alone (**Scheme 5**), affording 72 % conversion and 37 % ROP selectivity, alongside 14 % ring-enlargement products (benzene and cyclohexane) and only 1.6 % cracking products (**Table 3, Entry 1**). In contrast, Pt/Al₂O₃ only exhibited 5 % MCP conversion (albeit 100 % ROP selectivity, **Table 2, Entry 2**). The choice of zeolite is critical, apparent from Pt supported on a mixture of 80 wt% β -zeolite (Si:Al=25) and 20 wt% Al₂O₃, which showed good MCP conversion but very poor selectivity (3 %) to ring opening (**Table 3, Entry 2**). Galperin and co-workers postulated that the low ROP selectivity reflected extensive MCP isomerisation over the (Brønsted) acid sites to cyclohexane, and subsequent Pt catalysed dehydrogenation to benzene. Surprisingly, Pt on a solid base hydrotalcite support delivered modest MPC conversion and almost total ROP selectivity (**Table 3, entry 2**) via the nonselective mechanism to form 2-MP, 3-MP and n-H in a statistical distribution. This observation likely reflects almost complete suppression of acid-catalysed MCP isomerisation (favoured at the high temperature of 350 °C used),^{74, 102, 114, 181} with hydrogenolysis exclusively over metal sites. Similar conclusions were deduced for MCH ring opening over Pt/HY, wherein ring cracking dominates (97 %) over ring opening (2 %) (**Table 3, Entry 3**). As expected, increasing the reaction temperature to 400 °C favours aromatic products over Pt/zeolites (**Table 3, Entry 1**). Such conditions are hence ill-suited for SRO of MCP and MCH monocyclics over Pt/zeolites due to strong support acidity and dehydrogenation activity of Pt,^{182, 183} and there remains merit in revisiting such catalysts at lower temperature.

Table 3. Ring opening of various molecules over bifunctional metal/acid(-base) catalysts.

Entry	Catalyst	Catalyst properties	Feedstock	Reaction conditions	Conversion (%)	Product distribution (%)					Ref.
						RO	RC	DH	CP	RE	
Transition metal/solid acid catalysts											
1	Pt/HZSM-48	0.5 wt% Pt, 9 nm, (Si/Al=48), 218 m ² g ⁻¹ , Total acidity of 53.4 μmol.ammonia.g _{cat} ⁻¹	MCP	350 °C, 0.1 MPa H ₂ , 0.3 h ⁻¹ WHSV, H ₂ /feed=10, Pre-reduction at 400 °C for 4 h	71.8	37.3	-	-	5.4	59.6	180
				400 °C, 0.1 MPa H ₂ , 0.3 h ⁻¹ WHSV, H ₂ /feed=10, Pre-reduction at 400 °C for 4 h	84.5	19	-	-	25.5	50.1	
2a	Pt/H-Beta+Al ₂ O ₃	0.3 wt% Pt, 70 wt% H-Beta Si/Al=25, 30wt% Al ₂ O ₃ , ~3 nm, 415 m ² g ⁻¹	MCP	250 mg, 350 °C, 0.47 h ⁻¹ WHSV, H ₂ /feed=60, Pre-reduction at 450 °C for 30 minutes	58.4	2.8	-	-	1	95	114
	b	Pt/Hydrotalcite			0.28 wt% Pt, ~3 nm, 270 m ² g ⁻¹	35.2	98.5	-	0.5	1	
3	Pt/HY	1 wt% Pt, HY (Si/Al=5.3), Total acidity of 795 μmol.ammonia.g _{cat} ⁻¹	MCH	260 °C, 3 MPa H ₂ , 2.5 h ⁻¹ WHSV, H ₂ /feed=40, Pre-reduction at 400 °C for 2 h	29.2	2	97.6	-	0.4	-	184
4	Pt/ITQ21	1 wt% Pt, Si/Al ratio (25), 596 m ² g ⁻¹ , Brønsted acidity of 159 μmol.pyridine.g _{cat} ⁻¹	Tetralin	300 °C, 3 MPa H ₂ , 2.5 h ⁻¹ WHSV, H ₂ /feed=10, Pre-reduction at 450 °C for 2 h	99.9	5	20.1	5	45	-	73
5	Pt/HY	1 wt% Pt, Si/Al ratio (5.3), 450 m ² g ⁻¹ Total acidity of 1141 μmol.ammonia.g _{cat} ⁻¹	Tetralin	327 °C; 2 MPa H ₂ , 2.5 h ⁻¹ WHSV, H ₂ /feed=60, Pre-reduction at 400 °C for 2 h	92.5	14.9	-	0.99	50.5	-	81
			Decalin		27.4	11.1	10.9	0	5.4		
6	Pt/H-Beta	0.97 wt% Pt, 79.5 metal dispersion, Si/Al ratio (12.5),	Decalin	200 mg, 250 °C, 5 MPa H ₂ , 2 h ⁻¹ WHSV, H ₂ /feed=260, Pre-reduction at 440 °C for 2 h	80	28	43	-	8	-	185, 186
7	Pt/H-Beta	2 wt% Pt, Si/Al ratio (25), 752 m ² g ⁻¹ , 33% Pt dispersion, 3.4 nm Pt; Total acidity of 612 μmol.pyridine.g _{cat} ⁻¹	Decalin	100 mg, 250 °C, 2 MPa H ₂ , 1.7 h ⁻¹ WHSV, H ₂ /feed=13, Pre-reduction at 400 °C for 2 h	90	30.2	42	3.6	16.4	-	74
8	Pt/USY	0.3 wt% Pt, 586 m ² g ⁻¹ , 3.9 nm, Brønsted acidity of 155 μmol.pyridine.g _{cat} ⁻¹	Tetralin	260 °C, 4 MPa H ₂ , 2 h ⁻¹ WHSV, H ₂ /feed=750, Pre-reduction at 300 °C for 4 h	99.6	28.3	13	-	43.8	-	81, 186
10a	Ir/USY	0.9 wt% Ir, Si/Al ratio (80), 759 m ² g ⁻¹ , 388 μmol.ammonia.g _{cat} ⁻¹ of acidity, 0.9 wt% Ir, 2-3 nm	MCP	500 mg, 300 °C, 3 MPa H ₂ , Pre-reduction at 200 °C for 1 h	97.6	66	-	-	3	31	116, 187
	b				Ir/HZSM-5	83.4	45	-	-	10	
11a	Ir/USY	Si/Al ratio (80), 759 m ² g ⁻¹ , 388 μmol.ammonia.g _{cat} ⁻¹ of acidity, 0.9 wt% Ir, 2-3 nm	MCH	500 mg, 300 °C, 2.8 MPa H ₂ , 1.8 h ⁻¹ WHSV, H ₂ /feed=40, Pre-reduction at 260 °C for 1 h	51.6	27	43	-	13	17	116

b	Ir/HZSM-5	Si/Al ratio (80), 406 m ² g ⁻¹ , 290 μmol.ammonia.g _{cat.} ⁻¹ of acidity, 0.9 wt% Ir, 2-3 nm			38.1	11	18	-	30	39	
13 a	0.5Ir/H-Beta-25	Si/Al ratio (12.5), 489 m ² g ⁻¹ , 0.5 wt% Ir, 2.83 nm size, 39% Ir dispersion, Brønsted acidity of 544 μmol.pyridine.g _{cat.} ⁻¹	MCH	200 mg, 330 °C, 3 MPa H ₂ , 24 h ⁻¹ WHSV, H ₂ /feed=12.5, Pre-reduction at 400 °C for 1 h	93	6	62	-	31	1	188
b	0.6Ir/H-AlMCM-41	Si/Al ratio (15), 795 m ² g ⁻¹ , 0.6 wt% Ir, 3.42 nm size, 32% Ir dispersion, Brønsted acidity of 197 μmol.pyridine.g _{cat.} ⁻¹		400 mg, 330 °C, 3 MPa H ₂ , 12 h ⁻¹ WHSV, H ₂ /feed=12.5; Pre-reduction at 400 °C for 1 h	73	33	55	-	11	1	
c	0.7Ir/Na-AlMCM-41	Si/Al ratio (15), 745 m ² g ⁻¹ , 0.7 wt% Ir, 3.22 nm size, 34% Ir dispersion, Brønsted acidity of 79 μmol.pyridine.g _{cat.} ⁻¹			22	52	24	-	21	3	
14 a	2Ir/H-Beta-25	2 wt% Ir, SiO ₂ /Al ₂ O ₃ ratio (25), 573 m ² g ⁻¹ , 22.9% dispersion,	Decalin	500 mg, 325 °C, 6 MPa H ₂ , H ₂ /feed=10, Pre-reduction at 350 °C for 1 h	84	45	-	-	-	-	189
b	2Ir/H-Beta-300	2wt%Ir, SiO ₂ /Al ₂ O ₃ ratio (300), 521 m ² g ⁻¹ , 17.4% dispersion,			60	28	-	-	-	-	
15	3.4Ir/H-Cs-Beta	3.4 wt% Ir, 3.7 wt% Cs, SiO ₂ /Al ₂ O ₃ ratio (14), 573 m ² g ⁻¹ , 86% dispersion, Total acidity of 129 μmol.pyridine.g _{cat.} ⁻¹	Decalin	262 °C, 5.2 MPa H ₂	94	59	-	-	-	-	190
16	Ir/Cs-meso-Beta	3 wt% Ir, SiO ₂ /Al ₂ O ₃ ratio (18), 3.7 wt% Cs, 666 m ² g ⁻¹ , 1.7 nm Ir, Total acidity of 240 μmol.pyridine.g _{cat.} ⁻¹	Decalin	260 °C, 3.5 MPa H ₂ , 0.44 h ⁻¹ WHSV	89.2	72.6	-	-	-	-	139
17	Ir/SiO ₂ -Al ₂ O ₃	0.96 wt% Ir, 40 wt% SiO ₂ , 60 wt% Al ₂ O ₃ , 1.5±0.2 nm, 500 m ² g ⁻¹	Tetralin	50 mg, 350 °C, 4 MPa H ₂ , H ₂ /feed=10, Pre-reduction at 350 °C for 6 h	80	37	-	3	40	-	104
18	Ir/SiO ₂ -Al ₂ O ₃	0.96 wt% Ir, SiO ₂ /Al ₂ O ₃ ratio (80/20), 337 m ² g ⁻¹ , 2.4 nm Ir, 38% metal dispersion, Total acidity of 1820 μmol.pyridine.g _{cat.} ⁻¹	Decalin	200 mg, 325 °C, 3 MPa H ₂ , Pre-reduction at 500 °C for 1 h	62.3	42	10	2	5.5	-	191
19	1.2Ir/WO ₃ /γ-Al ₂ O ₃	24 wt% W, surface density (4.1 atoms W.nm ⁻²), 1.2 wt% Ir	MCH	300 °C, 5 MPa H ₂ , 0.2 h ⁻¹ WHSV, H ₂ /feed=24, Pre-reduction at 350 °C for 1 h	75	52	40	-	8	-	112
			Decalin	1000 mg, 300 °C, 3 MPa H ₂ , 1 h ⁻¹ WHSV, H ₂ /feed=10, Pre-reduction at 450 °C for 1 h	75	51	-	-	-		
20 a	Rh/HY	3 wt% Rh, Si/Al=2.6, <1 nm	MCP	200 mg, 0.00526 MPa H ₂ , H ₂ /feed=18, Pre-reduction at 400 °C for 2 h	7.7	66	-	-	-	-	87
	b Rh/NaY	3 wt% Rh, Si/Al=2.6, 1.5 nm			10	73	-	-	-		
21	Rh1/SiO ₂ -Al ₂ O ₃	Si/Al ratio (14.8), 514 m ² g ⁻¹ (support), 0.79 wt% Rh, 2.1 nm	MCH		100	32	-	-	-	-	192

22	Rh/SiO ₂ -Al ₂ O ₃	1.5 wt% Rh, SiO ₂ /Al ₂ O ₃ ratio (70/30), 34 % metal dispersion, Total acidity of 1579 $\mu\text{mol.pyridine.g}_{\text{cat.}}^{-1}$	Decalin	200 mg, 350 °C, 3 MPa H ₂ , Pre-reduction at 500 °C for 1 h	78	69	-	-	-	-	193
23	Pd/HY	1 wt% Pd, Si/Al ratio of (30), 589 m ² g ⁻¹ , 3.09 nm, Total acidity of 1950 $\mu\text{mol.ammonia.g}_{\text{cat.}}^{-1}$	Naphthalene	500 mg, 300 °C, 3 MPa H ₂ , 1 h ⁻¹ WHSV, Pre-reduction at 450 °C for 1 h	98	52.5	29.5	-	17.6	-	131
			Tetralin		71	38.3	-	1	43.8	-	
			Decalin		92	92	-				
24	Pd1/SiO ₂ -Al ₂ O ₃	Si/Al ratio (14.8), 514 m ² g ⁻¹ (support), 0.78 wt% Pd, 3.0 nm	MCH	1500 mg, 350 °C, 3.9 MPa H ₂ , 2 h ⁻¹ WHSV, H ₂ /feed=8, Pre-reduction at 500 °C for 1 h	51	1	-	-	-	-	192
25	W-MCM-48	Si/W=40, 1234 m ² g ⁻¹	MCP	200 mg, 450 °C, Pre-reduction at 500 °C for 12 h	1.8	-	-	-	-	-	194
26	Fe-TUD-1	Si/Fe=45, 640 m ² g ⁻¹	MCP	200 mg, 200 °C, 0.1 MPa H ₂ , Pre-reduction at 500 °C for 4 h	1.58	-	-	-	-	-	195
Bimetallic/solid acid catalysts											
27	Ni-W oxide/Al ₂ O ₃ -USY	3.6 wt% Ni, 14.8 wt% W, 18.6 wt% WO ₃ , 295 m ² g ⁻¹ , Total acidity of 271 $\mu\text{mol.pyridine.g}_{\text{cat.}}^{-1}$	Decalin	3000 mg, 300 °C; 5 MPa; 4 h ⁻¹ WHSV, H ₂ /feed=1000	88	26	28	-	24		196
28	Ni ₂ P/SiO ₂ -Al ₂ O ₃	117 m ² g ⁻¹ , Si/Al ratio (0.21), 20 nm Ni ₂ P, Total acidity of 382 $\mu\text{mol.pyridine.g}_{\text{cat.}}^{-1}$	Naphthalene	Pre-reduction at 650 °C for 3 h	80	10	70	15	5		197
29	Pt-Ir/Nb ₂ O ₅	0.5 wt% Pt, 0.5 wt% Ir, 82 m ² g ⁻¹ , 4.8±1.5 nm, Total acidity of 383 $\mu\text{mol.ammonia.g}_{\text{cat.}}^{-1}$	Decalin	1000 mg, 350 °C, 3 MPa H ₂ , 4.5 h ⁻¹ WHSV, Pre-reduction at 500 °C for 4 h	35	27	12	41	20	-	151
30 a b	Ni-MoC/HY	2.25 wt% Ni, 11.3 wt% Mo, Si/Al ratio (13.5), 492 m ² g ⁻¹ , Total acidity of 159 $\mu\text{mol.ammonia.g}_{\text{cat.}}^{-1}$	Decalin	100 mg, 220 °C, 5 MPa H ₂ , 1.5 h ⁻¹ WHSV, H ₂ /feed=60, Pre-reduction at 400 °C for 4 h	44.3	33.5	-	-	-	-	90
	Ni-MoC/HBeta	2.25 wt% Ni, 11.2 wt% Mo, Si/Al ratio (22.9), 395 m ² g ⁻¹ , Total acidity of 116 $\mu\text{mol.ammonia.g}_{\text{cat.}}^{-1}$			24.3	18	-	-	-	-	
31	Pt-Ir/HY	1.5 wt% Pt, 0.75 wt% Ir, Si/Al ratio (13.3), 641 m ² g ⁻¹ , Total acidity of 371 $\mu\text{mol.ammonia.g}_{\text{cat.}}^{-1}$	Decalin	100 mg, 220 °C; 5 MPa H ₂ , 1.5 h ⁻¹ WHSV, H ₂ /feed=60, Pre-reduction at 400 °C for 4 h	82.87	32	-	-	-	-	90
32	Pt-Ir/USY	1 wt% Pt, 1 wt% Ir, Si/Al ratio (16.6), 516 m ² g ⁻¹	Tetralin	500 mg, 275 °C, 3 MPa H ₂ , 2.5 h ⁻¹ WHSV, H ₂ /feed=10, Pre-reduction at 450 °C for 2 h	100	21.1	62.9	1.1	-	-	138
33	Rh2Pd1/SiO ₂ -Al ₂ O ₃	Si/Al ratio (14.8), 514 m ² g ⁻¹ (support), 0.28 wt% Rh, 0.28 wt% Pd, 2.3 nm	MCH	1500 mg, 350 °C, 3.9 MPa H ₂ , 2 h ⁻¹ WHSV, H ₂ /feed=8, Pre-reduction at 500 °C for 1 h	80	51	24	-	30	2	192
34	Ru-Pt/SiO ₂ -Al ₂ O ₃	0.51 wt% Pt, 0.48 wt% Ru, 40 wt% SiO ₂ , 60 wt% Al ₂ O ₃ , 447 m ² g ⁻¹ , Total acidity of 1238 $\mu\text{mol.ammonia.g}_{\text{cat.}}^{-1}$	Decalin	1000 mg, 350 °C, 3 MPa H ₂ , Pre-reduction at 400 °C for 5 h	19	16.4	1.6	0.2	0.8	-	198
35	Rh-Pd/SiO ₂ -Al ₂ O ₃	0.66 wt% Rh, 0.34 wt% Pd, SiO ₂ /Al ₂ O ₃ ratio (40/60), 514 m ² g ⁻¹	Decalin	1000 mg, 350 °C, 3 MPa H ₂ , 1 h ⁻¹ WHSV, Pre-reduction at 450 °C for 1 h	42	35	10	8	6	-	199

Product distribution is divided into 4 groups, dehydrogenation products, Ring contraction products, cracking products, and Ring opening products- Dehydrogenated products include naphthalene, tetralin, 1-methyl indan

Ring contraction products include C10 bicyclic compounds where one or both rings consist of less than 6 carbon atoms

Cracking products include C1-C9 products with lower molecular weight than that of decalin

Ring opening products include C10-alkylcyclohexanes and C10-alkylcyclopentanes

SRO of bicyclics (naphthalene, tetralin and decalin) over Pt/zeolite catalysts (Table 3, Entries 4-8) is significantly improved relative to monocyclics. Tetralin SRO was investigated over Pt/USY catalysts (275 °C, 3 MPa H₂)¹³⁸ occurred with 99 % conversion and 16 % ROP selectivity. The reaction proceeded via tetralin hydrogenation over Pt metal sites, to form cis- and trans-decalins, which subsequently underwent isomerisation via ring contraction over the acid support into methyl-perhydroindanes and dimethyl-octahydropentalenes (Scheme 8). This two stage mechanism was also evident in a similar study over Pt/H-ZSM-5.²⁰⁰ Such bifunctional catalysts require careful control of the acid strength, such that decalin isomerisation to the desired ROPs is efficient, but occurs without subsequent acid catalysed dealkylation or cracking.

Zeolite pore dimensions and topology can impact the yield and selectivity of desired ROPs from bicyclic molecules.^{82, 88} Pt doped ITQ-21, Beta and USY zeolites, which possess different framework structures were evaluated for tetralin SRO (300 °C, 3 MPa H₂);⁷³ physicochemical properties of these Pt/zeolites and associated ROP yields are summarised in Table 4. USY and Beta supports were selected to minimise the influence of acidity differences as they exhibit similar Brønsted acid site loadings. Maximum ROP yields for Pt/USY (16.1 wt%) and Pt/Beta (14.5 wt%) were lower than that for Pt-ITQ21 (20.1 wt%). Molecular-docking simulations for 1,2-*trans*-diethylcyclohexane (considered a representative ROP from tetralin) suggested diffusion was faster through the large pore six-12 membered rings in ITQ-12 than the four-12 membered rings present in USY and Beta.⁷³ Such results indicate that the formation and escape of ROPs from narrower 10 member-ring pores of the latter zeolites is highly unlikely. Unsurprisingly, simulations also predicted the greatest diffusion limitations for ROPs through the smallest pores of the Beta zeolite BEA structure, accounting for the low experimentally observed product yields,^{73,138} although the higher proportion of strong Brønsted acid sites in Pt/Beta could also explain the low ROP yield due to competing cracking reactions.

Table 4: Physicochemical properties (surface area and pore volumes) and relative acidity of zeolites determined by N₂ and pyridine adsorption. Reproduced from ref⁷³

Entry	Zeolite	Si/Al ratio	Surface area (m ² /g)	Pore volume (cm ³ /g)	Brønsted acidity ^a	ROP yield (wt%)
1	Pt/ITQ-21	25	596	0.93	100	20.1
2	Pt/USY	17	532	0.43	95	16.1
3	Pt/Beta	93	659	0.91	87	14.5

^aTaking the amount of Brønsted acid sites at 250 °C desorption on ITQ21 as 100.

Decalin is more reactive than tetralin, and thus frequently chosen to understand the opening of 6-ring bicyclics over bifunctional metal/acid catalysts. Kubička et al. investigated decalin ring opening over Pt promoted H-Beta-25, H-Y-12 and H-Mordenite-20 (at 250 °C and 2 MPa H₂),^{74, 77} revealing catalytic

activity decreased in the order Pt/H-Beta > Pt/H-Y > Pt/H-Mordenite. Reaction was proposed to proceed via Pt catalysed dehydrogenation of decalin to an olefin, which is then protonated by a Brønsted acid site. The resulting carbenium ion can then undergo isomerisation or ring opening (Scheme 3), restoring the Brønsted acid site, and forming an olefin which can be hydrogenated by Pt to yield an isomer or ROP. Yields of ROPs for Pt-modified zeolites reached 30 mol%, compared with just 8 mol% for the protonated zeolites alone (Table 3, Entry 7); conversely, the yield of cracking products over H-Beta decreased from 22 mol% to 4 mol% on Pt addition, possibly reflecting Pt nanoparticle nucleation at strong acid sites inside the zeolite channels. The importance of metal-acid synergy was further explored for Pt modified VPI-15 (a large pore zeolite lacking Brønsted acid sites) for decalin ring opening.²⁰¹ No skeletal isomerisation or ring opening was observed, confirming that Brønsted acidity is important for opening of 6-ring naphthenics. Arribas et al. also report that larger pore size zeolites (USY, beta and mordenite) are more selective to ROPs than medium pore size counterparts⁸⁸ The importance of zeolite topology on molecular diffusion and ROP product distribution was further evidenced by Corma et al.,⁸² who showed larger pore HY is well-suited to decalin SRO. Molecular transport and steric effects also influence the conversion of different decalin isomers: SRO of *cis*-decalin (at 260 °C and 2 MPa H₂)⁸¹ over Pt/HY catalysts was more selective to ROPs than the corresponding *trans* form (Table 3, Entry 5), the latter possessing more sterically hindered C–H bonds. In the case of cyclohexane SRO over Pt/zeolites (H-ZSM-5, H-USY, H-mordenite and H-Beta), the acid support alone drives ring opening and subsequent disproportionation of hexyl-carbenium intermediates followed by hydrogenation, resulting in a broad distribution of paraffin/aromatic products and rapid deactivation associated with heavy coking in a continuous flow microreactor.²⁰⁰ Dimerization of hexyl-carbenium ions is sterically hindered within the narrow pore channels of H-ZSM-5. Pt addition promotes fast, direct hydrogenation of hexyl-carbenium ions to hexanes, highlighting a strong metal-acid synergy.

Kinetic modelling has provided further insight into the roles of metal and acid during decalin ring opening. Kubicka et al. proposed a Langmuir-Hinshelwood (L-H) model for Pt/H-Beta over a wide range of reaction conditions (1–6 MPa H₂, 476–563 K and catalyst concentrations 10–40 g/l).²⁰² Decalin SRO is complex, with a network of >200 reaction products, and hence it is currently impossible to model every reaction steps. A simplified reaction mechanism was therefore considered (Figure 16), which included the skeletal isomerisation of decalin (reaction 1), ring opening of skeletal isomers (reaction 2) and cracking of ROPs (reactions 3 and 4). The resulting kinetic model predicted activation energies for reactions 1, 2 and 4 of 140, 170 and 196 kJ/mol, respectively, in good agreement with experiments,²⁰² with isomerisation being the most facile step, followed by ring opening, and cracking having the highest barrier (and hence favoured at high temperature).

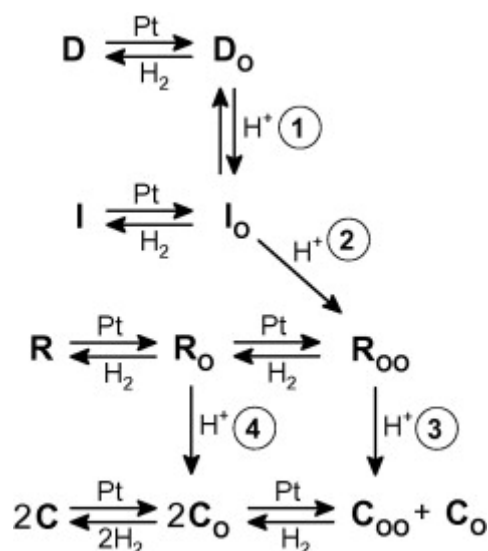


Figure 16. Modelled SRO reaction scheme for decalin over Pt/Beta zeolite. Only surface reactions are shown with adsorption/desorption steps omitted for clarity. Notation: D (decalin), I (skeletal isomers, R (ring opening products, e.g. C10-alkylnaphthenes) and C (cracking products with <10 carbons). Indices O and OO denote an olefin and diene, respectively. Reproduced with permission from Ref ²⁰².

Ir is also widely explored in bifunctional catalysts employing acidic supports. As discussed in the previous section, Ir/Al₂O₃ exhibits the highest ring opening activity of all noble metals for MCH, with ROP yields >80 % attainable at modest conversion (<30 %). However, ROP yields fall <20 % at high conversion due to deep hydrogenolysis (dealkylation of MCH).¹²² This limitation could be overcome if ring opening occurred after ring contraction (indirect ring opening), the latter being promoted by acidic supports. Pleasingly, modification of 1.2wt% Ir/Al₂O₃ and 1.2wt% Ir/ZrO₂-SiO₂ by acidic WO₃^{112, 203} (W surface densities between 0-5.3 W/nm²) increased ring opening selectivity to 77 % and 80 % at high MCH conversions of 75 % and 80 % respectively. In contrast, unpromoted Ir/ZrO₂-SiO₂ only exhibited 65 % ROP selectivity at 54% conversion (Table 3, Entry 19) while WO₃/Al₂O₃ alone was almost inert towards MCH, highlighting the benefits of incorporating metal and acid active sites. These observations were attributed to lowering of the activation energy for 6-membered ring hydrogenolysis over Ir/WO₃/ZrO₂-SiO₂ to 117 kJ/mol from 138 kJ/mol over Ir/ZrO₂-SiO₂. The initial rate of indirect ring opening (via ring contraction) is also reported to increase 50-fold over bifunctional catalysts like Ir/WO₃/Al₂O₃ compared to WO₃/Al₂O₃.¹¹² The preferred pathway for SRO over bifunctional catalysts appears ring contraction, followed by ring opening.^{75, 204} Mild acidic supports for Ir catalysts appear ideal for maximising MCH conversion and CN, while avoiding undesired cracking prevalent over strong solid acids.

Zeolites have been used to support Ir nanoparticles for MCP and MCH ring opening.¹¹⁶ The total acid strength of 0.9 wt% Ir/USY and 0.9 wt% Ir/H-ZSM5 was determined from NH₃ chemisorption at temperatures spanning 100-600 °C, being 388 and 290 μmol.g⁻¹ respectively (Table 3, Entries 10 and 11). The more acidic Ir/USY catalyst exhibited 27 % selectivity to ROPs and 43 % ring contraction, whereas Ir/H-ZSM-5 exhibited only 11 % ROPs and 18 % ring contraction; higher acidity of the USY support

enhancing isomerisation to ring contraction products, and hence increasing both MCH conversion and ROP yield. Similar observations were made for the SRO of MCP over the same catalysts (**Table 3, Entry 10**). The correct metal loading, particle size and support acidity are key to increasing ROP yield at high MCH conversion; poor mass transport through zeolite channels often promotes coking and pore blockage, and hence mesoporous or hierarchically porous solid acid supported could prove beneficial.^{205, 5, 9}

Establishing the correct balance between metal hydrogenolysis activity, and support acidity and porosity, ring opening studies have explored non-zeolitic supports. Mesoporous materials such as Al-MCM-41 are alternatives to zeolites, offering a high surface area, tunable mesoporosity (2-20 nm), and low to moderate Brønsted acidity.²⁰⁶ High surface areas combined with large pore sizes and volumes should improve the accessibility of in-pore active sites and enhanced reactant/product diffusion thereby minimising secondary reactions and coking. The influence of support acidity on 1,2-DMCH conversion was investigated over Ir/Al-MCM-41 for different Si:Al ratios, and in the presence of Na,¹⁸⁸ and benchmarked against a strong acid support (H-Beta-25). Total (Brønsted and Lewis) acidity of Ir/Na-MCM-41 (Si:Al = 20), Ir/H-Al-MCM-41 (45), Ir/H-Al-MCM-41 (20), and Ir/H-Beta-25 was determined by pyridine FTIR (**Figure 17a**), and confirmed the expected decrease in acidity with increasing Si:Al ratio and Na doping. 1,2-DMCH conversion and ROP selectivity (**Figure 17b**) were greatest for moderately acidic Ir/H-Al-MCM-41(45), whereas the more acidic Ir/H-Beta-25 favoured cracking at the expense of ring opening. In contrast, Ir/Na-MCM-41 (20) exhibited low 1,2-DMCH conversion due to acid site neutralisation, with reactivity confined to hydrogenolysis over Ir NPs.

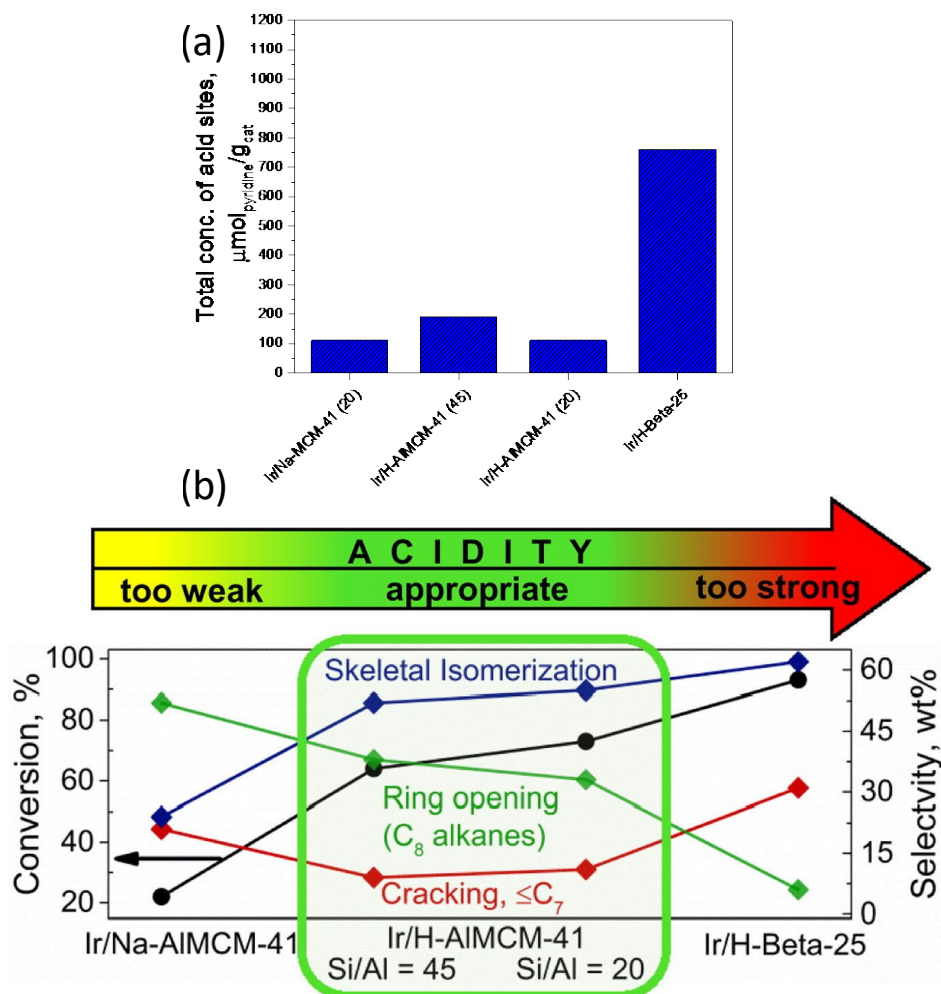


Figure 17. (a) Total acid site concentration over Ir/Na-MCM-41 (20), Ir/H-AIMCM-41 (45), Ir/H-AIMCM-41 (20) and Ir/H-Beta-25 catalysts. (b) Corresponding MCH conversions and selectivity for ring opening, isomerisation and cracking. Reproduced with permission from Ref ¹⁸⁸

Bifunctional Ir catalysts are also reported for SRO of bicyclic molecules (tetralin and decalin). 1 wt% Ir/SiO₂-Al₂O₃ catalysts with different SiO₂ content (30-80 wt%) were explored for decalin SRO at 300 °C and 5.2 MPa hydrogen pressure in a continuous fixed-bed reactor.¹⁹¹ Ir/SiO₂-Al₂O₃ (Si:Al=70:30) exhibited the highest decalin conversion (85 %) accompanied by a high ROP selectivity (62 %) (Table 3, Entry 18). Note that decalin SRO over monometallic Pt/SiO₂ and Ir/SiO₂ at 325 °C (i.e. non-acidic supports), favours dehydrogenation products,²⁰⁷ highlighting the requirement for acid sites to direct ring opening. Mesoporous supports such as Zr doped silica and amorphous SiO₂-Al₂O₃ (ASA) have also been studied for tetralin ring opening to limit cracking reactions.^{103, 104, 208} Selectivity to ROPs was approximately proportional to the acid:metal site ratio, with a low-loaded (<1 wt%) Ir/ASA (40 wt% silica) optimal for high ROP selectivity (>50 %) with minimal cracking (<10 %).¹⁰⁶ These catalysts also show promise for more realistic feedstocks, being tolerant to 100 ppm H₂S, albeit at a high reaction temperature (350 °C).

Ring opening of decalin over Pt or Ir modified zeolites generally gives C10 naphthenes with one remaining ring, so called open chain decanes (OCD). Formation of OCDs (discussed earlier) via decalin ring opening over bifunctional catalysts can still improve CN sufficient for diesel fuel applications. During

hydrotreating, cis-/trans- equilibrium mixtures of decalin undergo a series of reactions, including skeletal isomerisation and ring opening to single ring C₁₀ naphthenes (OCDs), in competition with undesired hydrocracking to <10 carbon atom hydrocarbons. From a practical perspective, a high degree of branching in OCDs formed by SRO is important for obtaining a high CN; OCDs are defined as decane isomers with $M = 142 \text{ g mol}^{-1}$ and molecular formula C₁₀H₂₂.

Decalin ring opening over a bimetallic Pt-Ir/H-Y zeolite (Si:Al = 13.3) gave a poor selectivity and yield of OCDs (5 % and 4 % respectively).⁹⁰ OCD yields can be improved by ion-exchange of zeolite frameworks to modulate acidity. For example, La³⁺ exchange into faujasite Na-X zeolite and subsequent metal modification produced Ir/La-X (Si:Al = 1.21) and Pt/La-X (Si:Al = 1.21) which respectively give 10 % and 12 % OCD yields.¹⁰⁷ Fine tuning of acid strength by ion-exchange of alkali cations into negative zeolite framework sites in 3 wt% Ir/H-Y (Si:Al = 2.41) is also reported,²⁰⁹ wherein, the Brønsted acid site density ($\mu\text{mol g}^{-1}$) at 200 °C decreased from Ir/Na, H-Y (191) > Ir/Rb, H-Y (160) > Ir/Li, H-Y (158) > Ir/K, H-Y (131) > Ir/Cs, H-Y (85). Na modified Ir/H-Y exhibited the highest OCD yield of 40 %. In contrast, a maximum yield of ROP+OCD products of 59 % (44 % OCDs) was reported for Cs ion-exchanged 3.4 wt% Ir/H-Beta(14) catalyst (Si:Al = 14 and 129 $\mu\text{mol}_{\text{H}^+} \cdot \text{g}^{-1}$ at 200 °C) (Table 3, Entry 15).¹⁹⁰ The opposing behaviour of Cs in suppressing and promoting SRO over Y and Beta zeolites respectively is attributed to two factors: (i) different acid strengths due to different Si:Al ratios; and (ii) a higher Ir content for the Beta zeolite resulting in enhanced hydrogenolysis activity. These materials were named High-Performance Ring opening Catalysts (HIPEROCS) due to their exceptional OCD yields, which are a consequence of large pores, a low number of Brønsted acid sites, and the high activity of Ir for endocyclic C-C bond hydrogenolysis (Figure 18a and Figure 18b bold arrows). Undesired side reactions in Figure 18b are favoured when the concentration and/or strength of acid sites are too high.^{107, 190, 210}

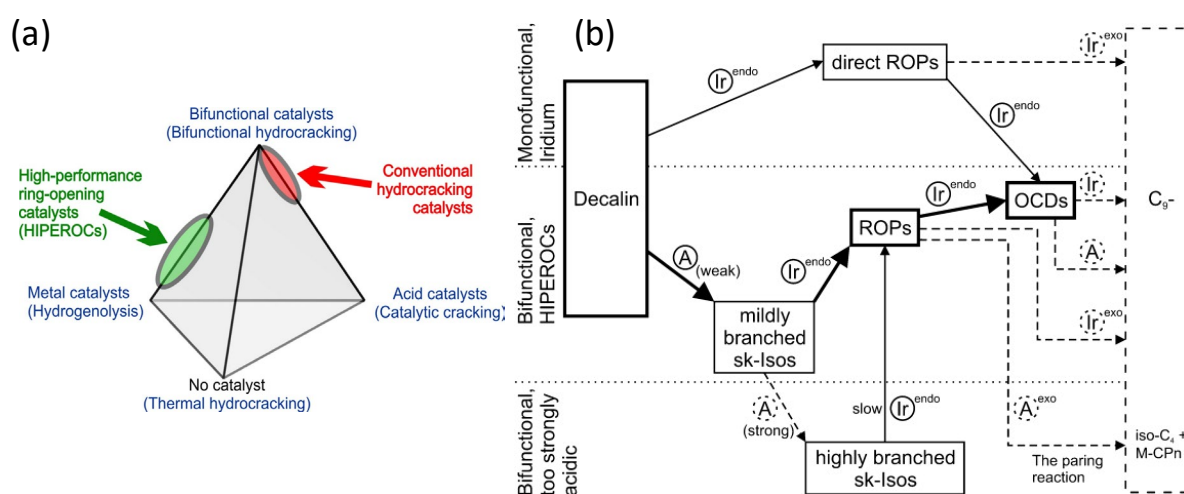


Figure 18. (a) Impact of metal and acid properties on different reaction pathways, and optimal balance achieved by high-performance ring opening catalysts (HIPEROCS). b) Proposed reaction network for decalin SRO to OCDs on HIPEROCS (bold arrows in centre of figure): A = Brønsted acid sites; dashed arrows show undesired reactions; Endo and Exo denote ring opening and demethylation, respectively. Reproduced with permission from Ref¹⁹⁰.

The introduction of mesopores in Beta zeolite via surfactant-assisted desilication has been explored as a means to improve mass transport via pore hierarchy. This approach improved ROP yield and selectivity during decalin SRO over bifunctional (weakly acidic) 3 wt% Ir and Pt/Cs- β -meso catalysts.¹³⁹ Figure 19 reveals a very high, maximum combined (ROP+OCD) yield of 72.6 wt% at 89.2 % decalin conversion (81.4 % selectivity) (Table 3, Entry 16), representing the highest reported yield to date, and superior to similar HIPEROC systems based on conventional (microporous) zeolites.¹⁹⁰

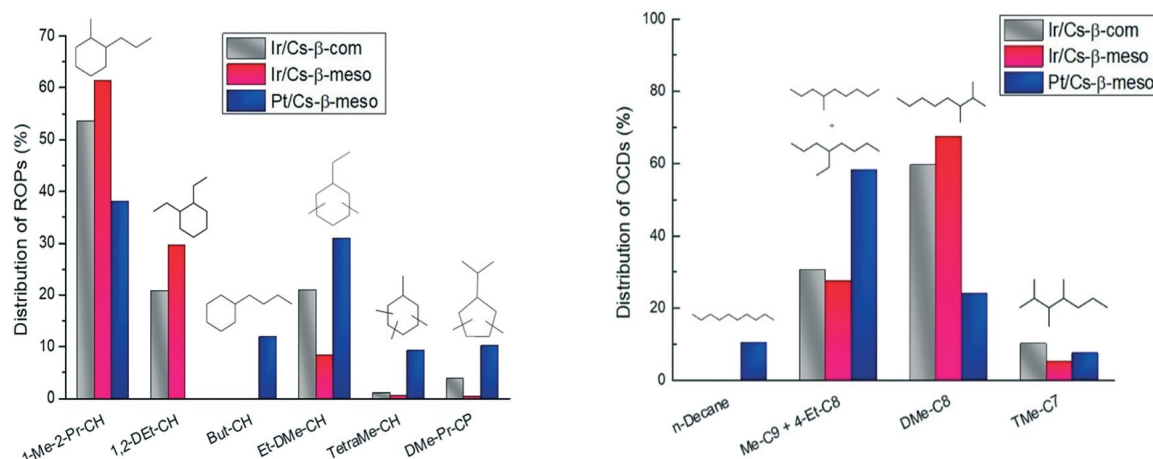


Figure 19. (a) Major ROP isomers from decalin SRO over Ir and Pt/Cs- β catalysts at 30–40 % conversion: 1-Me-2-Pr-CH = 1-methyl-2-propylcyclohexane; 1,2-DEt-CH = 1,2-diethylcyclohexane; But-CH = butylcyclohexane; Et-DMe-CH = ethyldimethylcyclohexanes; TetraMe-CH = tetramethylcyclohexane; DMe-Pr-CP = dimethylpropylcyclopentanes. (b) Distribution of OCDs from decaline SRO over Ir and Pt/Cs- β catalysts at 30–40 % conversion. Reproduced with permission from Ref¹³⁹.

Kinetic modelling of decaline SRO over Ir/H-Beta between 275–350 °C and 3–6 MPa H₂,¹⁸⁹ found ring opening of isomers exhibited the lowest activation energy (141 kJ/mol) and cracking the highest energy (159 kJ/mol). The ring opening barrier for Ir/H-beta was also lower than that for Pt/H-beta, consistent with the higher efficiency of Ir catalysts for decalin SRO.¹⁸⁹

Bifunctional Rh/zeolites are less studied for SRO of mono- and bicyclic molecules. MCP and MCH ring opening and ring enlargement (RE) is reported over Rh/HY, Rh/NaY, Rh/NaY(neutral), Rh/SiO₂ and a physical mixture of Rh/NaY+Rh/NaY(neutral) catalysts.⁸⁷ As per Table 2, Entry 32, Rh/SiO₂ exhibits 92.4 % selectivity to ROPs (2-MP, 3-MP and n-H) from MCP, with a statistical distribution of 2-MP:3-MP (2.28:1). Surprisingly, turnover frequencies at 200 °C based on rates of ring opening the aforementioned Rh catalysts were as follows: Rh/SiO₂ ($318 \times 10^{-4} \text{ s}^{-1}$) > Rh/NaY (neutral) ($112 \times 10^{-4} \text{ s}^{-1}$) > Rh/NaY ($30 \times 10^{-4} \text{ s}^{-1}$) > Rh/HY ($11 \times 10^{-4} \text{ s}^{-1}$). The low activity observed of Rh/HY was attributed to its propensity for ring enlargement products (low 2-MP/3-MP ratio) associated with Rh-proton adducts arising from the close proximity of metal clusters and acid sites (Table 3, Entry 20). A physical mixture of Rh₂O₃/HY zeolite and Mo-Ni oxide was also explored for naphthalene ring opening in the presence of water.¹²⁷ The physical mixture of catalysts exhibited 100 % naphthalene conversion and 18 % decalin and 51 % ROP selectivity.

Water addition increase the ROP yield to 63 %, ascribed to adsorption at the zeolite surface and concomitant inhibition of condensation reactions which generate heavy compounds from aromatics (Scheme 8). Pd/HY is also reported as a bifunctional catalyst for naphthalene ring opening.^{131, 132} Although initial conversion is very high (98 %) resulting in 53 % ROP yield (300 °C and 3 MPa H₂) (Table 3, Entry 23),¹³¹ selectivity to ROPs decreased to only 30 % after 5 h on stream due to carbon deposition (8.2 wt%) and corresponding micropore blockage (surface area falling from 589 m² g⁻¹ to 340 m² g⁻¹). Less carbon deposition was observed for tetralin and decalin SRO over Pd/HY (6.8 and 3.1 wt% respectively), suggesting that efficient hydrogenation of polyaromatics is critical to preventing deactivation.

Non-noble metals, including W, Mo and Fe, have been incorporated into mesoporous catalysts (Table 3, Entries 25 and 26) for MCP ring opening,^{194, 195, 211} wherein metal speciation gives rise to metallic and acidic (metal oxide) functions. W-MCM-48 (Si:W=40, 1234 m² g⁻¹, 2.3 nm pore diameter) was examined for MCP ring opening reaction at 450 °C under 1 bar H₂, but exhibited low conversion (<2 %) and no ring opening products. Mesoporous Fe/KIT-6, Mo/KIT-6 and Fe-Mo/KIT-6 prepared by solid-solid methods were also tested, but yielded only cracking products.²¹¹ MCP conversion followed the sequence 1.5Mo-0.3Fe/KIT-6 (0.29 %) > 0.3Fe/KIT-6 (0.26 %) > 1.5Mo/KIT-6 (0 %). Low MCP conversions (0.3-9.5 %) are also reported for a mesoporous Fe-TUD-1 catalyst,¹⁹⁵ for which it was concluded that small Fe clusters promoted multiple C-C bond cleavage, favouring C₁ molecules. These observations are expected since reactions were performed at 400 °C, where cracking is thermodynamically favoured, however single site Fe-O-Si species did exhibit selectivity towards MCP ring opening via a metallocyclobutane intermediate. Although it appears that MCP ring opening is governed by the hydrogenolysis activity of Fe and support acidity, lower temperature measurements for supports of varying pore size/network connectivity are required to conclude whether the internal porosity influences SRO for mesoporous Fe solid acid catalysts. Nevertheless, it seems clear that non-noble metals show poor activity towards MCP and promote deep cracking rather than ring opening.

In summary, ring opening of bicyclic naphthenes necessitates bifunctional catalysts, with the best ROP selectivity obtained with for noble metals on porous acid supports which possess a low concentration of Brønsted acid sites. The performance advantage of such bifunctional catalysts over metal-only catalysts derives from acid-catalysed isomerisation of 6-membered rings into 5-membered rings, which facilitate hydrogenolysis of resulting endocyclic C-C bonds, enabling the production of acyclic molecules without loss of carbon atoms. Selectivity for ROPs is higher for bifunctional metal/acid catalysts than metal-only counterparts. Bifunctional metal/acid catalysts can be divided into two classes: (1) metal/zeolite; and (2) metal/non-zeolite. Pt- and Ir-containing K, Cs, Rb-exchanged Y zeolites with low and weak Brønsted acidities are the most selective to ROPs, with an Ir modified, Cs⁺ ion-exchanged Beta zeolite (Si:Al = 14) offering optimal SRO performance. Bifunctional catalysts employing MCM-41, SiO₂-Al₂O₃ or ZrO₂-SiO₂/WO₃ solid acids (with weaker Brønsted acid sites) have also shown some promise, however ROP

yields remain far lower than zeolite analogues (e.g. **Table 3, Entry 16 vs Entry 18**). Further research on mesoporous and hierarchical porous bifunctional catalysts is required to optimise the metal-acid synergy and molecular mass transport, and thereby suppresses secondary reactions and associated coking.

4.2.2 Bimetallic/solid acid catalysts

As discussed in **Section 4.1.2**, bimetallic catalysts can be advantageous for achieving high ROP selectivity. Pt-Ir is one of the most promising combinations for SRO, and has been investigated in conjunction with Nb₂O₅ as a solid acid support¹⁵¹ Decalin SRO was compared for Pt/Nb₂O₅ and Ir/Nb₂O₅ at loadings of 0.3, 0.5 and 0.7 wt%, and 1 wt% Pt-Ir/Nb₂O₅ with different Ir:Pt molar ratios (0.5, 1 and 2) at 350 °C and 3.5 MPa H₂ (**Figure 20**). Highest selectivity for ROPs was observed for Ir(0.3)/Nb₂O₅ followed by Pt-Ir, with Pt the least selective. Pt addition increases selectivity to naphthalene at the expense of ROP due to its high dehydrogenation activity (**Table 3, Entry 29**);²¹² the hydrogenation \leftrightarrow dehydrogenation equilibrium for cyclic molecules shifts to the right at high temperatures (and reduced H₂ pressure).²¹³ Although bimetallic catalysts are often extolled as superior to monometallic counterparts, in this instance, Pt incorporation brings no benefits, with the lowest loading Ir/Nb₂O₅ catalyst (4.4 nm metal NPs) offering the optimal ROP selectivity and decalin conversion.

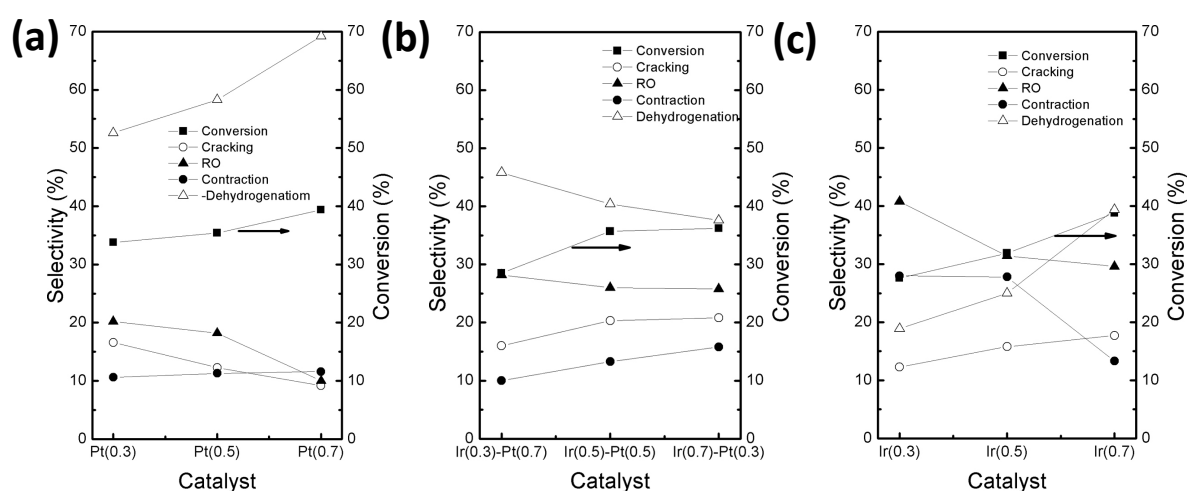


Figure 20. Decalin conversion and selectivity towards cracking, ring opening (RO), ring contraction and dehydrogenation products after 6 h of reaction for Nb₂O₅ supported (a) monometallic Pt, (b) bimetallic Pt-Ir, and (c) monometallic Ir catalysts. Reproduced with permission from Ref¹⁵¹.

Decalin ring opening over Ir modified Pt/Zr-MCM-41²¹⁴ delivered a maximum ROP selectivity of 26 % and yield of 16 % from decalin at 350 °C and 1.5 wt% Ir/0.75 wt% Pt. Increasing the reaction temperature to 400 °C enhanced decalin conversion to 56 %, but promoted undesired dehydrogenation.²¹⁵ Ir improved the thermal stability of Pt and ring opening selectivity. The behaviour was observed for Pt-

Ir/HY catalysts for decalin SRO with Ir and Pt contents between 0.5 to 1.5 wt%.²¹⁶ In contrast to the preceding niobia example, use of the HY zeolite support resulted in outstanding performance for a bimetallic Ir(1.0)Pt(1.0) catalyst at 350 °C, with high decalin conversion and a good ROP yield obtained (Table 3, Entry 31). Other noble bimetal combinations (Rh-Pd, Ir-Pd and Pt-Rh) are reported for SRO of mono- and bicyclic molecules, albeit with lower ROP yields than for Pt-Ir.

Supported Ni is considered a cost-effective alternative to noble metal catalysts due to its propensity for hydrogen activation under mild conditions (<300 °C and 3 MPa H₂).^{124, 217} Examples include NiW/Al₂O₃-USY (Table 3, Entry 27), Ni₂P/SiO₂-Al₂O₃ (Table 3, Entry 28), NiMoC/HY (Table 3, Entry 30a), and NiMoC/H-Beta (Table 3, Entry 30b)^{128, 129, 132, 137, 197, 218-221} and show promise for the partial hydrogenation of naphthalene to tetralin and decalin, which may subsequently react over acid sites to form isomerisation and ring opening products. NiMoC on different solid acid supports (HY, H-Beta, Al-SBA-15, and SiO₂-Al₂O₃) has also explored for decalin ring opening,⁹⁰ with HY and H-Beta variants offering the highest ROP yields, albeit typically <10 % and hence still inferior to (most costly) noble metal catalysts.¹⁹⁷

In summary, incorporating a second metal into bifunctional (metal/acid) catalysts has negligible benefits in terms of activity or ROP selectivity. Although Ir improves ring opening over Pt catalysts, Pt-Ir bimetallics are less selective, and no more active, than monometallic Ir catalysts; Pt catalysed dehydrogenation counters the hydrogenolysis performance of Ir. Bimetallics on acidic supports do not appear effective in suppressing cracking of ROPs from monocyclics, and deeper insight into the balance of metal-acid interactions is required. The influence of solid acid porosity (dimensions, hierarchy and connectivity) has yet to be explored, which may offer increased ROP selectivity and operating lifetime.

4.3 Comparison of transition metal vs bifunctional catalysts

Despite the plethora of catalyst formulations studied for SRO of mono- and bicyclic hydrocarbons, some common features emerge. Considering five membered rings (e.g. 2-MP), monometallic catalysts with hydrogenolysis activity are more selective to ROPs than bifunctional metal/solid acid catalysts, particularly when Pt and Ir are the chosen metal. Although, high MCP conversions are achievable over bifunctional catalysts, this requires elevated temperatures wherein cracking products are favoured. For monocyclics such as MCP, strongly acidic supports are undesirable since these also promote cracking of ROPs; neutral or weakly acidic supports (Al₂O₃ or SiO₂) are preferable in combination with noble metals. Mechanistically, a 'non-selective' mechanism is the optimum route to ROPs (2-MP and n-H) with an increased CN over < 2 nm Pt NPs. A 'selective' mechanism, operating via a metallocyclobutane intermediate to increase the n-H yield, would be more desirable, but is harder to direct, requiring metal-support adduct formation. Fine tuning of active metal NP size (and hence electronic and geometric properties of the active surface ensemble) can dramatically modify catalyst behaviour. Ir/γ-Al₂O₃ emerges as the most active catalyst for

MCP ring opening. Ir catalysts also the most active for high MCH conversion and good ROP selectivity, notably Ir/Al₂O₃ (and K, Na or Ni promoted variants). Iridium is also the only metal able to directly open the MCH ring; other metals require acid catalysed ring contraction prior to effecting hydrogenolysis and ring opening, necessitating a careful balance of acid and metal functions to obtain a high ROP selectivity.

Bimetallic catalysts have been successfully applied to indan ring opening, with the best systems exhibiting high selectivity for n-propyl benzene (n-PB) and 2-ethyl toluene (2-ET) products. As indan does not require a ring contraction step prior to ring opening (unlike tetralin and decalin), strong acid supports such as zeolites are not required, with Al₂O₃ proving adequate. Smaller NPs (<3 nm) of active metals are desirable to achieve C-C bond cleavage of the indan five membered ring to yield 2-ET and n-PB. Selectivity to ROPs for mono- and bimetallic catalysts follows the order Ir > Pt-Ir > Ru-Ir > Pd-Ir > Pt > Pd > Ru, highlighting the unique advantage of Ir for selective C-C bond cleavage. Note that while SRO of indan may be facile, it is not a good model naphthene for middle distillates, and associated studies are mainly useful for obtaining kinetic data on the reactivity of intermediates formed by ring contraction.

In the case of ring opening reactions involving two six membered rings, metal/solid acid catalysts are essential to cleave the C-C bond. Among transition metals exhibiting moderate to high activity for hydrogenolysis, Ir is the most selective for ring opening of C₆ molecules; other transition metals require acidic supports to catalyse contraction (to a C₅ ring) prior to C-C bond cleavage. The complexity of SRO for polycyclic molecules, and breadth of reaction conditions employed in the literature, hamper quantitative benchmarking of different catalyst formulations. Decalin is one of the few naphthenes for which a quantitative comparison of conversion and ROP yield under similar reaction conditions (Figure 21). In general, monometallic Ir catalysts (1-10 in Figure 21) exhibit the highest conversion and yield, although simple metal oxide supports (Al₂O₃, SiO₂ and Nb₂O₅), while attractive for industrial use because of their excellent mechanical and textural properties and low cost, do not provide sufficient strong Brønsted acid sites to drive significant ring opening. Analogous monometallic Pt catalysts (11-13) offer only modest conversion and favour dehydrogenation over ring opening resulting in low ROP yields. The combination of Ir and moderate acidity (Si:Al <25) zeolite supports afforded the most promising candidates for decalin SRO, with Ir/Cs-Beta-18 (7) and Ir/H-Beta-18 (6) exhibiting the highest RO yield (>70 wt%) outperforming all other zeolite supports (4-5 and 8-10) which were somewhat less active and selective. Beta zeolite also dramatically improves the activity and ring opening of Pt NPs (14), although protonated (15) and La doped HY (16) supports enable the highest ROP yield (35-45 wt%) for monometallic Pt catalysts. Pt-Ir bimetallics offer no significant advantage over Ir/acid catalysts, e.g, the best performing Pt-Ir/HY-3.16 only delivers ~56 wt% ROP (20). Judicial selection of the zeolite architecture and acidity thus appears even more significant than the choice of noble metal. Precious metal thrifting is a valuable strategy to improve the efficiency of Ir usage, exemplified by core@shell formulations such as Ir@Co for SRO of monocyclic rings,¹⁵⁰ although this strategy has not yet been extended to metal/acid variants for polycyclic naphthenes.

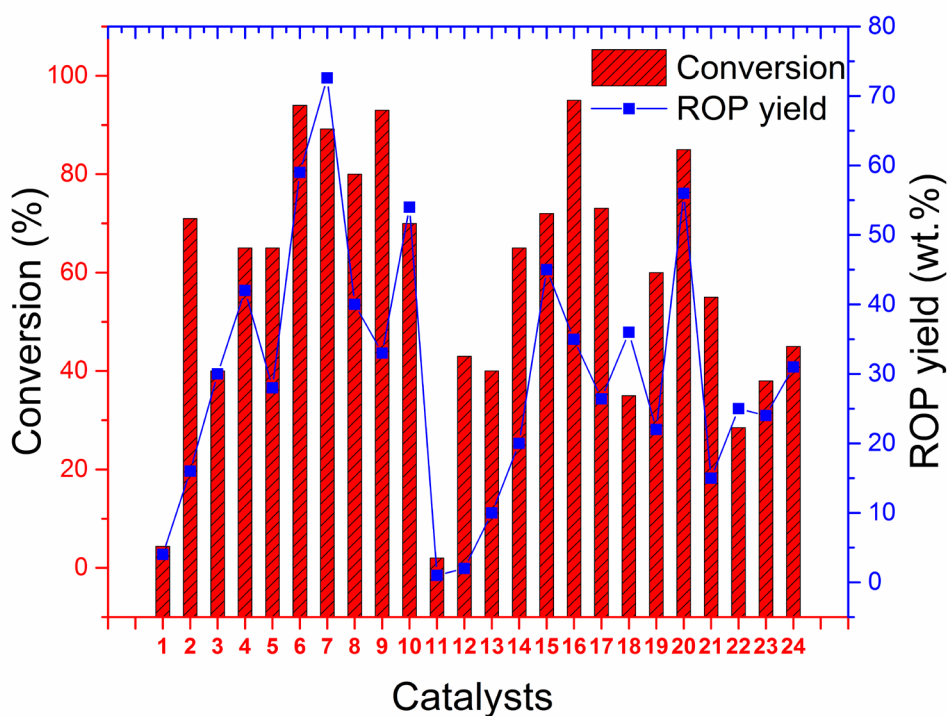


Figure 21. Decalin conversion and ring opening yield over different catalysts: (1) Ir/Al₂O₃; (2) Ir/SiO₂; (3) Ir/Nb₂O₅; (4) Ir/H-Beta-25; (5) Ir/H-Beta-300; (6) Ir/H-Beta-18; (7) Ir/Cs-Beta-18; (8) Ir/Cs-Beta-18-meso; (9) Ir/SiO₂-Al₂O₃-80; (10) Ir/La-HY-1.21; (11) Pt/Al₂O₃; (12) Pt/SiO₂; (13) Pt/Nb₂O₅; (14) Pt/Beta-25; (15) Pt/HY-3.16; (16) Pt/La-HY-1.21; (17) Pt/Al-SBA-15; (18) Rh/SiO₂-Al₂O₃; (19) Pd/SiO₂-Al₂O₃; (20) Pt-Ir/HY-3.16; (21) Pt-Ir/Zr-MCM-41; (22) Pt-Ir/Al₂O₃; (23) Pt-Ir/Nb₂O₅; (24) Rh-Pd/SiO₂-Al₂O₃. Metal loadings 1-3 wt%, 250-350 °C and 3-5 MPa H₂. Data compiled from Refs ^{81, 105, 107, 110, 132, 139, 151, 157, 189-192, 199, 202, 214}.

5. SRO of real feedstocks and sulfur poisoning

Ring opening of real oil feedstocks is challenging due to their molecular complexity which hinders product separation and quantitative analysis. LCO feedstocks contain a high concentration of polyaromatics (up to 90 wt%) and sulfur (4-6 wt%) resulting in low CN (18).²²² Fossil crude oil derived middle distillates are complex mixtures of thousands of compounds, with the major aromatic, naphthenic and benzo-naphthenic fractions comprising five- and six-membered rings bearing variable length alkyl groups and fused rings whose proportions depend on the final boiling point and oil characteristics.⁹⁸ Analysis of fossil crude oil from refineries indicates that the most abundant compounds are aromatics with two fused rings.^{11, 223} The complexity and high viscosity of LCO feedstocks dictates SRO at high H₂ pressure (>10 MPa) and temperature (400 °C).^{108,224} There are limited studies of SRO of real feedstocks using transition metal and bifunctional metal/acid catalysts (Table 5), and these focus on determining polyaromatic content and CN rather than reaction mechanisms.

Table 5. SRO of real oil feedstocks over **transition** metal and bifunctional metal/acid catalysts.

Entry	Catalyst	Feedstock type (boiling point range °C)	Density (g/cm ³)		Aromatic (wt%)		Sulfur (ppm)		CN		Ref.			
			Before	After	Before	After	Before	After	Before	After				
1	Pt-Pd/SiO ₂ - Al ₂ O ₃	LCO (180-360)	0.948	0.840	69.4	<3	19000	<1	27.2	45- 46	14			
2	NiW/AUSY-2	LCO (180-360)	-	-	56.9	19.8	920.2	23.9	25	39	225			
3	Pt/MSA	Hydro- desulfurized LCO (228-312)	0.888	0.827	-	-	-	-	34.2	43	70			
	Pt/ZSM-12			0.831								-	-	40
	Pt/USY			0.846								-	-	43
	Pt/Al ₂ O ₃			0.848								-	-	43
4	3.1%Ir/NaH-Y	Dearomatized	0.879	-	79.4	-	7900	31	33	43	108			
	4%Pt/NaH-Y	LCO (189-307)		-				-				25	53	
5	W-Ni/γ-Al ₂ O ₃	Shale oil (180- 360)	0.889	0.826	-	-	7500	47.9	33	51	226			
6	Ni-Mo/SiO ₂ - Al ₂ O ₃	LCO (189-360)	-	-	64.4	6.4	5000	27	32	50	64			
7	Ni-Mo/Al ₂ O ₃	LCO (180-360)	-	-	42.3	10.9	-	-	25	40	222			

Mesoporous ASA (Si:Al = 20) supported Pd-Pt (4:1 molar ratio) catalysts were explored under industrial conditions (285 °C, 12–48 h, H₂:feed = 600 N cm³/cm³ and LHSV = 1 h⁻¹) in a fixed-bed, lab-scale microreactor, for the treatment of a hydrogenated LCO feedstock containing 50 ppm sulfur.¹⁴ Approximately 80 % saturation of aromatic rings and an increase in CN from 36.6 to 44.1 was achieved, with the formation of <1 % of non-selective cracking products (Table 5, Entry 1). Process economics require that loss of oil through cracking to low-value light gases be minimised. Pd-Rh/SiO₂-Al₂O₃ are also reported for industrial feedstocks,⁹⁸ with the selectivity for ring opening compounds >60 % when lower Si:Al ratio supports were used. The Pd:Rh molar ratio (1:1 or 2:1) had little impact on activity. A seven-point improvement of CN from 39 to 46 was observed when reaction was performed at 280–300 °C, with <10% of non-selective cracking products formed. Pt/Al-SBA-15 (Pt loading 0-1.75 wt%) has also been explored for SRO of naphthenic compounds within hydrotreated light gas oil,¹⁰ affording a >90 % decrease in aromaticity and a maximum CN of 64 for a 1.5 wt% Pt loading. In contrast, Pt/HY was unable to improve the cetane index, mainly due to the formation of secondary cracking products, suggesting that the enhanced mass transport and milder acidity of mesoporous Al-SBA-15 are beneficial for SRO. This hypothesis is partially supported by the observation that Na-modified HY supports (with weaker acidity) enable selective Ir and Pt SRO catalysts.¹⁰⁸ Figure 22 shows the ring opening yields and Cetane Index (CI equivalent to CN) of a 3.1 % Ir/Na_{0.9}H_{0.1}-Y and 4.0 % Pt/Na_{0.88}H_{0.12}-Y catalyst during reaction (290 to 350 °C and 7.0 MPa H₂ in a down-flow fixed bed reactor) of dearomatized light cycle oil (DeAr-LCO) with an initial CN

of 41.7 (Table 5, Entry 4). The CI (CN) was calculated based on the fuel density and distillation range (ASTM D4737-04 method). Both Na-modified Ir and Pt catalysts exhibited low cracking yields and delivered a significantly improved CN, consistent with high SRO activity. In contrast, conventional Ir/USY and Ir/MSA (mesoporous silica alumina) showed high yields of cracking products, reflecting their stronger support acidity. At 20 % yield of cracking products, the CN for 3.1 wt% Ir/Na_{0.9}H_{0.1}-Y and 4.0 wt% Pt/Na_{0.88}, H_{0.12}Y increased to 53, compared to only 43 and 45 for as 2 wt% Ir/USY and 2 wt% Ir/MSA respectively.

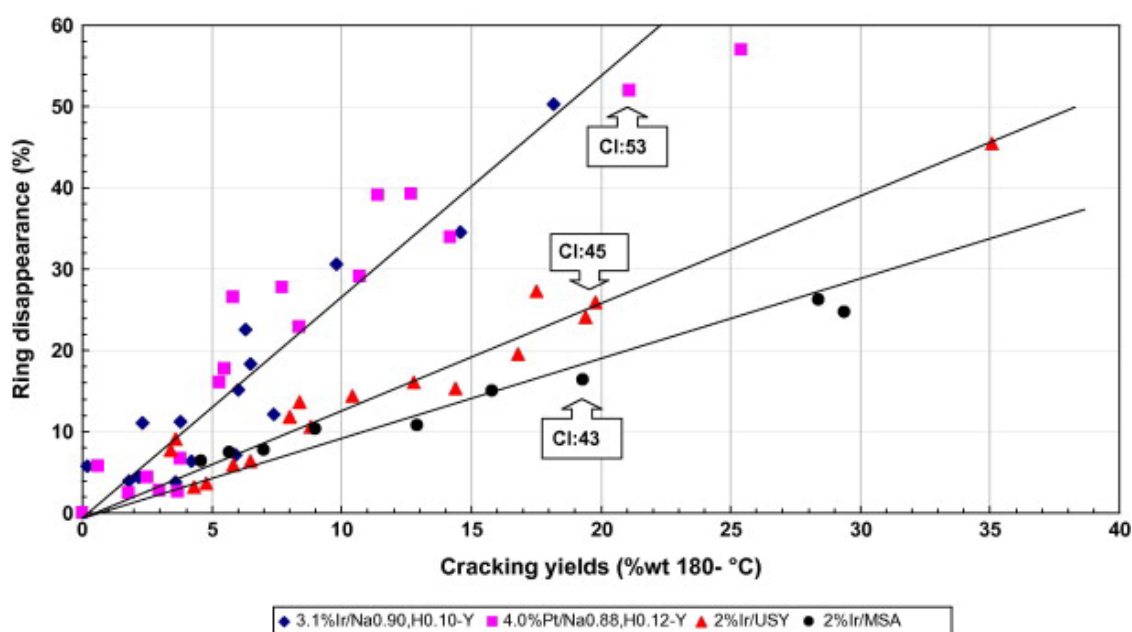


Figure 22. Comparison of high-performance, ring opening bifunctional catalysts using a LCO feedstock. Testing occurred in two stages: first, deep hydrodesulfurisation over a commercial sulfided NiMo catalyst; followed by deep dearomatization over the bifunctional catalysts. Reproduced with permission from Ref¹⁰⁸

Ring opening of hydrotreated light gas oil (HLGO) has also been investigated over less expensive Ni-Mo carbide catalysts using HY-zeolite,²²⁷ and benchmarked against Pt-Ir/HY. Ni-Mo carbide/HY improved the CN from 42 to 54 following SRO at 325 °C and 5 MPa H₂, outperforming Pt-Ir/HY (upgraded CN of 50). Stability tests revealed that the Ni-Mo carbide catalyst was stable for at least 168 h, whereas Pt-Ir/HY was deactivated after only 72 h, attributed to the greater resistance to coking of the former.

Sulfur tolerance is another desirable characteristic for effective SRO of real feedstocks, since residual H₂S at levels from 10 to 250 ppm can remain after hydrodesulfurisation in a refinery. Most noble metals are susceptible to sulfur poisoning, forming metal sulfides, resulting in a loss of conversion and selectivity to ring opening products,¹⁰⁶ however, metal-support interactions can weaken metal-sulfur bond, reducing their sensitivity to sulfidation.¹⁰⁶ Metals such as Pt exhibit structure-sensitivity for the SRO of MCP, hence it is also important to understand whether sulfur poisoning is also particle size dependent. To this end,

different bimetallic Pt catalysts (Pt-Ir, Pt-Re, Pt-Co and Pt-Cu) were pretreated with thiophene and subsequently evaluated for SRO (347 °C and 0.1 MPa H₂).¹⁴³ Thiophene exposure drastically lowered MCP conversion from >90 % for the parent catalysts to only 10 %. Sulfided catalysts also exhibited poor ROP yields (<9 % to 2-MP, 3-MP and n-hexane) and high (>90 %) benzene yields, suggesting that the sulfided catalysts lost metal hydrogenolysis activity but remained active for ring dehydrogenation. Exposure of an Ir/ASA catalyst to 50-200 ppm H₂S significantly impaired tetralin hydroconversion (350 °C and 4 MPa H₂),^{103, 106} favouring undesired dehydrogenation products (naphthalene). Catalytic activity was recovered after purging with H₂ and restoring S-free conditions, indicating preferential (reversible) inhibition of the metal hydrogenolysis function by sulfur. Pt, Ir or Pd (0.5 wt%) and cobalt (10 wt%) modified zirconium doped mesoporous silicas (Zr-MSU) are reported for tetralin conversion (at 315 °C, 4.5 MPa H₂) in the presence of 425 ppm dibenzothiophene (DBT).²⁰⁸ The Co₁₀Pt_{0.5} bimetallic maintained >90 % conversion to decalin in the presence of the sulfur feed for 5 h. Conversely, monometallic Pt was severely deactivated (conversion falling from 95 % to 20 %) by DBT, as widely reported in the literature.^{228, 229} Uniquely, Pt-S bonding appears to inhibit on-stream Co particle agglomeration thereby suppressing tetralin dehydrogenation. Ni catalysts would seem preferred candidates for hydroconversion of naphthenics in the presence of sulfur due to its lower cost relative to noble metals. Bifunctional NiW modified Zr-MSU was explored for tetralin conversion at 350 °C in the presence of <300 ppm DBT (H₂:tetralin molar ratio = 10.1 and 6 MPa H₂).²³⁰ Tetralin conversion of 80 % was attained despite the sulfur contaminant, but decreased to 59 % for [DBT] >1000 ppm. The formation of WS₂ at high sulfur concentrations was believed responsible for the lower conversion, possibly by hindering the metal/acid synergy necessary for SRO.

The preceding issue of noble metal deactivation by sulfur in the SRO of model compounds can be partly circumvented by LCO feed pretreatment by desulfurisation and dearomatisation processes. Non-noble metal sulfide catalysts are often used for the hydrodesulphurisation (HDS) of aromatic-rich LCOs, offering both hydrogenation and hydrogenolysis activity and inherent resistance to sulfur impurities, and consequently their potential as SRO catalysts has also been explored.^{230, 231} NiMo, NiW and CoMo are effective for hydrotreating and hydrocracking of middle distillates at temperatures spanning 300-450 °C and H₂ pressures of 3-5 MPa,^{64, 222, 232-235} and typically supported over γ -Al₂O₃, SiO₂ or TiO₂ due to their low cost and high hydrothermal stability.^{222, 232, 236} The effect of support acidity on HDS and dearomatisation was investigated over NiMo and CoMo supported on γ -Al₂O₃, alumina coated zeolite (ACZ) and TiO₂ for the hydrotreating of a LCO containing 4,700 ppm S and 72.5 wt% aromatics (360 °C and 5 MPa H₂ pressure). NiMo and CoMo both reduced the aromatic content <35 wt% irrespective of the support selection. It was postulated that the acidic ACZ support might favour hydrocracking reactions, thereby improving product quality, but under the deep desulfurisation conditions employed extensive cracking and coke formation was observed.²²² In some instances, migration of active promoters (e.g. Co or Ni) to external sites on the support surface is reported to enhance catalyst activity. For NiWS/Al₂O₃-USY,^{225, 230} a high

tetralin conversion (75–100 % at 340 °C, 4.0 MPa H₂ and a H₂:feed = 500) and ring opening selectivity (up to 39 % depending on support acidity) was achieved even in the presence of 920 ppm sulfur. Strong cooperation between metal sulfide and acid active sites was proposed to enhance SRO and restrict sulfur poisoning. The performance of NiWS/Al₂O₃-USY was validated against a hydrotreated LCO (57 vol% aromatics and CN = 25); the aromatic content was lowered to 19 % and CN raised to 37, reflecting good ring opening activity and limited cracking. Similar performance (31 wt% ROP yield) was observed over phosphorus modified NiW/USY-2/Al₂O₃ catalysts due to the synergy between acid and WS₂ hydrogenation sites.²³⁷ Bifunctional NiWS/SiO₂-Al₂O₃ has also been employed for decalin hydroconversion (350-380 °C and 5 MPa H₂) delivering a 17 % ROP yield even with the addition of 8000 ppm H₂S.²³⁸ A large reduction in the polyaromatic content of an LCO feed (from 64 wt% to 5 wt%) is reported for NiMoS/SiO₂-Al₂O₃ (380 °C and 6 MPa H₂);⁶⁴ however, the products did not satisfy diesel or gasoline fuel specifications, attributed to the harsh reaction conditions employed which promoted undesired hydrocracking in competition with desired hydrogenation, skeletal isomerisation and ring opening. Hence while sulfided NiMo or CoMo catalysts are effective for HDS, attempts to direct C-C bond cleavage under DDS conditions are less selective with SRO accompanied by cracking to light hydrocarbons.

6. Summary

SRO of naphthenic molecules is a key step in oil refining, which reduces particulate emissions from combustion of resulting diesel fuel by increasing the cetane number of poor quality LCO and waste pyrolysis oils (whether from plastics or lignocellulosic biomass). Various transition metal catalysts have been explored including noble and non-noble metal catalysts immobilised on neutral or acidic supports. Transition metals including Ni, Pd, Pt, Ir, Rh and Ru catalyse ring opening via hydrogenolysis pathways. However, their reactivity towards bicyclic reactants is lower than that for monocyclics, with bifunctional metal/solid acid catalysts required for the former. Iridium is the most active and selective metal for SRO of mono- and bicyclic naphthenes, with the less costly Pt, Pd and Ru less active and/or less selective for ring opening. Although Pd is less active than Ir, its higher ring opening selectivity suggests that active site identification and optimisation (possibly through surface alloying) should be pursued to improve activity. Ni would be the most desirable non-precious metal for SRO in terms of cost and hydrogenation activity, and promotes a similar surface reaction mechanism to Ir, but is less selective due to extensive cracking of ROPs (also observed for Ru). In general, bimetallic catalysts have not offered performance improvements over Ir, however the use of core-shell NPs has proved an effective means to maximise dispersion of this costly metal, and the synthesis of Ir single atom catalysts could offer another avenue to achieve metal thrifting. In contrast, bifunctional metal/acid catalysts show great promise for tuning SRO activity and selectivity; relative rates of ring opening and ring contraction are a strong function of the metal:acid ratio,

adjustable by varying both the support (acid site density and porosity) and metal (loading, particle size and use of promoters) properties. Strongly acidic catalysts are ill-suited for the ring opening of naphthenes due to their rapid deactivation through coking. Despite this promise, there remains a poor understanding of the nature of active sites, and their synergic interactions, in bifunctional catalysts, and these aspects are ripe for in-situ spectroscopic and computational studies to develop next-generation catalysts. Little is known about adduct formation at the metal/acid interface, believed responsible for directing metallocyclobutane pathways and concomitant large increases in CN. The role (if any) of Lewis acidity, and in-pore mass transport to active sites, is also poorly understood despite mesoporous Beta zeolite exhibiting some of the promising SRO results. Efficient mass transport of products out of catalyst particles is important to minimise undesired reactions of ROPs, and hierarchical micro- and mesoporous supports should enhance ROP selectivity while minimising coking and associated pore blockage and deactivation.

7. Challenges and Prospects

Significant progress has been made in the development of supported metal catalysts for the transformation of naphthenic components and associated upgrading of oil feedstocks to produce diesel fuels with desirable combustion properties. Bifunctional metal/acid catalysts offer the best combination of activity and ring opening selectivity for polycyclic compounds, facilitating endo C-C bond cleavage while mitigating cracking and dehydrogenation. Nevertheless, several challenges remain:

- (i) **Improved activity and selectivity.** Ring opening of polyaromatics is a unique form of hydroconversion, distinct from hydroisomerisation and hydrocracking. In the former chemistry, the molecular structure of the reactant is rearranged without loss of carbon, whereas in hydrocracking C-C bonds are broken non-selectively resulting in a broad distribution of C_n products including undesirable light volatiles and gases. Hydroisomerisation typically converts linear paraffins (n-alkanes) to their branched isomers, the opposite goal of SRO in which C-C bonds in rings are cleaved to produce linear (and some branched) alkanes. However, similar metal and acid active sites are involved in all three reaction classes, complicating the development of active SRO catalysts. Solving this challenge requires a deep understanding of metal/acid interactions, specifically how the proximity between active sites influences the chemistry of reactive intermediates (in the context of substrate channeling²³⁹) and whether metal and acid can alter one another's electronic and geometric structure.
- (ii) **Active metal dispersion and stability.** Most research has focused on low (~1-2 wt%) metal loadings to optimise SRO selectivity (avoiding cracking), but this necessarily lowers the number of potential active sites, problematic since current yields are not high enough for commercial application. Synthetic strategies such as the use of defective and ultra-high area supports (including precursors such as metal-

organic frameworks) offer a route to increasing the density of highly dispersed and thermally stable single atoms, clusters or NPs.

- (iii) Improved molecular mass transport to/from active sites. The most promising SRO catalysts are bifunctional materials employing microporous zeolites wherein diffusion of bulky naphthenics to in-pore active sites may be rate-limiting, and cracking over strong acid sites (a small fraction of which are likely present even for moderate Si:Al molar ratios) leading to pore blockage. Hierarchical porous supports offer the optimum balance of a high surface area and wider pores, the former essential for achieving high metal dispersion and the latter for enhancing mass transport.^{205, 240 241}
- (iv) Lowering metal cost. Most SRO studies address noble metals which (particularly Ir) can deliver high conversion and good selectivity from model and some real oil feeds. However, the cost of Earth scarce noble metals may be prohibitive, unless they can be efficiently recovered from spent catalysts and recycled. Although core@shell and single atom catalyst formulations can reduce precious metal loadings, it would still be preferable to find non-noble alternatives, with Ni, W and sulfided variants a promising starting point, especially given their superior tolerance to sulfur impurities in real feeds.
- (iv) Catalyst benchmarking. SRO is reported over a wide range of temperatures, H₂ pressures, reactor configurations and space velocities, and for diverse model and real feedstocks. Such variance greatly hinders quantitative comparisons of activity, selectivity and lifetime. Standardisation of testing conditions, and reporting of ROP selectivity at iso-conversion, would be beneficial to rapidly identify the most promising catalysts and derive quantitative structure-reactivity relationships. Use of parallel microreactors for screening multiple formulations under identical conditions should be explored.²⁴² Although defining and producing a real oil feed ‘standard’ composition is a thorny problem, this would greatly aid catalyst benchmarking, provided such test mixes were commercially available.

In addition to the preceding scientific challenges, industrial implementation of SRO technologies also requires comprehensive techno-economic (TEA) and life cycle analyses (LCA), particularly with regard to: (i) adding SRO processing units to existing refineries to produce diesel from lower quality crude oil; and (ii) co-processing of LCO with MSW or WPO pyrolysis oils to achieve catalytic ring opening of polycyclic molecules alongside cracking to e.g. propylene.²⁴³ To the authors’ knowledge no such peer-reviewed TEA/LCA studies are reported, and while such original research is beyond the scope of this review, are important areas for future research. The following discussion gives some indication of potential GHG reductions from waste to fuels and catalytic SRO processes. Catalysts for SRO have been developed and patented by several petroleum refineries, including ENI,¹⁹⁰ Akzo Nobel,²⁴⁴ and Exxon Mobil,²⁴⁵ with pilot

scale units developed by Saras Ricerche e Tecnologie SpA,¹⁰⁰ for the industrial upgrading of LCO in a two-stage hydroprocessing configuration (hydrotreatment/desulfurization, followed by SRO) with intermediate gas removal. In 2020, the Preemraff Lysekil refinery,²⁴⁶ formerly known as the Scanraff oil refinery, commissioned an agricultural residue pyrolysis oil conversion project for diesel production. Although cracking reactions do not produce useful diesel, higher value olefin by-products may offset lower fuel yields. The environmental impact of incorporating an SRO processing unit in a refinery for diesel production can be estimated from current carbon footprints of crude oil conversion. Well-to-wheel analysis of transportation fuel production from crude oil reveals the global average greenhouse gas (GHG) emission associated with a barrel of oil is 10.3 gram CO₂(eq)/MJ,²⁴⁷ with most of this from oil refining (10.2 gram CO₂(eq)/MJ for gasoline and 5.4 for diesel,²⁴⁸ **Figure 23**) linked to distillation and hydrogen production.

We envisage that SRO will operate in tandem with hydrotreating, albeit most likely as a separate reactor. Since SRO catalysts operate at or below reaction conditions used in hydrotreatment for diesel production (typically 350°C and 80 Bar H₂),²⁴⁹ incorporation of a SRO step should not significantly increase the overall carbon footprint. However, hydrogen costs are expected to rise although these are expected to be offset by emergence of cost-effective green hydrogen. Hydrogen is also typically in a 10 mole excess in hydrotreating, hence costs for separation and recycling hydrogen are unlikely to significantly increase on addition of a SRO unit, although capital costs will be higher because of the additional reactor and a separation unit to remove cracked products. At current oil prices of \$80 per barrel, catalyst costs for a refinery (where recycling schemes exist) are a small fraction of the plant operation, and hence the choice of noble on non-noble metal catalysts will have little impact on sustainability, particularly if metal thrifting strategies are exploited. Nevertheless, since the optimum noble metal containing SRO catalyst to date is based on Ir(Pt) catalysts (~3 wt% metal loading) on an alkaline earth metal exchanged H-Beta zeolite support, it would be desirable to reduce metal loadings and develop more economical syntheses of mesoporous zeolites to enable scale-up for refineries while mitigating the environmental impact of catalyst production.²⁵⁰ Many Ni SRO catalysts operate at >50 wt% metal loadings, and considering current demands for energy storage applications, the price of Ni is likely to rise; commercial SRO processes are this likely to focus on more robust noble metals for the foreseeable future.

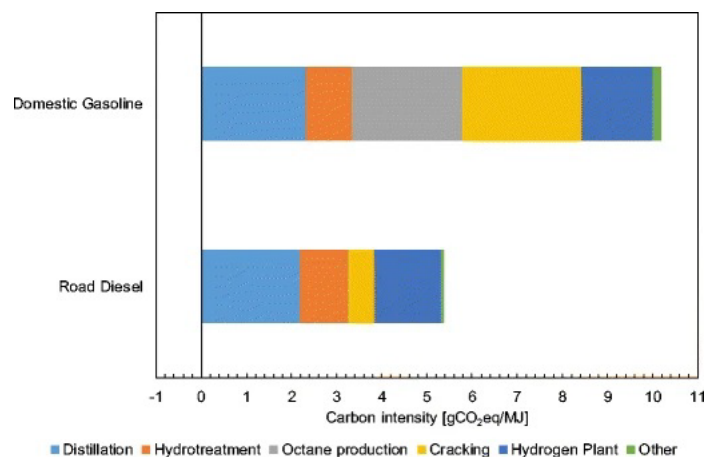


Figure 23: Carbon footprint for units employed in crude oil refining to gasoline or diesel. Reproduced with permission from ref 248.

If the oil feedstock is blended with e.g. MSW pyrolysis oils, then a different Waste-to-wheel scenario emerges, in which the exploitation of waste streams offers significant GHG savings versus landfill or incineration. An LCA study of fuel production from North Carolina MSW reveals 1250 g CO₂(eq)/kg(MSW) are produced.²⁵¹ Assuming a 50 % yield of bio-oil with an energy density of ~17 MJ/kg,²⁵² the carbon footprint of MSW derived fuel would be (2x1250)/17 = 147g CO₂ (eq)/MJ. Although higher than from crude oil refining, this footprint is countered by significant GHG emission savings from the diversion of MSW away from landfill.²⁵¹ Pyrolysis oil production from MSW, comprising yard waste (49.1 %), paper (9.1 %), plastics (LDPE, HDPE, PET and PP, 6.26 %), textile (4.85 %), food waste (1.19 %), polystyrene (0.41 %) and rubber (0.32 %) reduced GHG emissions by 42 % compared to waste landfilling.²¹ Future techno-economic and life cycle analyses could provide useful insight into the optimum fate of polycyclic fractions, and whether SRO competes favourably with cracking and distillation to alternative products. Catalyst and process development (at least in the open literature) has focused on maximising selectivity to ROPs while minimising cracking. An alternative strategy, alluded to above and which requires further investigation, is to deliberately select SRO catalysts which support some cracking (e.g. to C3 or C4 alkanes or alkenes) to create higher value chemicals. As global energy infrastructure transitions to renewables, oil refineries may in future shift their focus towards increased chemicals production; this will likely impact on existing petrochemical markets since oil refineries operate at a larger scale than chemical plants. Some new refineries are already targeting significant petrochemical production instead of solely transportation fuels with the aim of converting 40–60 % of feedstock into chemicals such as p-xylene, benzene, ethylene and propylene.²⁰³

In summary, liquid transportation fuels are likely to remain an important component of the energy mix for the foreseeable future, particularly for diesel use in heavy duty/long distance vehicles. Ring opening catalysis is anticipated play a critical role in valorising lower grade crude oil feedstocks (and oils sourced from waste and biomass pyrolysis) by improving fuel quality and reducing the environmental impact of particulate emissions. A detailed techno-economic analysis would prove invaluable for guiding the

feedstock and catalyst selection, process operating conditions, and targeted products (high CN diesel components versus light chemicals).

8. Acknowledgments

We thank Southern Oil and the Australian Department for Business for funding under the Cooperative Research Centres Projects (CRCP) Grants Scheme (CRCPEIGHT000194) and the ARC (LP190100849).

9. References

1. V. G. Yadav, G. D. Yadav and S. C. Patankar, *Clean Technologies and Environmental Policy*, 2020, **22**, 1757-1774.
2. *BP Statistical Review of World Energy 2021, 70th edition*, 2021.
3. L. Rivera-González, D. Bolonio, L. F. Mazadiego, S. Naranjo-Silva and K. Escobar-Segovia, *Sustainability*, 2020, **12**, 472.
4. *World Energy Outlook 2021*, IEA, Paris International Energy Authority, 2021.
5. A. Osatiashtiani, B. Puértolas, C. C. S. Oliveira, J. C. Manayil, B. Barbero, M. Isaacs, C. Michailof, E. Heracleous, J. Pérez-Ramírez, A. F. Lee and K. Wilson, *Biomass Conversion and Biorefinery*, 2017, **7**, 331-342.
6. B. Sørensen, in *Renewable Energy (Third Edition)*, ed. B. Sørensen, Academic Press, Burlington, 2004, DOI: <https://doi.org/10.1016/B978-012656153-1/50018-2>, pp. 29-209.
7. V. Chintala, *Renewable and Sustainable Energy Reviews*, 2018, **90**, 120-130.
8. *World Energy Outlook 2020*, IEA, Paris International Energy Authority, 2020.
9. J. C. Manayil, A. Osatiashtiani, A. Mendoza, C. M. A. Parlett, M. A. Isaacs, L. J. Durndell, C. Michailof, E. Heracleous, A. Lappas, A. F. Lee and K. Wilson, *ChemSusChem*, 2017, **10**, 3506-3511.
10. K. C. Mouli, O. Choudhary, K. Soni and A. K. Dalai, *Catalysis Today*, 2012, **198**, 69-76.
11. B. H. Cooper and B. B. L. Donniss, *Applied Catalysis A: General*, 1996, **137**, 203-223.
12. G. B. McVicker, M. Daage, M. S. Touvelle, C. W. Hudson, D. P. Klein, W. C. Baird, B. R. Cook, J. G. Chen, S. Hantzer, D. E. W. Vaughan, E. S. Ellis and O. C. Feeley, *Journal of Catalysis*, 2002, **210**, 137-148.
13. R. Cataluña and R. da Silva, *Journal of Combustion*, 2012, **2012**, 738940.
14. M. Jacquin, D. J. Jones, J. Rozière, A. J. López, E. Rodríguez-Castellón, J. M. Trejo Menayo, M. Lenarda, L. Storaro, A. Vaccari and S. Albertazzi, *Journal of Catalysis*, 2004, **228**, 447-459.
15. E. Dobrzyńska, M. Szewczyńska, M. Pośniak, A. Szczotka, B. Puchałka and J. Woodburn, *Environmental Pollution*, 2020, **259**, 113772.
16. A. C. Lloyd and T. A. Cackette, *Journal of the Air & Waste Management Association*, 2001, **51**, 809-847.
17. M. Han, D. N. Assanis and S. V. Bohac, *Combustion Science and Technology*, 2009, **181**, 496-517.
18. M. Lindgren, K. Arrhenius, G. Larsson, L. Bäfver, H. Arvidsson, C. Wetterberg, P.-A. Hansson and L. Rosell, *Atmospheric Environment*, 2011, **45**, 5394-5398.
19. X.-c. Lü, J.-g. Yang, W.-g. Zhang and Z. Huang, *Energy & Fuels*, 2005, **19**, 1879-1888.
20. <https://www.acea.auto/figure/passenger-car-fleet-by-fuel-type/>, (accessed December, 2021).
21. V. Chhabra, A. Parashar, Y. Shastri and S. Bhattacharya, *Industrial & Engineering Chemistry Research*, 2021, **60**, 1473-1482.
22. G. A. Marrero, J. Rodríguez-López and R. M. González, *SERIEs*, 2020, **11**, 203-241.
23. E. Zervas and C. Lazarou, *International Journal of Energy Research*, 2007, **31**, 192-203.
24. J. Hendrikse, M. Grutters and F. Schäfer, in *Identifying Ignitable Liquids in Fire Debris*, eds. J. Hendrikse, M. Grutters and F. Schäfer, Academic Press, 2016, DOI: <https://doi.org/10.1016/B978-0-12-804316-5.00003-4>, pp. 7-16.
25. G. Rong, Y. Zhang, J. Zhang, Z. Liao and H. Zhao, *Industrial & Engineering Chemistry Research*, 2018, **57**, 1547-1559.
26. S. Bezergianni, A. Dimitriadis, O. Kikhtyanin and D. Kubička, *Progress in Energy and Combustion Science*, 2018, **68**, 29-64.

27. S. Fraser, in *Distillation*, eds. A. Górak and H. Schoenmakers, Academic Press, Boston, 2014, DOI: <https://doi.org/10.1016/B978-0-12-386876-3.00004-1>, pp. 155-190.
28. G. C. Laredo, P. M. Vega Merino and P. S. Hernández, *Industrial & Engineering Chemistry Research*, 2018, **57**, 7315-7321.
29. Y. Oh, H. Noh, H. Park, H. Han, T.-B. Nguyen and J. K. Lee, *Catalysis Today*, 2020, **352**, 329-336.
30. C. Tóth, D. Sági and J. Hancsók, *Topics in Catalysis*, 2015, **58**, 948-960.
31. R. B. Ahmad Ghaddar, Rising use of plastics to drive oil demand to 2050: IEA, <https://www.reuters.com/article/us-petrochemicals-iaa-idUSKCN1ME2QD>, (accessed January, 2022).
32. K. D. Sharma and S. Jain, *Social Responsibility Journal*, 2020, **16**, 917-948.
33. F. Ateş, N. Miskolczi and N. Borsodi, *Bioresource Technology*, 2013, **133**, 443-454.
34. C. Dorado, C. A. Mullen and A. A. Boateng, *ACS Sustainable Chemistry & Engineering*, 2014, **2**, 301-311.
35. W. Shi, Y. Gao, S. Song and Y. Zhao, *Industrial & Engineering Chemistry Research*, 2014, **53**, 11557-11565.
36. C. L. Williams, C.-C. Chang, P. Do, N. Nikbin, S. Caratzoulas, D. G. Vlachos, R. F. Lobo, W. Fan and P. J. Dauenhauer, *ACS Catalysis*, 2012, **2**, 935-939.
37. J. M. J. M. Ravasco and R. F. A. Gomes, *ChemSusChem*, 2021, **14**, 3047-3053.
38. T. R. Carlson, Y.-T. Cheng, J. Jae and G. W. Huber, *Energy & Environmental Science*, 2011, **4**, 145-161.
39. Y. Zheng, J. Wang, C. Liu, X. Lin, Y. Lu, W. Li and Z. Zheng, *Journal of the Energy Institute*, 2020, **93**, 1833-1847.
40. Y.-T. Cheng and G. W. Huber, *Green Chemistry*, 2012, **14**, 3114-3125.
41. J. Q. Bond, A. A. Upadhye, H. Olcay, G. A. Tompsett, J. Jae, R. Xing, D. M. Alonso, D. Wang, T. Zhang, R. Kumar, A. Foster, S. M. Sen, C. T. Maravelias, R. Malina, S. R. H. Barrett, R. Lobo, C. E. Wyman, J. A. Dumesic and G. W. Huber, *Energy & Environmental Science*, 2014, **7**, 1500-1523.
42. X. Zhang, H. Lei, L. Zhu, M. Qian, X. Zhu, J. Wu and S. Chen, *Applied Energy*, 2016, **173**, 418-430.
43. G. Nie, X. Zhang, L. Pan, M. Wang and J.-J. Zou, *Chemical Engineering Science*, 2018, **180**, 64-69.
44. P. Sushma, *IOP Conference Series: Materials Science and Engineering*, 2018, **455**, 012066.
45. S. Kaza, L. Yao, P. Bhada-Tata and F. Van Woerden, *What a waste 2.0: a global snapshot of solid waste management to 2050*, World Bank Publications, 2018.
46. S. Bezergianni, A. Dimitriadis, G.-C. Faussone and D. Karonis, *Energies*, 2017, **10**.
47. R. Geyer, J. R. Jambeck and K. L. Law, *Science Advances*, 2017, **3**, e1700782.
48. M. Z. H. Khan, M. Sultana, M. R. Al-Mamun and M. R. Hasan, *Journal of Environmental and Public Health*, 2016, **2016**, 7869080.
49. S. L. Wong, N. Ngadi, T. A. T. Abdullah and I. M. Inuwa, *Renewable and Sustainable Energy Reviews*, 2015, **50**, 1167-1180.
50. D. Zhao, X. Wang, J. B. Miller and G. W. Huber, *ChemSusChem*, 2020, **13**, 1764-1774.
51. A. Lopez-Uribebarrenechea, I. de Marco, B. M. Caballero, M. F. Laresgoiti and A. Adrados, *Journal of Analytical and Applied Pyrolysis*, 2012, **96**, 54-62.
52. Y. Zhang, D. Duan, H. Lei, E. Villota and R. Ruan, *Applied Energy*, 2019, **251**, 113337.
53. Plastic Odyssey: Around the world powered by plastic, <http://www.ifsma.org/tempannounce/aga44/Plastic%20Odyssey%20Brochure.pdf>, (accessed January, 2022).
54. K. Moorthy Rajendran, V. Chintala, A. Sharma, S. Pal, J. K. Pandey and P. Ghodke, *Materials Today Communications*, 2020, **24**, 100982.
55. W. Ferdous, A. Manalo, R. Siddique, P. Mendis, Y. Zhuge, H. S. Wong, W. Lokuge, T. Aravinthan and P. Schubel, *Resources, Conservation and Recycling*, 2021, **173**, 105745.
56. F. Campuzano, A. G. Abdul Jameel, W. Zhang, A.-H. Emwas, A. F. Agudelo, J. D. Martínez and S. M. Sarathy, *Energy & Fuels*, 2020, **34**, 12688-12702.
57. G. C. Laredo, P. Pérez-Romo, J. Escobar, J. L. Garcia-Gutierrez and P. M. Vega-Merino, *Industrial & Engineering Chemistry Research*, 2017, **56**, 10939-10948.
58. M. Attia, S. Farag and J. Chaouki, *Catalysts*, 2020, **10**, 1381.
59. A. Alvarez-Majmutov, S. Badoga, J. Chen, J. Monnier and Y. Zhang, *Energy & Fuels*, 2021, **35**, 9983-9993.
60. M. B. Griffin, K. Lisa, H. Wang, A. Dutta, K. A. Orton, R. J. French, D. M. Santosa, N. Wilson, E. Christensen, C. Nash, K. M. Van Allsburg, F. G. Baddour, D. A. Ruddy, E. C. D. Tan, H. Cai, C. Mukarakate and J. A. Schaidle, *Energy & Environmental Science*, 2018, **11**, 2904-2918.
61. V. A. Valles, Y. Sa-ngasaeng, M. L. Martínez, S. Jongpatiwut and A. R. Beltramone, *Fuel*, 2019, **240**, 138-152.
62. J. Shen and N. Semagina, *ACS Catalysis*, 2014, **4**, 268-279.

63. A. Martínez, M. A. Arribas and S. B. C. Pergher, *Catalysis Science & Technology*, 2016, **6**, 2528-2542.
64. G. Escalona, A. Rai, P. Betancourt and A. K. Sinha, *Fuel*, 2018, **219**, 270-278.
65. H. Du, C. Fairbridge, H. Yang and Z. Ring, *Applied Catalysis A: General*, 2005, **294**, 1-21.
66. R. C. Santana, P. T. Do, M. Santikunaporn, W. E. Alvarez, J. D. Taylor, E. L. Sughrue and D. E. Resasco, *Fuel*, 2006, **85**, 643-656.
67. H. Shi, X. Li, G. L. Haller, O. Y. Gutiérrez and J. A. Lercher, *Journal of Catalysis*, 2012, **295**, 133-145.
68. A. Galadima and O. Muraza, *Fuel*, 2016, **181**, 618-629.
69. I. Fechete and J. C. Védrine, *Comptes Rendus Chimie*, 2018, **21**, 408-418.
70. V. Calemma, R. Giardino and M. Ferrari, *Fuel Processing Technology*, 2010, **91**, 770-776.
71. P. T. M. Do, S. Crossley, M. Santikunaporn and D. E. Resasco, in *Catalysis: Volume 20*, The Royal Society of Chemistry, 2007, vol. 20, pp. 33-64.
72. J. Govindhakannan, K. Chandra Mouli, A. Phoenix, C. F. Fairbridge and A. K. Dalai, *Fuel*, 2012, **97**, 400-410.
73. M. A. Arribas, A. Corma, M. J. Díaz-Cabañas and A. Martínez, *Applied Catalysis A: General*, 2004, **273**, 277-286.
74. D. Kubička, N. Kumar, P. Mäki-Arvela, M. Tiitta, V. Niemi, H. Karhu, T. Salmi and D. Y. Murzin, *Journal of Catalysis*, 2004, **227**, 313-327.
75. J.-W. Park, K. Thomas, J. van Gestel, J.-P. Gilson, C. Collet, J.-P. Dath and M. Houalla, *Applied Catalysis A: General*, 2010, **388**, 37-44.
76. R. Moraes, K. Thomas, S. Thomas, S. Van Donk, G. Grasso, J.-P. Gilson and M. Houalla, *Journal of Catalysis*, 2012, **286**, 62-77.
77. D. Kubička, N. Kumar, P. Mäki-Arvela, M. Tiitta, V. Niemi, T. Salmi and D. Y. Murzin, *Journal of Catalysis*, 2004, **222**, 65-79.
78. P. Castaño, A. G. Gayubo, B. Pawelec, J. L. G. Fierro and J. M. Arandes, *Chemical Engineering Journal*, 2008, **140**, 287-295.
79. A. Raichle, Y. Traa, F. Fuder, M. Rupp and J. Weitkamp, 2001, **40**, 1243-1246.
80. H. S. Cerqueira, P. C. Mihindou-Koumba, P. Magnoux and M. Guisnet, *Industrial & Engineering Chemistry Research*, 2001, **40**, 1032-1041.
81. M. Santikunaporn, J. E. Herrera, S. Jongpatiwut, D. E. Resasco, W. E. Alvarez and E. L. Sughrue, *Journal of Catalysis*, 2004, **228**, 100-113.
82. A. Corma, V. González-Alfaro and A. V. Orchillés, *Journal of Catalysis*, 2001, **200**, 34-44.
83. Å. Slagtern, I. M. Dahl, K. J. Jens and T. Myrstad, *Applied Catalysis A: General*, 2010, **375**, 213-221.
84. C. Berger, A. Raichle, R. A. Rakoczy, Y. Traa and J. Weitkamp, *Microporous and Mesoporous Materials*, 2003, **59**, 1-12.
85. H. B. Mostad, T. U. Riis and O. H. Ellestad, *Applied Catalysis*, 1990, **58**, 105-117.
86. H. B. Mostad, T. U. Riis and O. H. Ellestad, *Applied Catalysis*, 1990, **63**, 345-364.
87. T. J. McCarthy, G. D. Lei and W. M. H. Sachtler, *Journal of Catalysis*, 1996, **159**, 90-98.
88. M. A. Arribas, A. Martínez and G. Sastre, in *Studies in Surface Science and Catalysis*, eds. R. Aiello, G. Giordano and F. Testa, Elsevier, 2002, vol. 142, pp. 1015-1022.
89. P. T. Do, W. E. Alvarez and D. E. Resasco, *Journal of Catalysis*, 2006, **238**, 477-488.
90. K. C. Mouli, V. Sundaramurthy and A. K. Dalai, *Journal of Molecular Catalysis A: Chemical*, 2009, **304**, 77-84.
91. R. Kramer and H. Zuegg, *Journal of Catalysis*, 1984, **85**, 530-535.
92. S. L. González-Cortés, S. Dorkjampa, P. T. Do, Z. Li, J. M. Ramallo-López and F. G. Requejo, *Chemical Engineering Journal*, 2008, **139**, 147-156.
93. S. Dokjampa, T. Rirksomboon, D. T. M. Phuong and D. E. Resasco, *Journal of Molecular Catalysis A: Chemical*, 2007, **274**, 231-240.
94. H. Ziaei-Azad and N. Semagina, 2014, **6**, 885-894.
95. K. Foger and H. Jaeger, *Journal of Catalysis*, 1989, **120**, 465-472.
96. B. Coq, E. Crabb and F. Figuéras, *Journal of Molecular Catalysis A: Chemical*, 1995, **96**, 35-48.
97. F. G. Gault, in *Advances in Catalysis*, eds. D. D. Eley, H. Pines and P. B. Weisz, Academic Press, 1981, vol. 30, pp. 1-95.
98. M. Taillades-Jacquín, D. J. Jones, J. Rozière, R. Moreno-Tost, A. Jiménez-López, S. Albertazzi, A. Vaccari, L. Storaro, M. Lenarda and J.-M. Trejo-Menayo, *Applied Catalysis A: General*, 2008, **340**, 257-264.
99. N. Catherin, E. Blanco, L. Piccolo, D. Laurenti, F. Simonet, C. Lorentz, E. Leclerc, V. Calemma and C. Geantet, *Catalysis Today*, 2019, **323**, 105-111.
100. U. Nylén, L. Sassu, S. Melis, S. Järås and M. Boutonnet, *Applied Catalysis A: General*, 2006, **299**, 1-13.

101. L. Brito, G. D. Pirngruber, E. Guillon, F. Albrieux and J. A. Martens, **n/a**.
102. B. A. Lerner, B. T. Carvill and W. M. H. Sachtler, *Journal of Molecular Catalysis*, 1992, **77**, 99-108.
103. S. Nassreddine, S. Casu, J. L. Zotin, C. Geantet and L. Piccolo, *Catalysis Science & Technology*, 2011, **1**, 408-412.
104. L. Piccolo, S. Nassreddine, G. Toussaint and C. Geantet, 2012, **5**, 1717-1723.
105. S. A. D'Ippolito, L. Pirault-Roy, C. Especel, F. Epron and C. L. Pieck, *Fuel Processing Technology*, 2018, **177**, 6-15.
106. S. Nassreddine, L. Massin, M. Aouine, C. Geantet and L. Piccolo, *Journal of Catalysis*, 2011, **278**, 253-265.
107. S. Rabl, A. Haas, D. Santi, C. Flego, M. Ferrari, V. Calemma and J. Weitkamp, *Applied Catalysis A: General*, 2011, **400**, 131-141.
108. V. Calemma, M. Ferrari, S. Rabl and J. Weitkamp, *Fuel*, 2013, **111**, 763-770.
109. D. Kubička, N. Kumar, T. Venäläinen, H. Karhu, I. Kubičková, H. Österholm and D. Y. Murzin, *The Journal of Physical Chemistry B*, 2006, **110**, 4937-4946.
110. A. Haas, S. Rabl, M. Ferrari, V. Calemma and J. Weitkamp, *Applied Catalysis A: General*, 2012, **425-426**, 97-109.
111. E. Blanco, L. Di Felice, N. Catherin, L. Piccolo, D. Laurenti, C. Lorentz, C. Geantet and V. Calemma, *Industrial & Engineering Chemistry Research*, 2016, **55**, 12516-12523.
112. R. Moraes, K. Thomas, S. Thomas, S. Van Donk, G. Grasso, J.-P. Gilson and M. Houalla, *Journal of Catalysis*, 2013, **299**, 30-43.
113. G. Diaz, F. Garin, G. Maire, S. Alerasool and R. D. Gonzalez, *Applied Catalysis A: General*, 1995, **124**, 33-46.
114. L. B. Galperin, J. C. Bricker and J. R. Holmgren, *Applied Catalysis A: General*, 2003, **239**, 297-304.
115. M. Vaarkamp, P. Dijkstra, J. Vangrondelle, J. T. Miller, F. S. Modica, D. C. Koningsberger and R. A. Vansanten, *Journal of Catalysis*, 1995, **151**, 330-337.
116. D. P. Upare, S. Yoon and C. W. Lee, *Catalysis Letters*, 2012, **142**, 744-752.
117. A. Djeddi, I. Fechete and F. Garin, *Catalysis Communications*, 2012, **17**, 173-178.
118. K. Hayek, R. Kramer and Z. Paál, *Applied Catalysis A: General*, 1997, **162**, 1-15.
119. G. Jacobs, F. Ghadiali, A. Pisanu, A. Borgna, W. E. Alvarez and D. E. Resasco, *Applied Catalysis A: General*, 1999, **188**, 79-98.
120. R. Kramer and H. Zuegg, *Journal of Catalysis*, 1983, **80**, 446-456.
121. C. G. Walter, B. Coq, F. Figueras and M. Boulet, *Applied Catalysis A: General*, 1995, **133**, 95-102.
122. A. Piegsa, W. Korth, F. Demir and A. Jess, *Catalysis Letters*, 2012, **142**, 531-540.
123. R. Nageswara Rao, N. You, S. Yoon, D. P. Upare, Y.-K. Park and C. W. Lee, *Catalysis Letters*, 2011, **141**, 1047-1055.
124. F. Li, X. Yi, J. Zheng, H. Jin and W. Fang, *Catalysis Communications*, 2009, **11**, 266-271.
125. P. T. Williams and E. Slaney, *Resources, Conservation and Recycling*, 2007, **51**, 754-769.
126. A. Gutiérrez, J. M. Arandes, P. Castaño, M. Olazar and J. Bilbao, *Fuel*, 2012, **94**, 504-515.
127. Q. Wang, H. Fan, S. Wu, Z. Zhang, P. Zhang and B. Han, *Green Chemistry*, 2012, **14**, 1152-1158.
128. J.-I. Park, J.-K. Lee, J. Miyawaki, Y.-K. Kim, S.-H. Yoon and I. Mochida, *Fuel*, 2011, **90**, 182-189.
129. S.-U. Lee, Y.-J. Lee, J.-R. Kim and S.-Y. Jeong, *Applied Catalysis B: Environmental*, 2017, **219**, 1-9.
130. M. Chawla, S. Rafiq, F. Jamil, M. R. Usman, S. Khurram, M. Ghauri, N. Muhammad, A. a. H. Al-Muhtaseb and M. Aslam, *Journal of Cleaner Production*, 2018, **198**, 683-692.
131. S. J. Ardakani and K. J. Smith, *Applied Catalysis A: General*, 2011, **403**, 36-47.
132. K. Jaroszewska, A. Masalska, K. Bączkowska and J. R. Grzechowiak, *Catalysis Today*, 2012, **196**, 110-118.
133. P. Samoila, M. Boutzeloit, C. Especel, F. Epron and P. Marécot, *Applied Catalysis A: General*, 2009, **369**, 104-112.
134. B. Pawelec, A. M. Venezia, V. La Parola, E. Cano-Serrano, J. M. Campos-Martin and J. L. G. Fierro, *Applied Surface Science*, 2005, **242**, 380-391.
135. H. Chen, H. Yang, O. Omotoso, L. Ding, Y. Briker, Y. Zheng and Z. Ring, *Applied Catalysis A: General*, 2009, **358**, 103-109.
136. S. Dokjampa, T. Rirksomboon, S. Osuwan, S. Jongpatiwut and D. E. Resasco, *Catalysis Today*, 2007, **123**, 218-223.
137. I. Cuauhtémoc-López, A. Jiménez-Vázquez, L. A. Estudillo-Wong, G. Torres-Torres, H. Pérez-Vidal, M. Barrera-Salgado, R. López-González and D. De la Cruz-Romero, *Catalysis Today*, 2021, **360**, 176-184.
138. M. a. A. Arribas, P. Concepción and A. n. Martínez, *Applied Catalysis A: General*, 2004, **267**, 111-119.
139. N. Suárez, M. A. Arribas, A. Moreno and A. Martínez, *Catalysis Science & Technology*, 2020, **10**, 1073-1085.

140. X. Dong, P. Zheng, A.-G. Zheng, H.-F. Li, G.-F. Xia, M.-F. Li, R.-Y. Zheng and B.-Q. Xu, *Catalysis Today*, 2018, **316**, 162-170.
141. R. Kramer and M. Fischbacher, *Journal of Molecular Catalysis*, 1989, **51**, 247-259.
142. H. Glasl, K. Hayek and R. Kramer, *Journal of Catalysis*, 1981, **68**, 397-405.
143. M. J. Dees, M. H. B. Bol and V. Ponec, *Applied Catalysis*, 1990, **64**, 279-295.
144. A. Djeddi, I. Fechete and F. Garin, *Applied Catalysis A: General*, 2012, **413-414**, 340-349.
145. P. Samoila, F. Epron, P. Marécot and C. Especel, *Applied Catalysis A: General*, 2013, **462-463**, 207-219.
146. A. Le Valant, F. Drault, C. Maleix, C. Comminges, R. Beauchet, Y. Batonneau, L. Pirault-Roy, C. Especel and F. Epron, *Journal of Catalysis*, 2018, **367**, 234-243.
147. A. Djeddi, I. Fechete and F. Garin, *Topics in Catalysis*, 2012, **55**, 700-709.
148. G. Bellussi, A. Haas, S. Rabl, D. Santi, M. Ferrari, V. Calemma and J. Weitkamp, *Chinese Journal of Catalysis*, 2012, **33**, 70-84.
149. A. Djeddi, I. Fechete, O. Ersen and F. Garin, *Comptes Rendus Chimie*, 2013, **16**, 433-441.
150. Z. Wang, A. Zheng, R. Zheng, M. Li, H. Li, G. Xu and G. Xia, *RSC Advances*, 2016, **6**, 105063-105069.
151. V. M. Benitez, S. P. de Lima, M. do Carmo Rangel, D. Ruiz, P. Reyes and C. L. Pieck, *Catalysis Today*, 2017, **289**, 53-61.
152. U. Nylén, J. F. Delgado, S. Järås and M. Boutonnet, *Applied Catalysis A: General*, 2004, **262**, 189-200.
153. H. Ziaei-azad, C.-X. Yin, J. Shen, Y. Hu, D. Karpuzov and N. Semagina, *Journal of Catalysis*, 2013, **300**, 113-124.
154. J. Shen, X. Yin, D. Karpuzov and N. Semagina, *Catalysis Science & Technology*, 2013, **3**, 208-221.
155. Y. Miki, S. Yamadaya and M. Oba, *Journal of Catalysis*, 1977, **49**, 278-284.
156. D. P. Upare, S. Yoon and C. W. Lee, *Journal of Porous Materials*, 2013, **20**, 1129-1136.
157. S. A. D'Ippolito, L. B. Gutierrez, C. R. Vera and C. L. Pieck, *Applied Catalysis A: General*, 2013, **452**, 48-56.
158. M. A. Vicerich, M. Oportus, V. M. Benitez, P. Reyes and C. L. Pieck, *Applied Catalysis A: General*, 2014, **480**, 42-49.
159. L. M. Kustov, E. D. Finashina, V. I. Avaev and B. G. Ershov, *Fuel Processing Technology*, 2018, **173**, 270-275.
160. Z.-J. Zhao, L. V. Moskaleva and N. Rösch, *Journal of Catalysis*, 2012, **285**, 124-133.
161. F. Calle-Vallejo, J. Tymoczko, V. Colic, Q. H. Vu, M. D. Pohl, K. Morgenstern, D. Loffreda, P. Sautet, W. Schuhmann and A. S. Bandarenka, *Science*, 2015, **350**, 185.
162. S. Kuld, M. Thorhauge, H. Falsig, C. F. Elkjær, S. Helveg, I. Chorkendorff and J. Sehested, *Science*, 2016, **352**, 969.
163. F. E. Shephard and J. J. Rooney, *Journal of Catalysis*, 1964, **3**, 129-144.
164. K. Foger and J. R. Anderson, *Journal of Catalysis*, 1979, **59**, 325-339.
165. J. G. van Senden, E. H. van Broekhoven, C. T. J. Wreesman and V. Ponec, *Journal of Catalysis*, 1984, **87**, 468-477.
166. G. Del Angel, B. Coq, R. Dutartre and F. Figueras, *Journal of Catalysis*, 1984, **87**, 27-35.
167. D. Teschner, D. Duprez and Z. Paál, *Journal of Molecular Catalysis A: Chemical*, 2002, **179**, 201-212.
168. E. Christoffel, F. Fetting and H. Vierrath, *Journal of Catalysis*, 1975, **40**, 349-355.
169. H. Shi, O. Y. Gutiérrez, G. L. Haller, D. Mei, R. Rousseau and J. A. Lercher, *Journal of Catalysis*, 2013, **297**, 70-78.
170. H. Shi, O. Y. Gutiérrez, A. Zheng, G. L. Haller and J. A. Lercher, *The Journal of Physical Chemistry C*, 2014, **118**, 20948-20958.
171. Z. Paál and P. TÉTÉNYi, *Nature*, 1977, **267**, 234-236.
172. W. Yu, M. D. Porosoff and J. G. Chen, *Chemical Reviews*, 2012, **112**, 5780-5817.
173. N. Györffy, A. Wootsch, S. Szabó, I. Bakos, L. Tóth and Z. Paál, *Topics in Catalysis*, 2007, **46**, 57-64.
174. V. Akhmedov and K. J. Klabunde, *Journal of Molecular Catalysis*, 1988, **45**, 193-206.
175. M. Chamam, K. Lázár, L. Pirault-Roy, I. Boghian, Z. Paál and A. Wootsch, *Applied Catalysis A: General*, 2007, **332**, 27-36.
176. M. Chamam, A. Wootsch, L. Pirault-Roy, I. Boghian and Z. Paál, *Catalysis Communications*, 2007, **8**, 686-692.
177. R. J. Fenoglio, G. M. Nuñez and D. E. Resasco, *Applied Catalysis*, 1990, **63**, 319-332.
178. M. A. Vicerich, V. M. Benitez, C. Especel, F. Epron and C. L. Pieck, *Applied Catalysis A: General*, 2013, **453**, 167-174.
179. O. V. Masloboishchikova, T. V. Vasina, E. G. Khelkovskaya-Sergeeva, L. M. Kustov and P. Zeuthen, *Russian Chemical Bulletin*, 2002, **51**, 249-254.

180. Y. Park, Y. C. Kim, J. Kim, Y.-K. Park, Y. S. Choi, J. M. Kim and J.-K. Jeon, *Catalysts*, 2019, **9**, 531.
181. G. C. Bond, *Applied Catalysis A: General*, 1997, **149**, 3-25.
182. M. C. Tsai, C. M. Friend and E. L. Muetterties, *Journal of the American Chemical Society*, 1982, **104**, 2539-2543.
183. W. L. Manner, L. H. Dubois, G. S. Girolami and R. G. Nuzzo, *The Journal of Physical Chemistry B*, 1998, **102**, 2391-2402.
184. M. Santikunaporn, W. E. Alvarez and D. E. Resasco, *Applied Catalysis A: General*, 2007, **325**, 175-187.
185. C. A. A. Monteiro, D. Costa, J. L. Zotin and D. Cardoso, *Fuel*, 2015, **160**, 71-79.
186. Q. Wang, Z.-G. Hou, B. Zhang, J. Liu, W.-Y. Song, D.-S. Xue, L.-Z. Liu, D. Wang and X.-G. Chen, *Petroleum Science*, 2018, **15**, 605-612.
187. D. P. Upare and C. W. Lee, *Fuel Processing Technology*, 2014, **126**, 243-248.
188. H. Ziaei-Azad and A. Sayari, *Journal of Catalysis*, 2016, **344**, 729-740.
189. A. H. Alzaid and K. J. Smith, *Applied Catalysis A: General*, 2013, **450**, 243-252.
190. D. Santi, T. Holl, V. Calemme and J. Weitkamp, *Applied Catalysis A: General*, 2013, **455**, 46-57.
191. S. A. D'Ippolito, A. D. Ballarini and C. L. Pieck, *Energy & Fuels*, 2017, **31**, 5461-5471.
192. S. A. D'Ippolito, C. Especel, L. Vivier, S. Pronier, F. Epron and C. L. Pieck, *Journal of Molecular Catalysis A: Chemical*, 2015, **398**, 203-214.
193. S. A. D'Ippolito, L. Pirault-Roy, C. Especel, F. Epron and C. L. Pieck, *RSC Advances*, 2017, **7**, 46803-46811.
194. I. Fechete, B. Donnio, O. Ersen, T. Dintzer, A. Djeddi and F. Garin, *Applied Surface Science*, 2011, **257**, 2791-2800.
195. S. Haddoum, I. Fechete, B. Donnio, F. Garin, D. Lutic and C. E. Chitour, *Catalysis Communications*, 2012, **27**, 141-147.
196. L. Yuan, S. Guo, Z. Li, H. Cui, H. Dong, L. Zhao and J. Wang, *RSC Advances*, 2017, **7**, 9446-9455.
197. S. Cui, G. Wang, Y. Yang and B. Liu, *Fuel*, 2018, **225**, 10-17.
198. L. Piccolo, S. Nassreddine, M. Aouine, C. Ulhaq and C. Geantet, *Journal of Catalysis*, 2012, **292**, 173-180.
199. S. A. D'Ippolito, C. Especel, L. Vivier, F. Epron and C. L. Pieck, *Applied Catalysis A: General*, 2014, **469**, 532-540.
200. G. Onyestyák, G. Pál-Borbély and H. K. Beyer, *Applied Catalysis A: General*, 2002, **229**, 65-74.
201. D. Kubička, N. Kumar, P. Mäki-Arvela, T. Venäläinen, M. Tiitta, T. Salmi and D. Y. Murzin, in *Studies in Surface Science and Catalysis*, eds. J. Čejka, N. Žilková and P. Nachtigall, Elsevier, 2005, vol. 158, pp. 1669-1676.
202. D. Kubička, T. Salmi, M. Tiitta and D. Y. Murzin, *Fuel*, 2009, **88**, 366-373.
203. S. Lecarpentier, J. van Gestel, K. Thomas, J.-P. Gilson and M. Houalla, *Journal of Catalysis*, 2008, **254**, 49-63.
204. G. B. McVicker, O. C. Feeley, J. J. Ziemiak, D. E. W. Vaughan, K. C. Strohmaier, W. R. Kliewer and D. P. Leta, *The Journal of Physical Chemistry B*, 2005, **109**, 2222-2226.
205. C. M. A. Parlett, K. Wilson and A. F. Lee, *Chemical Society Reviews*, 2013, **42**, 3876-3893.
206. A. Sayari, D. Shee, N. Al-Yassir and Y. Yang, *Topics in Catalysis*, 2010, **53**, 154-167.
207. M. A. Vicerich, V. M. Benitez, M. A. Sánchez and C. L. Pieck, *Catalysis Letters*, 2015, **145**, 910-918.
208. A. Infantes-Molina, J. Mérida-Robles, E. Rodríguez-Castellón, J. L. G. Fierro and A. Jiménez-López, *Applied Catalysis B: Environmental*, 2007, **73**, 180-192.
209. S. Rabl, D. Santi, A. Haas, M. Ferrari, V. Calemme, G. Bellussi and J. Weitkamp, *Microporous and Mesoporous Materials*, 2011, **146**, 190-200.
210. J. Weitkamp, *ChemCatChem*, 2012, **4**, 292-306.
211. A. Boulaoued, I. Fechete, B. Donnio, M. Bernard, P. Turek and F. Garin, *Microporous and Mesoporous Materials*, 2012, **155**, 131-142.
212. N. Jiang, K. S. R. Rao, M.-J. Jin and S.-E. Park, *Applied Catalysis A: General*, 2012, **425-426**, 62-67.
213. J. M. Orozco and G. Webb, *Applied Catalysis*, 1983, **6**, 67-84.
214. K. C. Mouli, V. Sundaramurthy, A. K. Dalai and Z. Ring, *Applied Catalysis A: General*, 2007, **321**, 17-26.
215. L. Zhang, M. Zhou, A. Wang and T. Zhang, *Chemical Reviews*, 2020, **120**, 683-733.
216. S. A. D'Ippolito, L. B. Gutierrez and C. L. Pieck, *Applied Catalysis A: General*, 2012, **445-446**, 195-203.
217. S. Qiu, X. Zhang, Q. Liu, T. Wang, Q. Zhang and L. Ma, *Catalysis Communications*, 2013, **42**, 73-78.
218. H. Liu, C. Liu, C. Yin, B. Liu, X. Li, Y. Li, Y. Chai and Y. Liu, *Catalysis Today*, 2016, **276**, 46-54.
219. G. Yun, Q. Guan and W. Li, *RSC Advances*, 2017, **7**, 8677-8687.
220. M. Usman, D. Li, R. Razaq, U. Latif, O. Muraza, Z. H. Yamani, B. A. Al-Maythalyony, C. Li and S. Zhang, *Journal of Environmental Chemical Engineering*, 2018, **6**, 4525-4530.

221. S.-U. Lee, Y.-J. Lee, J.-R. Kim and S.-Y. Jeong, *Journal of Industrial and Engineering Chemistry*, 2018, **66**, 279-287.
222. N. Azizi, S. A. Ali, K. Alhooshani, T. Kim, Y. Lee, J.-I. Park, J. Miyawaki, S.-H. Yoon and I. Mochida, *Fuel Processing Technology*, 2013, **109**, 172-178.
223. Y. Al Obaidi, M. Kozminski, J. Ward, M. Johnson and J. M. Guevremont, *Industrial & Engineering Chemistry Research*, 2018, **57**, 12029-12035.
224. C. Peng, Z. Zhou, Z. Cheng and X. Fang, *Energy & Fuels*, 2019, **33**, 1090-1097.
225. L. Wang, B. Shen, F. Fang, F. Wang, R. Tian, Z. Zhang and L. Cui, *Catalysis Today*, 2010, **158**, 343-347.
226. H. Wang, F. Dai, Z. Li and C. Li, *Energy & Fuels*, 2015, **29**, 4902-4910.
227. K. Chandra Mouli and A. K. Dalai, *Applied Catalysis A: General*, 2009, **364**, 80-86.
228. L. J. Simon, J. G. van Ommen, A. Jentys and J. A. Lercher, *Catalysis Today*, 2002, **73**, 105-112.
229. C. Song and A. D. Schmitz, *Energy & Fuels*, 1997, **11**, 656-661.
230. D. Eliche-Quesada, J. Mérida-Robles, P. Maireles-Torres, E. Rodríguez-Castellón, G. Busca, E. Finocchio and A. Jiménez-López, *Journal of Catalysis*, 2003, **220**, 457-467.
231. Y. Wang, B. Shen, K. Hao, J. Li, L. Wang, B. Feng and Q. Guo, *Catalysis Communications*, 2012, **25**, 59-63.
232. V. Chandra Srivastava, *RSC Advances*, 2012, **2**, 759-783.
233. T. Kabe, W. H. Qian, S. Ogawa and A. Ishihara, *Journal of Catalysis*, 1993, **143**, 239-248.
234. N. Kunisada, K.-H. Choi, Y. Korai, I. Mochida and K. Nakano, *Applied Catalysis A: General*, 2004, **276**, 51-59.
235. P. Vozka, D. Orazgaliyeva, P. Šimáček, J. Blažek and G. Kilaz, *Fuel Processing Technology*, 2017, **167**, 684-694.
236. H. Topsøe, B. S. Clausen and F. E. Massoth, in *Catalysis: Science and Technology*, eds. J. R. Anderson and M. Boudart, Springer Berlin Heidelberg, Berlin, Heidelberg, 1996, DOI: 10.1007/978-3-642-61040-0_1, pp. 1-269.
237. Y. Wang, B. Shen, L. Wang, B. Feng, J. Li and Q. Guo, *Fuel Processing Technology*, 2013, **106**, 141-148.
238. L. Di Felice, N. Catherin, L. Piccolo, D. Laurenti, E. Blanco, E. Leclerc, C. Geantet and V. Calemma, *Applied Catalysis A: General*, 2016, **512**, 43-51.
239. M. A. Isaacs, C. M. A. Parlett, N. Robinson, L. J. Durndell, J. C. Manayil, S. K. Beaumont, S. Jiang, N. S. Hondow, A. C. Lamb, D. Jampaiah, M. L. Johns, K. Wilson and A. F. Lee, *Nature Catalysis*, 2020, **3**, 921-931.
240. K. Li, J. Valla and J. Garcia-Martinez, *ChemCatChem*, 2014, **6**, 46-66.
241. M. A. Isaacs, N. Robinson, B. Barbero, L. J. Durndell, J. C. Manayil, Christopher M. A. Parlett, C. D'Agostino, K. Wilson and A. F. Lee, *Journal of Materials Chemistry A*, 2019, **7**, 11814-11825.
242. K. Arve, P. Mäki-Arvela, K. Eränen, M. Tiitta, T. Salmi and D. Y. Murzin, *Chemical Engineering Journal*, 2014, **238**, 3-8.
243. X. Zhou, H. Yan, X. Feng, H. Zhao, Y. Liu, X. Chen and C. Yang, *Industrial & Engineering Chemistry Research*, 2020, **59**, 20086-20101.
244. 1997.
245. 1998.
246. Preemraff Lysekil Refinery, <https://www.nsenergybusiness.com/projects/preemraff-lysekil-refinery/>).
247. S. Masnadi Mohammad, M. El-Houjeiri Hassan, D. Schunack, Y. Li, G. Englander Jacob, A. Badahdah, J.-C. Monfort, E. Anderson James, J. Wallington Timothy, A. Bergerson Joule, D. Gordon, J. Koomey, S. Przesmitzki, L. Azevedo Inês, T. Bi Xiaotao, E. Duffy James, A. Heath Garvin, A. Keoleian Gregory, C. McGlade, D. N. Meehan, S. Yeh, F. You, M. Wang and R. Brandt Adam, *Science*, 2018, **361**, 851-853.
248. V. Gordillo, N. Rankovic and A. F. N. Abdul-Manan, *The International Journal of Life Cycle Assessment*, 2018, **23**, 1527-1541.
249. C. Peng, X.-c. Fang, R.-h. Zeng, R. Guo and W.-y. Hao, *Catalysis Today*, 2016, **276**, 11-18.
250. Q. Sun, N. Wang and J. Yu, *Advanced Materials*, **n/a**, 2104442.
251. H. Wang, L. Wang and A. Shahbazi, *Journal of Cleaner Production*, 2015, **87**, 511-519.
252. V. K. Guda, P. H. Steele, V. K. Penmetsa and Q. Li, in *Recent Advances in Thermo-Chemical Conversion of Biomass*, eds. A. Pandey, T. Bhaskar, M. Stöcker and R. K. Sukumaran, Elsevier, Boston, 2015, DOI: <https://doi.org/10.1016/B978-0-444-63289-0.00007-7>, pp. 177-211.